3-2000

Collection of Detonation Signatures and Characterization of Spectral Features

Jay A. Orson

COLLECTION OF DETONATION SIGNATURES AND CHARACTERIZATION OF SPECTRAL FEATURES

THESIS

Jay A. Orson, 1st Lieutenant, USAF

AFIT/GSO/ENP/00M-01

DEPARTMENT OF THE AIR FORCE
AIR UNIVERSITY

AIR FORCE INSTITUTE OF TECHNOLOGY

Wright-Patterson Air Force Base, Ohio

AFIT/GSO/ENP/00M-01

COLLECTION OF DETONATION SIGNATURES AND CHARACTERIZATION OF SPECTRAL FEATURES

THESIS

JAY A. ORSON, 1st LIEUTENANT, USAF
AFIT/GSO/ENP/00M-01

The views expressed in this thesis are those of the author and do not reflect the official policy or position of the United States Air Force, Department of Defense, or the U.S. Government.

AFIT/GSO/ENP/00M-01

COLLECTION OF DETONATION SIGNATURES AND CHARACTERIZATION OF SPECTRAL FEATURES

Presented to the Faculty

Graduate School of Engineering and Management

Air Force Institute of Technology

Air University

Air Education and Training Command

In Partial Fulfillment of the Requirements for the

Degree of Master of Science in Space Operations

Jay A. Orson, B.S.

1st Lieutenant, USAF

March 2000

AFIT/GSO/ENP/00M-01

COLLECTION OF DETONATION SIGNATURES AND CHARACTERIZATION OF SPECTRAL FEATURES

Jay A. Orson, B.S.
1st Lieutenant, USAF

Approved:

Glen Perram (Chairman)	6 MAR00 date
Jeffery Little (Member)	5 Mar 2000 date
Howard Evans (Member)	29 Feb 2000 date
Jim Engel (Member)	29 Feb 2000 date

Acknowledgements

I would like to take this opportunity to express my love and appreciation for my wife, Barbara, and my two sons, Kohl and Keithen, who were always my number one fans. Their support, sacrifice, and devotion over the past eighteen months have been my constant motivation.

I am indebted for the guidance and support provided by my advisor Lt Col Glen Perram, the support of my sponsor NAIC/DXDI for funding two TDY's to see bombs blow up, and the efforts of my committee members Lt Col Little, Howard Evans and Jim Engel.

Finally, would like to express sincere thanks to Tom Fitzgerald for the *Matlab* coding assistance and joint sensor fusion efforts, as well as the gracious learning provided by the DXDO collection team members. Their help made two deployments to Bravo Twenty a huge success as well as enjoyable, even at o'dark 0300. May super tools and the Bird Farm ever live in NAS Fallon.

Jay Orson

Table of Contents

List of Figures

List of Tables

Abstract

The remote observations of the temporal and spectral characteristics of the infrared (IR) emissions from exploding ordnance have been correlated with explosion conditions. A Bomem MR-154 Fourier Transform Interferometer with two detectors, InSb and HgCdTe, and a 75 mrad telescope was used to record spectra in the 1.3 - 20 μm range. Data was collected at spectral resolutions of 16 cm^{-1} and 4 cm^{-1} and temporal resolutions of 0.045 s and 0.123 s respectively. Two field tests were conducted: (1) a set of dynamic drop explosions and (2) a series of static detonations.

In most events, the temporal profile for certain bands indicate a rapid, intense signature, followed by a secondary maximum and a long-term decay of up to several seconds. A second class of temporal profiles were characterized by an event initiation, followed by an increase in apparent radiance to one maximum, followed by a long-term decay. Sensor fusion between the FTIR instrument and four 200 Hz InSb radiometers is quite promising. The FTIR temporal profiles, calibrated for absolute radiance, compare within 8% in three independent bands and within 30% in the fourth band. The degree of temporal overlap as a function of frequency for a pair of detonation events, provides a direct indication of the ability to discriminate between explosion conditions. Overlap analysis provides quantification of the repeatability of an explosive condition, and the discrimination between look angle and explosive type. Additional preliminary analysis mechanistically describes all events as decaying gray bodies.

COLLECTION OF DETONATION SIGNATURES AND CHARACTERIZATION OF SPECTRAL FEATURES

I. Introduction

Overview

Remote sensing is changing the way mankind looks at the world. From medical diagnostics, ballistic missile defense, terrain mapping of Mars, to identifying groceries in the supermarket, remote sensing effects everyone. Remote sensing is "the combination of techniques used to gather and process information about an object without direct physical contact" (6, 1-4). It has many ramifications for the Department of Defense (DOD). The DOD uses sensing techniques for battlefield management, battle-space characterization, weapons guidance, technical intelligence and threat identification.

One of the first uses of remote sensing by the US Army Air Corps was taking pictures of troop movements in WWI. Today, remote sensing is not limited to visual pictures of troop movements, but includes sensing most of the electromagnetic spectrum. This 'sensed' spectrum ranges from short wavelength x-rays, to visual photos, to infrared, to longer wavelength radio waves. Each spectral range can be used to detect unique information about unknown objects or events. For example: X-rays detect solar flares, visual photographs provide military intelligence or pictures for disaster relief, infrared determines agricultural crop conditions as well as theater missile defense, and radio waves monitor changing conditions in the polar icecaps.

Currently, the Navy Tactical Exploitation of National Capabilities (TENCAP) office in partnership with the National Air Intelligence Center's division of data exploitation (NAIC/DXD) are sponsoring research in the area of infrared Measurement and Signals Intelligence (MASINT) detection of explosions. "This effort explores the potential use of space-based MASINT sensors to support combat units in the area of Battle-Space Characterization" (17,1). This program has sponsored a series of tests where ordnance was detonated under field conditions.

This thesis effort focused on the infrared collection of detonation signatures from the Radiant Brass 3A and 3B tests. Fifty-six detonation events were collected over the spectral range of 500 to 6000 wavenumbers (cm^{-1}) with .047 seconds time resolution. Collection was accomplished with a Bomem MR-154 Fourier Transform Infrared spectroradiometer. These events were a combination of dynamic F-18 delivered ordnance as well as static detonations.

The collection of detonation signatures is no simple task. Detonation events by their very nature are mechanisticcally complex and highly variable. Explosions involve chemistry and physics under extreme conditions and therefore are difficult to describe and predict. The spectral signatures sensed by the MR-154 have large variations caused by the munitions themselves, the event environment, the collection method, and subsequent processing. This thesis focuses on the collection of infrared signatures from detonation events and the subsequent analysis of the temporal and spectral features collected. Great effort has been taken to preserve the true nature of the collected signature and to accurately control the variables.

Event Features

How do explosion mechanisms give rise to observed features in data? To answer this question, a simple discussion of bomb phenomenology is needed. The explosion mechanisms produce three primary 'sensed' features, an explosion initiation, a secondary afterburn, and a decay period. The explosion initiation is due to the initial spike of energy caused by the nearly instantaneous conversion of the explosive from chemical potential energy to kinetic energy. The time scale of this feature is less than 1 μs (8,1).

The afterburn feature is due to the residual products of the detonation itself. In an underoxidized explosion these residuals are themselves fuels (5, 133). After the initial pressure pulse of the explosion reaches equilibrium pressure with the surrounding environment, oxygen and air remix with the residual explosion by-products. This mixing of oxygen and residual fuel ignites and causes the energetic afterburn fireball. This feature starts milliseconds after the initiation feature and can last for up to a second. The third feature is the decay of the explosion itself. When the afterburn has consumed all the residual fuel, the event decays back to ambient conditions. This feature lasts between 1-3 seconds. These three features make up the primary time history of the 'sensed' explosion and are detailed in Figure1.1.

The second dimension of features present in a detonation signature is the spectrum. This spectrum is dominated by the gray body effect of the explosion mechanisms. The detonation event deposits large amounts of kinetic energy into the environment. Kinetic energy is divided into two categories, directed translational kinetic energy and random internal kinetic energy. Translational kinetic energy is associated with the external motion of particles and bomb fragments.

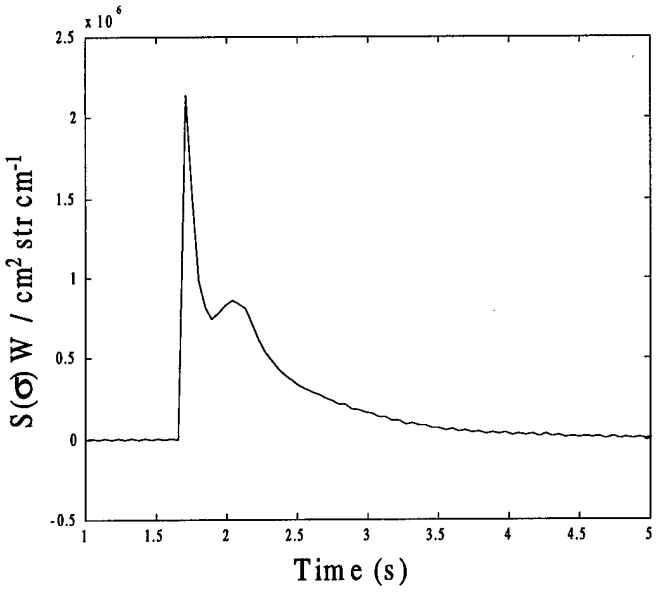

Figure 1.1. Time History for an Explosive A, Size Large Event

Random internal kinetic energy is the total quantity of energy associated with the presence, relative positions, and movements of all component molecules, atoms, and subatomic units (5, 94). In thermodynamics, the average random kinetic energy is characterized by temperature. If the radiation and motion is in equilibrium, the temperature can further be related to the radiation emitted by the event via equation 1.1, the Planck Distribution:

$$S(\lambda) = \varepsilon(\lambda)\frac{2\pi hc^2}{\lambda^5}\frac{1}{e^{ch/\lambda kT} - 1} \qquad (1.1)$$

where

$S(\lambda)$ = spectral energy = W/ m^2
$\varepsilon(\lambda)$ = emissivity as a function of wavelength
λ = radiation wavelength
h = Planck's constant = 6.626×10^{-34} W sec^2
T = absolute temperature in Kelvin
c = velocity of light = 2.9979×10^8 m/sec
k = Boltmann's constant = 1.38×10^{-23} W sec/K

The wavelength of maximum emittance (λ_m), and a simplified form for total emittance (M), of the Planck distribution are given by:

$$\lambda_m = a/T \tag{1.2}$$

$$M = \sigma T^4 \tag{1.3}$$

where

a = constant = 2898 μm K
σ = constant = 5.669 x 10^{-8} W m^{-2} K^{-4}

Since the explosion mechanism imparts energy to all particles in the atmosphere as well as all explosive byproducts, a continuous spectrum partially based on equation 1.1 is collected. If $\varepsilon(\lambda) = 1$, equation 1.1 describes the radiation emitted from a black body. When $\varepsilon \neq 1$, but is constant, the output from equation 1.1 is a called a 'gray' body. When $\varepsilon \neq 1$ and is a function of wavelength, it is described as a selective radiator.

In an interview with Bill Miller the statement was made that a detonation could be "primarily described as a gray body" (18). Assuming this is true, some general characteristics of a detonation event can be derived. For example, estimate the temperature of a typical explosion initiation feature as 1800°K, the afterburn feature 1100°K, and the decay feature 400°K. Assuming a black body emitter, Table 1.1 provides the approximate range of the emitted spectra, the maximum wavelength, and the total energy of the three temporal signatures of a typical detonation event.

Table 1.1 Spectral Range of Event Emitted Radiation

Feature	Upper Bound (μm)	Lower Bound (μm)	λ_m (μm)	M (w/cm^2)
Initiation	20 +	.4	1.61	59.50
Afterburn	20 +	.8	2.63	8.30
Decay	20 +	3.0	9.66	0.05

The values in Table 1.1 are approximate and are derived by plotting equation 1.1 and subjectively determining the 95% limits of the area under the curve. Notice the spectral range of a detonation event is extremely large, .4 μm to well above 20 μm. This range is much larger than the combined spectral width of the detectors used for this work. The total energy radiated from the source changes by over four orders of magnitude throughout the event lifetime. Couple a need for spectral resolution with a very fast event time evolution and you get the primary collection tradeoff, spectral resolution versus temporal resolution. This tradeoff will be discussed further in the Experiment chapter.

Problem Statement

Battle-space characterization and technical intelligence are priorities in the DOD and have direct affect on the warfighter. A fundamental goal of the Radiant Brass test program is "developing and demonstrating new ways to provide situational awareness information to the operational warfighter" (17, 1). Studying infrared signatures of conventional munitions deployed in field conditions is a direct characterization of the battle-space. Little infrared spectral information is available on the signatures of these weapons. Previous spectral collection attempts during Radiant Brass testing have provided minimal to mixed results. The objective of this thesis was to collect robust infrared spectral signatures of detonation events, discern spectral bands that best discriminate the ordnance, and to possibly provide insight into the identification of ordnance or event conditions.

Scope

This thesis will concentrate on collection of high quality spectral and radiometric signatures from conventional munitions detonated in field conditions. A radiometric comparison with other collection team's measurements will be made to validate data. The frequency content of the spectrum will be analyzed by overlapping temporal time traces by frequency. The repeatability of events and the affects of look angle will be quantified. Finally, a preliminary principal component analysis will be discussed and the possibilities for further battle-space characterization explored.

Summary of current knowledge

The source under study is munitions detonations performed during the Navy TENCAP sponsored testing, dubbed Radiant Brass. This testing consisted of a series of five tests conducted at the Navel Air Station, (NAS) Fallon, NV. Testing started in June 1998 and was completed October 1999. Throughout the program various contractors and government agencies have supported Radiant Brass by deploying sensors to the test range and collecting event signatures. These teams are commonly called ground truth teams. The primary data requirements for these collection teams were radiometric in nature. Spectral information was an ancillary objective. No spectral data is available from the first Radiant Brass test and a limited data set is available from the second test.

The first Radiant Brass test was designed to,

> "obtain well calibrated, radiometric, optical signatures on these bombs together with accurate, well documented data on the devices themselves, the nature of the explosive events and their effects and the atmospheric characteristics along the observer-to-target line of sight" (13, 2).

This test consisted of six different ground truth teams with various different instrument packages. A total of 89 events took place over 4 days with a combination of static and

dynamic air dropped tests. After post processing and calibration, two different ground truth team's radiometric data was compared. In Band B, 2.7-3.15 μm, the comparison was within 70%. In Band D, 4.45-4.75 μm, the comparison results were a factor of 2.5 (13, 43). Despite these differences, radiometric goals were reached and the test was considered a success. All attempts at spectral measurements failed and spectroscopic goals were not achieved.

The second test Radiant Brass 2A was an air delivered ordnance test. The primary objective for this test was the same as the first test. The secondary objective was to assess whether the many discrepancies discovered in the first test relate to bomb delivery angle, ground penetration depth, aircraft release manner, look angle of bomb to observers line of sight, and ground surface interaction. There were two primary ground truth teams for this test. One collection team had numerous technical difficulties and only 3 out of 27 events were collected. A Bomem Model MR-200 Fourier Transform Infrared (FTIR) spectroradiometer was deployed by a Bomem representative. This equipment managed to collect 12 of the 27 events. Overall this test was judged to be unproductive as little radiometric data was collected (14,13).

The third test, Radiant Brass 2B, was a success. This test was a static recreation of Radiant Brass 2A and objectives were similar. Two different ground truth teams deployed four radiometer suites with similar spectral filters. Both teams had very successful collections. Between the two teams, every event was captured. Fifty-three out of 67 events had multiple collects for all radiometer pairs. Data comparisons between ground truth were good in three of the four bands and were off by a factor of 2 in the fourth band (15, 28).

AFIT, was invited to independently deploy a FTIR spectroradiometer to collect signatures during this test. Capt Hauser deployed a Bomem MR-154 FTIR spectroradiometer to the site and collected a large majority of the events. Three limitations of this data collection were apparent. One, the field of view (FOV) of the spectrometer was limited to 2.5 mrad. This was approximately an eleven meter diameter FOV at the event source. With such a small FOV, pointing of the spectrometer at the appropriate event was an issue. When the spectrometer was aligned properly, the detonation event would over fill the spectrometer FOV. Two, detector saturation occurred on many events. This leads to uncertainty in the absolute radiance and spectral signature. The third issue was the FTIR collection rate. The deployed equipment's temporal resolution was limited to 3.6 scans per second at 16 cm^{-1} resolution and .9 scans per second at 2 cm^{-1} resolution. At these scan rates, the FTIR was averaging out temporal features in the detonation event. Despite these limitations the collected data did show promise for identification and warranted further research (10, 1-86).

Due to the inherent difficulties and costs associated with collection of bomb detonations, little spectral data is available on conventional munitions. The analysis in this thesis is limited to the spectral data collected from the Radiant Brass 2A and 2B tests and signatures collected from the Radiant Brass 3A and 3B tests.

Approach

The experimental equipment to be used for collection of spectral signatures was a Bomem FTIR MR-154 spectrometer. This instrument was an upgraded version of the spectrometer deployed for the Radiant Brass 2B test. The upgrade allowed for faster data collection, the use of two simultaneous detectors, and real time video. All three of these

features were utilized for this thesis. This collection system was comprised of two primary components, the spectrometer itself with its associated optics and the data control computer. The spectrometer was placed on a tripod in clear view of the exploding ordnance. Optics on the front of the spectroradiometer, were used to collect source radiation and help control the system field of view. The field of view of the system was approximately a 300 m diameter circle at 4 km. Two detectors, an Indium Antimonide (InSb) and a Mercury, Cadmium, Telluride (HgCdTe) determined radiance information. The deployed instrument is shown in the Figure 1.2:

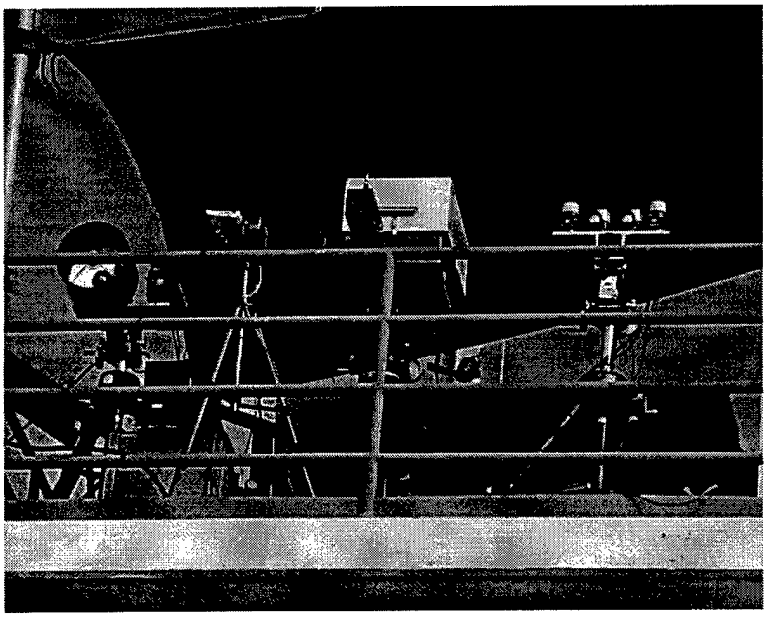

Figure 1.2. Spectroradiometer Deployment

The liquid nitrogen dewer visible on the left side of the FTIR provided a stable cold reference source. The video signal was monitored at the spectroradiometer to improve pointing accuracy.

The data control computer was kept in a separate controlled environment and connected to the spectroradiometer by a serial cable. The video signal was distributed in

the vicinity of the control PC to provide real time images to the PC operator and for permanent record on Hi-8 digital tape. All measured signatures were stored on the control PC after each event. The equipment was calibrated on site with a variable temperature black body.

Collection procedures and data analysis followed the guidelines of the DOD Tactical Missile Signatures (TMS) Measurement Standards Handbook created by the Joint Tactical Missile Signatures (JTAMS) program (1). Onsite collection was subject to the control of the test director and ground collection team leader.

The Bomen *Acquire* software processed the spectral signatures. After proper calibration and data scrubbing the spectrum was outputted in ASCII format. Code was written to further manipulate the data. *Matlab* was chosen as the software analysis tool for its strengths as a vector and matrix operation software as well as its ability to process large amounts of data. *Matlab* code compared integrated FTIR spectral bands with collected radiometric data and overlapped two event time histories by wavenumber bin.

This completes the introduction material for the collection and analysis of conventional ordnance spectral signatures. Chapter II will provide a detailed discussion of FTIR operations, calibration theory, spectral to radiometric conversions, bomb phenomenology and signature variables. Chapter III will discuss the experiment in detail. Processes and analysis performed are presented in chapter IV. Collection results and analysis are examined in chapter V. Finally, chapter VI will formulate conclusions and offer recommendations for future study.

II. Theory

Introduction

Remote sensing is the acquisition of information about an object without physical contact. This information is acquired by detecting and measuring some characteristic of the object. Different object environment interactions can be detected such as emitted electromagnetic spectrum, acoustic vibrations or perturbations in the surrounding gravity field. Various types of information can be sensed from these object environment interactions. Commonly use types of information include spatial, spectral and intensity (7, 1).

This chapter will provide the basic theory needed for a reader not familiar with many remote sensing subjects. The first section will provide an understanding of basic remote sensing principles. The second section will describe the method of information collection, including the FTIR concept of operations, radiance calibration theory and sensor fusion. A review of the sensed object, detonations, will be covered in the bomb phenomenology section. Finally, variables associated with the collection, source and analysis will be discussed.

Infrared Remote Sensing

Electromagnetic energy is the primary method through which information is transmitted from an object to the sensor (7, 22). Spectral information is the frequency dependence of electromagnetic energy. For the present work, the spectrum of interest is the infrared region. This region of the spectrum is especially well suited for detecting ordnance detonations for three reasons. One, the center frequency of spectral emission is

centered in IR region for the afterburn and decay, see Table 1.1. Two, the lifetime of the afterburn and decay features is two to four seconds. This time window is much larger than the nearly instantaneous visual flash of the detonation initiation. Finally, the contrast in emittance between a detonation event and the corresponding IR background is very large. This allows for easier detection.

The spectral background is comprised of emitted and reflected radiation. Figure 2.1 details the background emission sources as well as many commonly used IR terms.

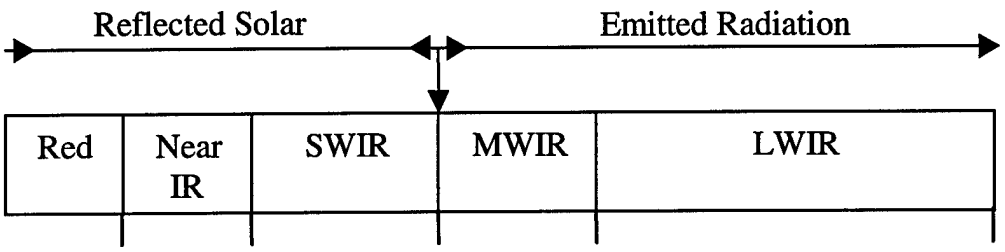

Figure 2.1. IR Spectral Regions [μm (cm^{-1})]

SWIR stands for Short Wave Infrared while MWIR and LWIR are Mid Wave Infrared and Long Wave Infrared respectively. The two background emission sources vary over the course of a day. SWIR is comprised of reflected solar radiation and disappears at night. During the day, the MWIR is a combination of reflected and emitted radiation while at night it is only emitted. The LWIR is always emitted radiation (6, 2-3).

A detonation event, by its nature, is an emitter of radiation. The amount of energy released in a detonation is large. This provides a sharp contrast to the low energy levels of the IR background. Figure 2.2 shows the intensities of the Nevada desert in August versus a detonation event. Each curve is taken within 20 milliseconds. This event was collected at 16 cm^{-1} resolution with the HgCdTe detector.

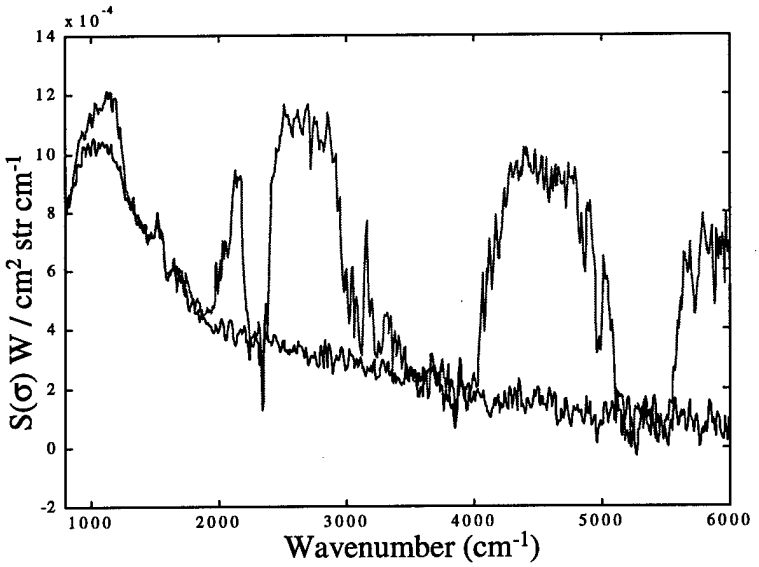

Figure 2.2. Event Background (Purple) and
Detonation Spectrum (Green)

Notice the large amount of emitted background around 1000 cm^{-1} corresponding to the temperature of the desert floor. From this figure it is apparent that the background will need to be subtracted from each source event.

Many texts use wavelength as its unit of length measurement. In spectroscopic discussions, wavenumber is more commonly used. The conversion between wavenumber and wavelength is:

$$\lambda(\mu m) = \left(\frac{10000}{\sigma(cm^{-1})} \right) \tag{2.1}$$

Equation 2.1 makes it easy to covert between one unit of measure and the other. Since the spectroradiometer software outputs all information in cm^{-1}, these units will be used primarily in this thesis. The wavelength to wavenumber conversion is not linear in wavelength. Higher wavenumber equates to lower wavelength so figure 2.2 trends longer wavelength to shorter wavelength, left to right. The wavelength unit of measure, trends in the opposite direction. Some commonly used wavelengths with the corresponding

wavenumber are listed in table 2.1. The terms lower and upper refer to shorter and longer wavelengths respectively.

Table 2.1. Wavelength to Wavenumber Conversion

λ(μm)	cm^{-1}	Notation
1.1	9090	Lower SWIR boundary
1.7	6000.0	Lower boundary of collected spectrum
2.5	3950.0	Lower boundary H_2O absorption
2.9	3425.0	Upper boundary H_2O absorption
3.0	3333.3	SWIR / MWIR breakpoint
4.2	2400.0	Lower boundary CO_2 absorption
4.5	2210.0	Upper boundary CO_2 absorption
4.9	2050.0	Lower boundary H_2O absorption
5.0	2000.0	MWIR / LWIR breakpoint
8.0	1250.0	Upper boundary H_2O absorption
15.2	660.0	Lower boundary CO_2 absorption
20.0	500.0	Upper boundary of collected spectrum

Electromagnetic energy also transports intensity or energy information. A number of quantities are commonly used to describe the energy transport of information. These quantities are summarized in Table 2.2.

Table 2.2. Radiation Quantities (7, 32)

Quantity	Symbol	Units	Equation	Defining Equation
Radiant energy	Q	Joules	N/A	N/A
Radiant energy density	W	$Joule/m^3$	2.2	$W = \frac{dQ}{dV}$
Radiant flux	Φ	Watt	2.3	$\Phi = \frac{dQ}{dt}$
Radiant flux density (Irradiance)	E	$Watt/m^2$	2.4	$E = \frac{d\Phi}{dt}$
Radiant intensity	I	Watt/str	2.5	$I = \frac{d\Phi}{dt}$
Radiance	L	$Watt/m^2$ str	2.6	$L = \left(\frac{dI}{dA}\right) * \cos(\theta)$
Spectral Radiance	S(σ)	Watt/ (cm^2 str cm^{-1})	N/A	Expression for radiance units produced by MR-154

Radiant energy is an important measure in a bomb detonation signature. Total emittance from a detonation event should relate directly to the size of the explosive used. A more detailed description of the spectral and the energy measurement methods performed by the FTIR spectroradiometer will be described in the next section.

Fourier Transform Infrared Spectroscopy Concept of Operation

A Bomem, model MR-154, Fourier Transform Infrared (FTIR) spectroradiometer was the primary piece of collection equipment used to collect detonation signatures for this work. A spectroradiometer collects both spectral and energy information.

Interferometery. The MR-154 uses a Michelson interferometer to create an interferogram of the input signal. Fourier transforming the interferogram creates the spectra. Some spectral detectors use dispersion optics to spatially separate wavelength information. One advantage of the FTIR technique is all frequencies of the input source are falling on the detector at all times. Figure 2.3 details the Michelson Interferometer.

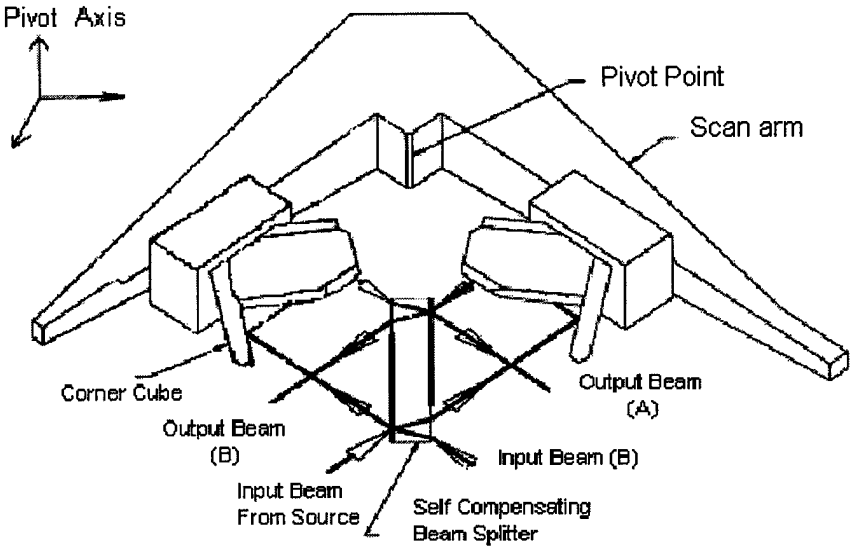

Figure 2.3. MR-154 Scan Arm (2, 2-5)

Prior to becoming the input beam in Figure 2.3, the source energy is gathered by the collection optics and collimated in the collimator optics. Upon striking the beamsplitter, the incident beam is split into two different paths. As the scan arm moves, the optical path length changes between the two beams. The two optical paths are recombined to create constructive and destructive interference patterns based on the differences in the optical path lengths. In general, intensities for all arm positions in both scan directions are added together to get one interferogram. Fourier transforming the interferogram subsequently decomposes intensity information into a spectrum. A more complete description of Fourier transform spectroscopy can be found in many texts such as Interference of Electromagnetic Waves, chapter 5 (4). In normal operations, one scan of the Michelson interferometer is defined as the forward and reverse sweep of the scan arm. In zero scan mode, a scan is only one sweep direction.

The nature of the FTIR collection method provides inherent broadband capability. No optical filtering is used and the spectral bandwidth is dependant on the detector not the system itself. This provides great flexibility as different detectors can be used with different frequency responses. The maximum optical path length difference of the system limits the spectral resolution. Within the system limits, the control computer can make quick resolution changes.

Digitizing of the interferogram requires precise monitoring of the optical path in the interferometer. The MR-154 uses an internal He-Ne laser, 15798 cm^{-1}, to determine the optical path difference feedback for the system (2, 2-6). This laser ensures very stable optical path length measurements.

In the FTIR spectroradiometer, the Michelson interferometer creates the spectral information. To measure intensity, the MR-154 collects data on two different detectors simultaneously. A liquid nitrogen cold reference source is attached to the MR-154 for an accurate cold body reference. Measuring the intensity information is a function of the cold reference source, choice of detector, and most importantly calibration.

Radiometric Calibration. Energy is the second type of information collected by the MR-154. Energy information is only as good as the calibration. Without proper calibration the output of the FTIR is just an electronic response to the source input. Measuring the energy responsivity of a collection system requires the user to create a sequence of known signal levels, and to measure the instrument's response as a function of those signal levels. A known black body source is used to provide the sequence of signal levels. A detailed measurement equation for a blackbody source is equation 2.7 (1,9-15).

$$V_{meas} = A_{opt} A_{bb} \frac{G_{elec}}{R^2} \int L\,(\lambda) Det(\lambda) Tr_{opt}(\lambda) Tr_{filt}(\lambda) Tr_{atm}(\lambda) d\lambda \qquad (2.7)$$

where

A_{opt} = area of instrument optical aperture
A_{bb} = area of blackbody emitter
R = distance from calibration source to instrument
$L_\lambda(\lambda)$ = blackbody spectral radiance W/cm^2 sr cm^{-1}
$Det(\lambda)$ = detector wavelength dependent power responsivity
$Tr_{opt}(\lambda)$ = instrument optics wavelength dependent transmission
$Tr_{filt}(\lambda)$ = spectral filter transmission
$Tr_{atm}(\lambda)$ = atmospheric transmission
G_{elec} = electronic gain

Equation 2.7 relates primarily to a radiometric measurement. Since a spectroradiometer collects energy information as a function of wavenumber (σ) a more appropriate equation is equation 2.8.

$$S_{meas}(\sigma) = A_{opt}A_{bb}\frac{G_{elec}}{R^2}[L(\sigma)Det(\sigma)Tr_{opt}(\sigma)Tr_{filter}(\sigma)Tr_{atm}(\sigma)] \quad (2.8)$$

This equation is valid because all spectroradiometer measurements are functions of wavenumber and the sampling bin size. The MR-154 has no filter so $Tr_{filt}(\lambda)$ can be neglected. All system wavenumber dependant terms, $Det(\sigma)$ and $Tr_{opt}(\sigma)$, as well as A_{opt} and G_{elec} can be grouped into one on term $K(\sigma)$. With these manipulations you get:

$$S_{meas}(\sigma) = \frac{A_{bb}}{R^2}K(\sigma)[L(\sigma)Tr_{atm}(\sigma)] \quad (2.9)$$

Further assume the transmission losses due to the atmosphere are negligible due to the short distances during a calibration and $Tr_{atm}(\sigma)$ disappears. For a calibration sequence the A_{bb}/R^2 is constant and can be combined into $K(\sigma)$. Lastly, when the event or calibration does not completely fill the system field of view, $L(\sigma)$ can be expanded to:

$$S_{Meas}(\sigma) = K(\sigma)[L_{bb}(\sigma) + L_{back}(\sigma) + M^{Stray}(\sigma)] \quad (2.10)$$

where

$L_{bb}(\sigma)$ = black body source radiance
$L_{back}(\sigma)$ = source background radiance
$M^{Stray}(\sigma)$ = system stray radiance term

The units of $S_{Meas}(\sigma)$ in Equation 2.10 is W/cm^2 str cm^{-1}.

To eliminate the source background, two measurements are taken at each calibration reference temperature, a source plus background and a background. These two reference measurements are subtracted to eliminate $L_{back}(\sigma)$. Theoretically, this leaves only the contribution of the black body (bb) source in the S, L, and M quantities. Once $L_{back}(\sigma)$ is subtracted, the equation becomes:

$$S_{bb}(\sigma) = K(\sigma)(L_{bb}(\sigma) + M^{Stray}(\sigma)) \quad (2.11)$$

A proper calibration procedure requires collection of a minimum of two reference temperatures, commonly called hot (H) and cold (C). With these two background subtracted reference measurements, $M^{stray}(\sigma)$ and $K(\sigma)$ are found by equations:

$$K(\sigma) = \frac{S_H(\sigma) - S_L(\sigma)}{L_H(\sigma) - L_L(\sigma)} \tag{2.12}$$

$$M^{Stray}(\sigma) = \frac{L_H(\sigma)S_C(\sigma) - L_L(\sigma)S_H(\sigma)}{S_H^s(\sigma) - S_C^{Meas}(\sigma)} \tag{2.13}$$

Once $M^{stray}(\sigma)$ and $K(\sigma)$ are determined, the equation to calibrate successive measurements is (2, 2-30):

$$S^{Calibrated}(\sigma) = S_{Meas}(\sigma)K^{-1}(\sigma) - M^{Stray}(\sigma) \tag{2.14}$$

Equation 2.14 is essentially a mathematic correction applied to a 'sensed' unknown signal. This calibration is only valid if all operating parameters of the system remain constant between reference point acquisition and the unknown measurement. Since the MR-154 collects data on both sweep directions of the interferometer, two sets of calibration constants are created.

The uncertainty in calibration is due to many error sources. These error sources include reference source errors, calibration drift, systems errors and intrinsic linearity. Calibration errors are a separate issue from measurement errors. Field calibration uncertainties should fall within 2 to 5 percent and field measurement uncertainties should be 5 to 20 percent (1, 9-10).

Intrinsic linearity is a big assumption in Equation 2.14. This requires linearity in the system and detector. For the large radiance and spectral range required to measure a detonation event, linearity in the InSb detector is a valid assumption. For the HgCdTe

detector a quadric calibration is more appropriate. The details of a quadratic calibration can be found in the users manual (3, 109-111).

Measurement Process. A properly deployed and well-calibrated system provides useful, accurate measurements of the emissions from an unknown source. A discussion of the software architecture used to collect and process measurements is required. The process has two steps, calibration and unknown acquisition.

The Bomem *Acquire* software package controls the Bomem MR-154. In general, one interferogram is collected using the forward and reverse scans of the Michelson interferometer. Each measurement is a number of interferograms averaged together. The number of interferograms to average is selectable by software. *Acquire* also controls what spectral range each detector will collect, how many successive measurements will be collected, and the time interval between measurements.

To produce a measurement, the first step is to complete the calibration process. At least two radiometric reference points must be collected. The cold and hot reference points should straddle the anticipated unknown temperature. In *Acquire*, each reference point has the same user selectable variables as a measurement. Once Equation 2.14 is applied to the appropriate reference points, a radiometric correction file is created. This process is detailed in the left half of Figure 2.4.

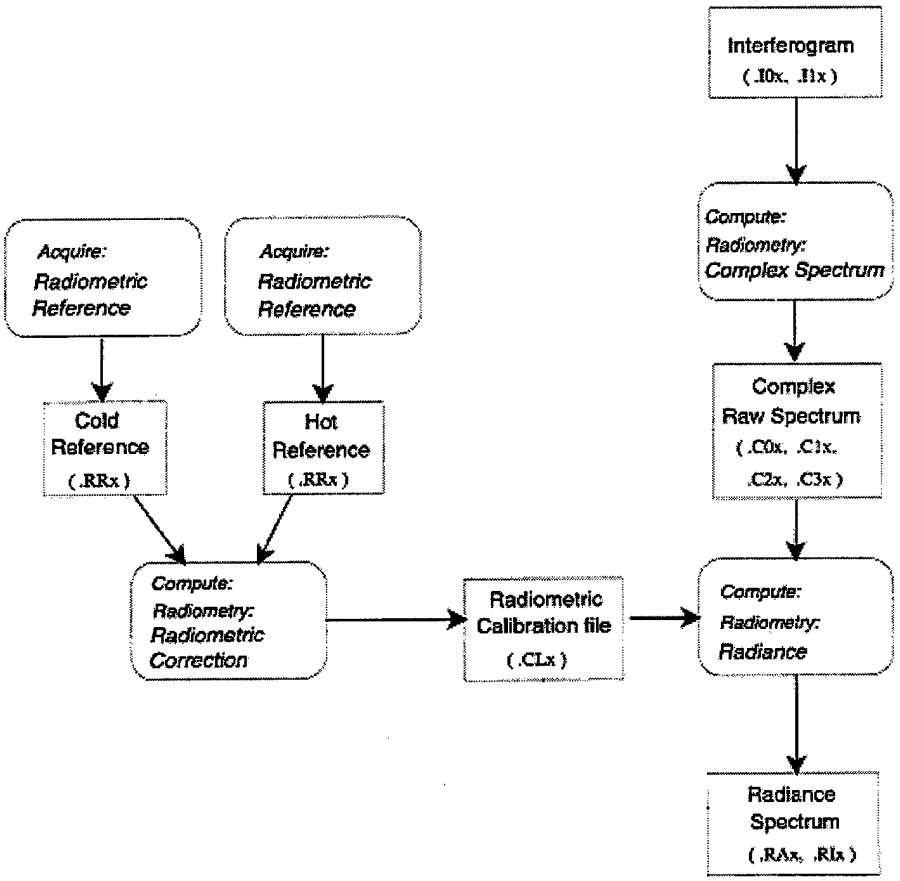

Figure 2.4. Software Measurement Process (3, 7)

The second step is to collect a measurement from an unknown source. This is accomplished directly in the Acquire software program. The spectral range, number of scans to average as a measurement, and number of measurements is input into *Acquire*. The system collects the event data and *Acquire* outputs an interferogram file. To process the interferogram, a cosine apodization function is applied. This corrected interferogram is transformed via a fast Fourier transform (FFT), to create a complex raw spectrum file. Applying the radiometric calibration file to the complex raw spectrum file creates the final radiance measurement.

Each block in Figure 2.4 that contains a bracketed quantity represents a specific output file from the *Acquire* software. The bracketed quantities refer to the file extension attached to a user-defined filename. A 'x' refers to the detector position, A or B, which is being processed. The *Acquire* software also provides limited data manipulation functions. An example of these functions is the background subtraction.

Sensor Fusion, Spectral to Radiometric Conversion

Sensor fusion is a nebulous term relating to using information from multiple sensors to more completely describe an event. For this work, sensor fusion is the comparison of the Wyle Labaratory's radiometric data to the MR-154 data (9). Comparing different ground truth team's data is an objective method of determining the validity of collected data. This follows the Joint Tactical Missile Signature procedures outlined further in Chapter III. This section will detail the theory used to compare two different collection instruments with dissimilar measurement techniques.

To start with, a radiometer collection platform normally uses a photovoltaic or photoconductive detector to collect energy. It continuously measures energy over the appropriate frequency range of the detector. A filter is used to limit the spectral range to a specific band. In Equation 2.7, $Tr_{filt}(\lambda)$ becomes important. Also, a radiometer does not discriminate where in the filter pass band the energy comes from. Its output is an integration of all energy in the filter band received at the detector in a time collection interval. In general, radiometric collection platforms collect data at faster rates than a spectroradiometer and therefore have better temporal resolution.

The Radiant Brass program required reporting of certain frequency bands in units of apparent intensity, W/ str μm. This is quite different than the units of W/cm^2 str cm^{-1}

outputted by the Bomem MR-154. To accomplish this comparison, the first assumption is the source being measured is a Lambertian disk. The radiant flux of a Lambertian source on the collector is derived by:

$$E(\sigma) = \pi L_{source} \sin^2(\theta) \tag{2.15}$$

for z >> r, let:

$$\sin^2(\theta) \approx \frac{r^2}{r^2 + z^2} \tag{2.16}$$

$$\Phi(\sigma) = \pi L_{source} A_{opt} \, r^2 \Big/ r^2 + z^2 \tag{2.17}$$

where all values are in cm.

r = radius of source
z = distance from source to collection optics
θ = angle between source and optics

Equation 2.16 represents a small angle approximation. This is valid for all collection geometries. Equation 2.17 gives the energy collected by the detector, neglecting system effects. The source emittance is assumed to be a plane wave by the time it reaches the collection optics. Neglecting M_{stray} and expanding $K(\sigma)$ from Equation 2.11 yields:

$$S_1(\sigma) = K_{cal}(\sigma) A_{opt} \pi \frac{r_1^2}{r_1^2 + z_1^2} L_1(\sigma) \tag{2.18}$$

$S_1(\sigma)$ provides a calibrated measurement of the source $L_1(\sigma)$. In equation 2.18, πr_1^2 is the source area A_1 and $r_1^2 + z_1^2 \approx z_1^2$ when z >> r. If $S_1(\sigma)$ is a blackbody measurement and the aperture size is increased for a second measurement, $L_1(\sigma)$ is constant but $S_2(\sigma)$ will increase due to the larger area of source. By comparing two

measurements in the form of Equation 2.18, the relationships 2.21 through 2.22 are derived. Let:

$$\Omega_n = \pi r \frac{r_n^2}{r_n^2 + z_n^2} = \frac{A_n}{z_n^2} \tag{2.19}$$

$$K_n(\sigma) = K_{cal}(\sigma) A_{opt} \Omega_n \tag{2.20}$$

Then:

$$\frac{K_1(\sigma)}{\Omega_1} = \frac{K_2(\sigma)}{\Omega_2} \tag{2.21}$$

$$S_2(\sigma) = S_1(\sigma) \frac{\Omega_2}{\Omega_1} \tag{2.22}$$

Equation 2.20 provides a method of accounting for the difference in the size of the source Lambertian disk by using the ratios of the areas of the sources and the distances to the source.

Moving back to intensity, the general form for converting radiance to intensity is:

$$I = \int L_1 A_1 d\sigma \tag{2.23}$$

By neglecting $M_{stray}(\sigma)$ in equation 2.11, the following relationship is derived for a calibrated measurement.

$$I(\sigma) = S_1(\sigma) \frac{A_1}{K_1(\sigma)} \tag{2.24}$$

Take two measurements, a detonation event and the calibration reference point, and apply the relationships in 2.19 – 2.22 provides:

$$I(\sigma) = S_{bomb}(\sigma) \frac{A_{bomb}}{K_{cal} \frac{\Omega_{bomb}}{\Omega_{cal}}} \tag{2.25}$$

$$I(\sigma) = S_{bomb}(\sigma)\frac{A_{cal}z_{bomb}^2}{z_{cal}^2} \tag{2.26}$$

Equation 2.26 determines the apparent intensity of the source in W/str cm^{-1} based on a calibrated measurement and a scaling factor relating A_{cal}, z_{bomb} and z_{cal}. This result greatly simplifies calculations as accounting for the time varying area of the detonation event is no longer a factor in calculating the apparent intensity. To finish the sensor fusion, a simple summation of energy in the proper filter band and conversion of cm^{-1} to μm is all that is required to convert the calibrated spectral signature to units of W/str μm. This technique is limited to the following conditions; distances z_1 and z_2 are known, both sources can be considered Lambertion, both sources are smaller than the FOV of the system, and no changes to the collection system are made between calibration and the measurements.

Bomb Phenomenology

Explosions were previously described as mechanistically complex. This section discusses bomb phenomenology by describing the explosive material, explosion dynamics and characteristic equilibrium equations for two explosives. This description is primarily based on Cooper's text, chapters 2, 3 and 7.

Most explosives consist of carbon, hydrogen, nitrogen, and oxygen. These elements form the organic compounds that become the explosive. Two common examples of explosives are cyclotrimethylene-trinitramine or cyclonite (RDX) and trinitrotoluene (TNT). These organic compounds are commonly described by the schematics in Figure 2.4.

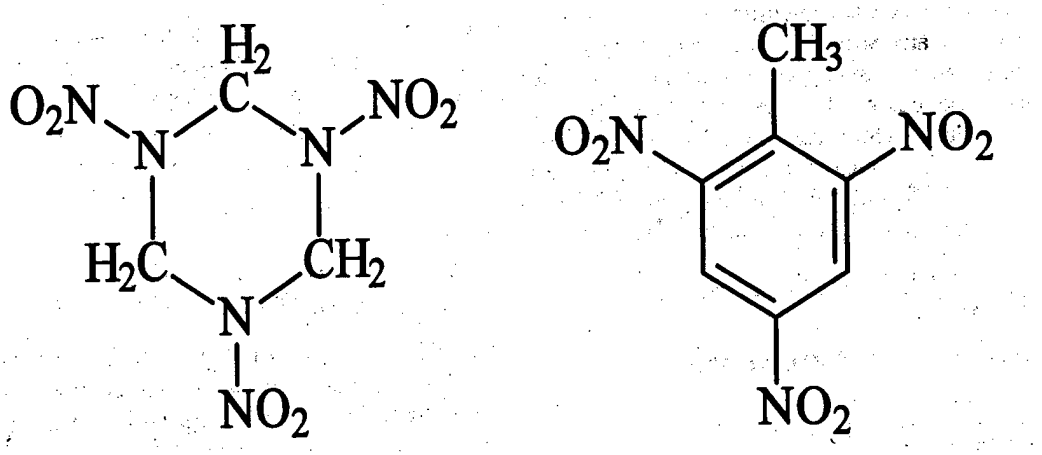

Figure 2.4. RDX (left) and TNT (right) (5, 23)

The first phase of an explosion is the detonation. In a simplistic discussion, the explosion is some fusing event. This initial fusing event breaks the chemical bonds holding the explosive together. The explosive fragments are contained in the bomb casing and form a gaseous mixture. This gaseous mixture contains both fuels (C or CH_2) and oxidizers (O or NO_2). The oxidizers react or burn the fuels releasing vast amounts of energy in the form of heat. This heating increases the temperature and pressure of the gaseous mixture to extremely high pressures. This high pressure ruptures the bomb casing and the burning explosive fragments are dispersed into a detonation zone. This detonation zone expands until equilibrium pressure is reached with the surrounding environment. This gaseous expansion starts the pressure pulse that emanates outward from the center of the explosion.

The global reactions involved in the oxidation of RDX is given by:

$$C_3H_6\ N_6O_6 \rightarrow 3N_2 + 3H_2O + 3CO + \Delta H_{DRDX} \qquad (2.26)$$

where ΔH_{DRDX} is the heat of detonation for RDX, 335.4 kcal/g mole (5,132).

The global reaction for TNT is given by equation 2.27.

$$C_7H_5N_3O_6 \rightarrow 1.5N_2 + 2.5H_2O + 3.5CO + 3.5C + \Delta H_{DTNT} \quad (2.27)$$

In this equation, ΔH_{DTNT} is the heat of detonation for TNT, 247.5 kcal/g mole (5,132). The actual oxidation process is much more complex than what is provided in equations 2.26 and 2.27. According to explosive models supplied by William Miller, over 150 molecules are involved in the detonation reactions (18).

After the detonation reaches equilibrium pressure with the surrounding atmosphere, the explosive fragments as well as explosive binder are distributed throughout this equilibrium zone. The fuels not fully oxidized, mix with oxygen in the air and continue to burn. The primary fuels are the residual CO and C left over in the global equations 2.26 or 2.27. This secondary oxidization is commonly called the afterburn.

This secondary reaction can be very energetic. The afterburn of TNT is primarily from the reactions of:

$$3.5CO + 3.5C + 5.25O_2 \rightarrow 7CO_2 + \Delta H_R \quad (2.28)$$

where ΔH_R is the heat of the reaction, 566 kcal/g mole. The heat generated from the reactions in equation 2.28 produce twice the heat liberated from the detonation itself (5, 133). This large amount of heat is distributed over a much greater and less dense volume, therefore the temperature of this volume doesn't necessarily increase.

Variables

Detonation events are extremely variable. The variability 'sensed' in a measured detonation event is a conglomeration of many factors. These factors will be grouped into three categories, source, collection and processing. Some factors are independent where other factors are dependant, but all factors are additive making the problem of

identification a difficult one. For every good experimental thesis, great pains are taken to create a test environment where all but a few variables are controlled. Achieving this is much more difficult when studying field detonations. Good collection methodology and test program planning can only reduce the number of variables and amount of uncertainty for each event. Table 2.3 is a compiled list of variables.

Test planning and collection methodology will attempt to control or at least quantify as many variables as possible. This discussion is detailed in the next chapter. One variable that warrants further discussion is atmospheric absorption.

Table 2.3. Variables in a Detonation Event.

Source	**Collection**	**Processing**
Atmospheric conditions and distance to event	Azimuth Look Angle between bomb axis and collection	Time averaging windows
Static versus dynamic deployment	Elevation angle of collection to event	Background subtraction
Explosive type	System noise	Zero reference level loss
Amount of explosive	Temporal resolution of Instrument	'Ringing' in FFT
Ordnance case tolerance	Spectral resolution of instrument	Signal aliasing
Fusing mechanism	Field of view of instrument	Calculation rounding
Target interaction	Calibration Uncertainties	Down sampling techniques
Orientation of the explosive	Measurement Uncertainties	Interpolation methods
Manner of bomb release	Changing collection environment	
Angle which bomb enters the ground		
Depth of penetration of explosive		

Any time electromagnetic energy propagates through the atmosphere it is affected by atmospheric absorption and scattering. The atmosphere is comprised of many different molecules. Each molecule will absorb different frequencies of electromagnetic

radiation due to quantum mechanical interactions. These quantum mechanical interactions include electronic, vibrational and rotational modes of the molecule. Due to the energy levels associated with IR radiation, electronic transitions are not prevalent. The vibrational and rotational modes are the strong absorbing mechanisms. A more detailed description of vibrational and rotational absorption modes can be found in Fundamentals of Molecular Spectroscopy, by Struve. The molecules that absorb electromagnetic radiation in the IR spectrum include H_20, CO_2, and O_3. Figure 2.6 summarizes the typical atmospheric absorption present in the atmosphere.

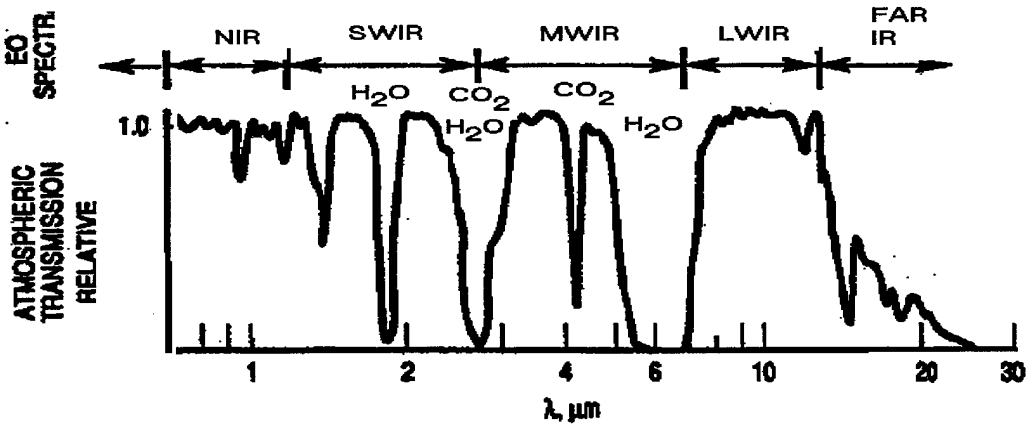

Figure 2.6. Molecules and Absorption (19, 67)

Notice H_20 and CO_2 have many absorption bands. Each large band is related to a vibrational mode. The width of the absorption is due to the rotational modes. An O_3 absorption spectrum around 10 μm is not included in this figure. This absorption feature of O_3 is only found in large concentrations around 100 km in altitude. All optical paths for this work were parallel to the earth's surface and O_3 absorption is negligible.

Concentrations of H_20, CO_2, and O_3 are dependent on atmospheric conditions. These change from day to day. The amount of absorption is a function of the concentration of particulate matter and the distance to the source. Atmospheric

absorption is commonly described with a transmission coefficient between zero and one. A coefficient of one means no attenuation and coefficients near zero are totally attenuated. Figure 2.7 is an example of transmission coefficients the night of Oct 26, 1999 at NAS Fallon Bravo 20, Nevada.

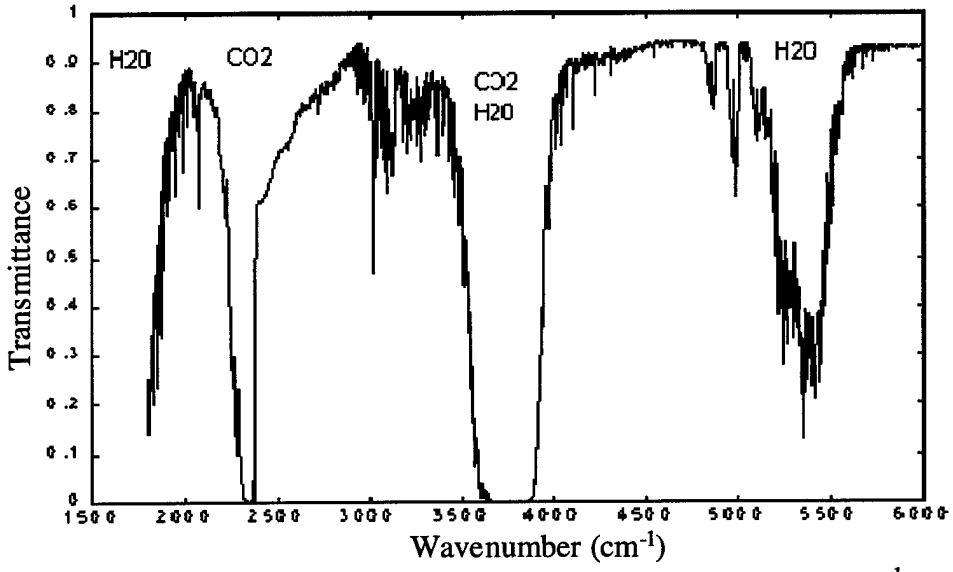

Figure 2.7. Transmission Coefficients for 2500 Meters [x axis cm^{-1}]

The primary absorption molecules are identified in this figure. The coefficients used in Figure 2.7 were calculated using MODTRAN code based on weather condition present during actual testing.

The total attenuation of the atmosphere is a combination of absorption and scattering. Particulates in the atmosphere with radii between .1 and 10 μm have the ability to obscure visibility in the visual, NIR, and SWIR regions (7, 279). The amount of scattering is based on the particulates cross-sectional area and the frequency of the source radiation. Clouds, smoke, and dust particles are examples of these particulates.

III. Experiment

Introduction

The field collection of detonation events is a taxing experiment. Besides the variables discussed in chapter one, each event's energy and spectrum vary over its lifetime. The environment of the collection equipment is dictated by mother nature and can vary over the course of the collection period. Finally, the turn around time between some air dropped events is less than four minutes -- providing little time for trouble shooting equipment errors. To mitigate these variables, the Radiant Brass program followed the Tactical Missile Signature (TMS) procedures to provide optimum control over the test experiment.

This chapter describes the experiment in detail. The discussion starts with a brief description of the relevant TMS processes. Experiment collection tradeoffs are addressed. Two experiments were conducted with different assumptions and variables. Due to the differences in each experiment, they are described separately. The subjects covered for each experiment include: test objectives, test organization, and equipment deployment.

Radiant Brass and TMS Methodology

The Tactical Missile Signatures process described by Augustine is a DOD standard as well as a guidance tool for planning, executing, collecting and reporting missile signatures. It is primarily focused on the collection of infrared and ultraviolet spectra. An ordnance signature is similar in many ways to a missile rocket plume. The test director for the Radiant Brass Program followed TMS guidelines.

While deployed on site, AFIT collection was subject to the decisions of the test director, test coordinator, chief scientist and ground truth deployment team leader. These individuals were in charge of logistics, communications, data quality and overall test objectives. Communications between the Naval Strike and Air Warfare Center (NSAWC) personal, Explosive Ordnance Disposal teams (EOD), safety officials, and ground collection teams, commonly called ground truth teams, were a vital role of these officials.

The TMS process provides guidelines for anyone responsible for collection, analysis and reporting of ground truth data. The TMS process divides experiment planning and execution into three phases; pretest, on-site and posttest activities. "Pretest analysis activities are primarily for planning purposes. On-site analysis activities are oriented toward data quality assurance. Posttest activities extract information from the data" (1, 8-5).

Pretest activities focused on data analysis and signal prediction. A primary area of concern in this phase was how to configure the MR-154 to avoid detector saturation. From previous data, it was determined the size of a detonation event at 4750 m was approximately the same size as a .2" aperture at 70". At these settings, the MR-154 collected measurements from a 1000°C black body to establish the detector gain configurations that avoided saturation. Five user selectable gains (A-E) exist on the MR-154. The detector gains were determined to be C for the HgCdTe and B for the InSb. The position of the detectors was also fixed as the transmission losses in the MR-154 differ by detector position. Another decision from pretest analysis was to have the calibration configuration simulate the event explosion. The chosen configuration was a

0.2" aperture at approximately 70" with temperature reference points of 700°C and 900°C. A medium FOV Bomem optics, model SMY04, was acquired to eliminate FOV issues present in RB2B data.

The final pretest activity was range safety certification training. No one was allowed on a Fallon Training Complex without safety training. Daily pre and post deployment safety briefings were required.

The TMS on-site procedures include irradiance predictions, calibration checks, common source analysis, quick look assessments and data storage inspection. The on-site procedures are discussed in the next chapter, Experimental Procedures and Analysis.

TMS posttest analysis includes calibration, data reduction, comparison with theoretical models or other collected data sources and formal reporting. Routine posttest procedures are described in the next chapter. Sensor fusion results are contained in chapter V while formal reporting is completed by this document.

Collection Tradeoffs

Throughout chapters one and two, collection tradeoffs were mentioned. These tradeoffs affect the collection methodology and final data products. Tradeoffs are an extension of TMS pretest objectives. The most important collection tradeoff is spectral resolution versus temporal resolution. The choice of spectral resolution, detector ranges and quantities of detectors affects temporal resolution. Since little spectral information was viable from previous Radiant Brass tests, the primary collection focus was to measure the largest spectral range possible without compromising temporal resolution. This is not a simple goal as spectral and temporal resolutions are inversely proportional.

The final configuration of the collection equipment was chosen to use both detectors to maximize spectral range of the collected event signature. The spectral range of the HgCdTe was set to be 500 to 6000 cm^{-1} and the InSb, 1800 to 6000 cm^{-1}. To offset the decrease in time resolution caused by dual detectors, all event measurements were taken in zero scan mode utilizing only one sweep direction of the Michelson Interferometer. These two decisions temporally offset each other. Finally, events were to be collected at 16 cm^{-1} with 0.047-second resolution until sufficient quantity of events were successfully collected for each set of test conditions. Spectral resolution could then be increased to 4 cm^{-1} with 0.245-second resolution.

The spectral range collected covers most of the SWIR, the MWIR and LWIR regions to include the 8-12 μm atmospheric pass band. In the collection configuration both detectors have some overlap in spectral range for comparison between detectors. The choice to use primarily 16 cm^{-1} resolution allowed the greatest consistency with data collected from Radiant Brass 2A and 2B tests.

Radiant Brass 3A

Test Description. The RB3A test was conducted at the Fallon Range Training Complex, Range Bravo 20, over the period 2-5 August 1999. This test range is located approximately 35 miles north-northeast of Fallon Nevada. Bravo 20 is a dry lakebed at 4,000 ft above sea level. Two towers are located on Bravo 20 with full electrical power to facilitate collection equipment. From the third floor balcony and roof of the west tower, an unobstructed view is possible in all directions. The tower and unobstructed view is shown in Figures 3.1 and 3.2:

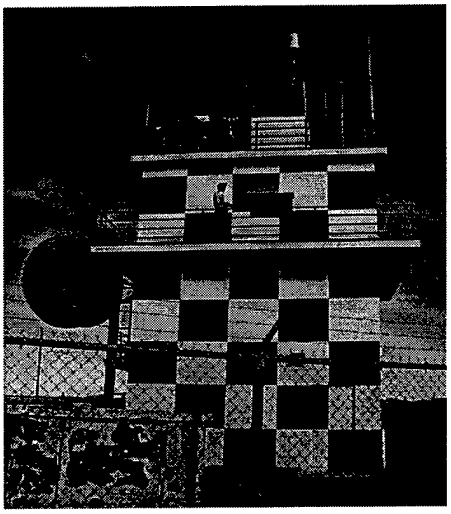

Figure 3.1. West Tower

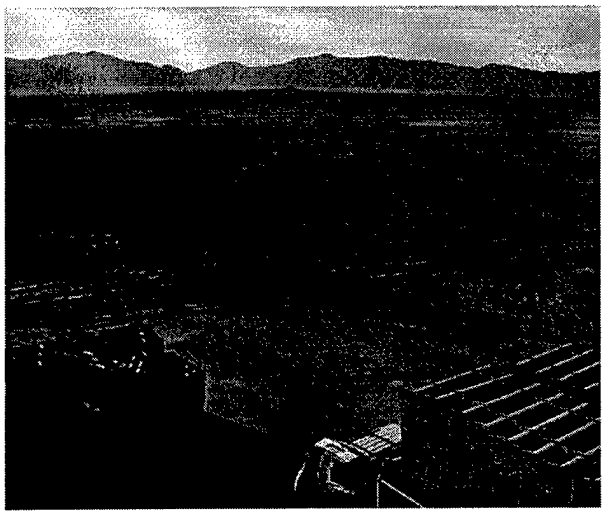

Figure 3.2. Unobstructed View of Target Area

The instruments can be seen under the tarp on the roof of the tower in Figure 3.1. The primary target area is Lone Rock, the dark colored outcropping feature seen centered on the top of Figure 3.2.

The primary purpose of the test was to collect munitions signatures deployed in normal operational configurations against ground targets. The ordnance was delivered by F-18's supported by the Naval Strike and Air Warfare Center (NSAWC) personnel. Naval Pacific Meteorology and Oceanography Detachment (NPMOD) provided meteorological support. The NSAWC pilots recorded aircraft attitude parameters at ordnance release so that vector impact dynamics could be calculated with the Joint Munitions Effectiveness Manual Model (JMEM). Prior test analysis provided indication that the observed event signatures may depend on the observers look angle with respect to bomb axis and/or the bomb target interaction with the ground surface (Miller RB3A).

The test was three days in length. Each day had 14 events scheduled. The target and thus the projected impact surface remained constant all three days. Two ground truth

teams were positioned in the West Tower of Bravo 20, Wyle Labs and AFIT. The distance to the target from the tower was 4825 m. The primary test variable that was altered was the angle between collector observation and bomb impact vector. The approximate F-18 run in vector on day one was 155° or directly away from the West tower, day two was 355° degrees or towards the West Tower and day three was 65° or perpendicular to collector boresight. The target for the F-18s is the square between Lone Rock and the sand dunes. The approximate F-18 aircraft vector is displaced from the actual target for clarity. The test layout for RB3A and RB3B is provided in Figure 3.3.

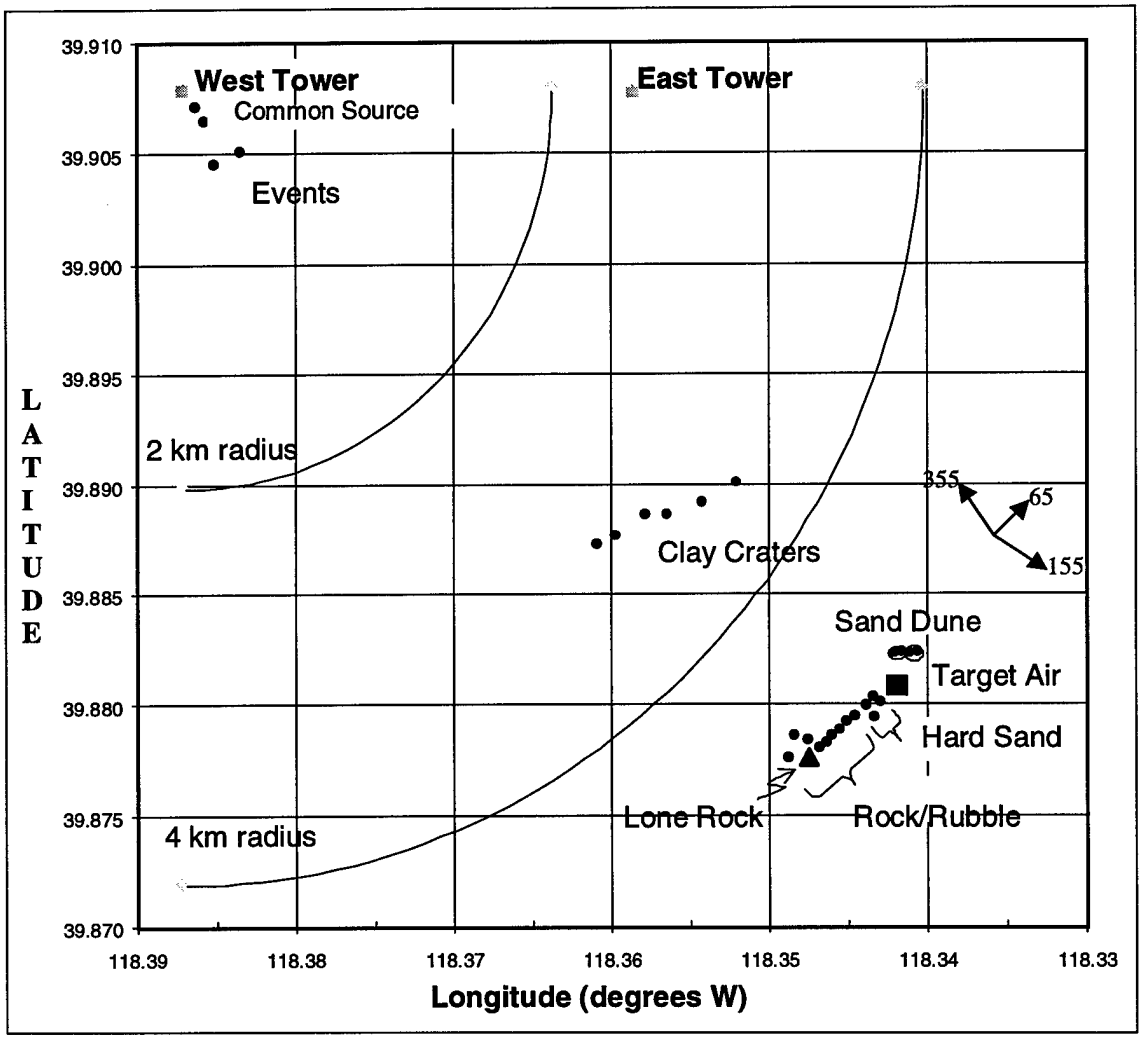

Figure 3.3. RB3A and RB3B Test Layout (17, 9)

Each day the scheduled events varied by aircraft heading, amount of explosive and explosive type. Ordnance was quantified by four amounts of explosive; extra small, small, medium, or large. Extra small is defined as less than 100 lbs, small is 100-400 lbs, medium is 400 to 600 lbs, and large is greater than 600 lbs of explosive. A complete description of collected events and conditions are provided later in this chapter. The types of explosives used are shown in Table 3.1.

Table 3.1 – TNT Weight Ratios (Multipliers) for Explosive Materials (17, 5)

Name	Composition	Peak Pressure	Impulse Pressure
C-4	RDX – 91%, Placticizer – 9%	1.37	1.09
H-6	RDX – 45.1%, TNT – 29.2%, Aluminum – 21%, Wax – 4.7%	1.38	1.15
RDX	Cyclotrimethylene-trinitramine	1.19	1.16
Tritonal	TNT – 80%, Aluminum – 20%	1.07	.96
Source of information: NAVY EODB 60A-1-1-4. *Technical Manual, Explosive Ordnance Disposal Procedures, Protection of Personnel & Property*, Revision 3, 11 April 1998.			

Equipment deployment. The equipment deployment followed the experiment approach detailed in Chapter I. The Bomem MR-154 was configured as described in the tradeoff section and pretest analysis. The HgCdTe was placed in detector position A and InSb in B. The cold reference source was connected in its appropriate position. The proper resolution was selected by rotary switch on the side of the MR-154. The temperature controller was set to 44°C, regulating the operational temperature of the MR-154 above expected ambient conditions. This was to mitigate measurement errors by minimizing the temperature changes of the system. Once the MR-154 was stabilized at 44°C, the system was reset to establish a new zero point reference. All aperture stops were set to 6.4 mm, the widest possible FOV.

The detector gains were set at C for the HgCdTe and B for the InSb as determined in pretest analysis. The detector gain is an electronic amplification of the detector-sensed intensity. The gain can be varied from A- E.

The cold reference source and the two detectors were cooled with liquid nitrogen. This regulates the temperatures to 77°K for optimum sensitivity. The liquid nitrogen levels were monitored between each event and filled at least every two hours.

The Bomem model SMY04 optics were attached to the collimator, secured by 3 screws, and focused at infinity to collect source radiation. The FOV of the SMYO4 was 74 milliradians or a 360 m diameter FOV at the target point. This leads to approximately a 120 m drop error radius perpendicular to bore sight. The FOV was bore sighted using real-time video.

Real-time video was recorded for each event. This video provided a means of determining if the event was in the spectroradiometer FOV. The video cable was attached to the input collimator of the MR-154. A custom cable connected the spectroradiometer to the camera control unit. RG-59 cable connected the camera control unit to the video display unit located on the roof. RG-59 cable connected the video display unit to the Sony Model EVO-9850 Hi-8 recorder located on the third floor. A Xybion UED100 video encoder superimposed the GPS time on the video.

The spectroradiometer was secured to its tripod and placed on the third floor roof of the West tower in clear view of the target. A tarp was place over the top of all equipment to eliminate most of the direct desert sunlight. A 100 ft serial cable connected the MR-154 to the control personal computer (PC) located on the third floor of the tower. The spectroradiometer and control PC setups are displayed in Figures 3.4 and 3.5.

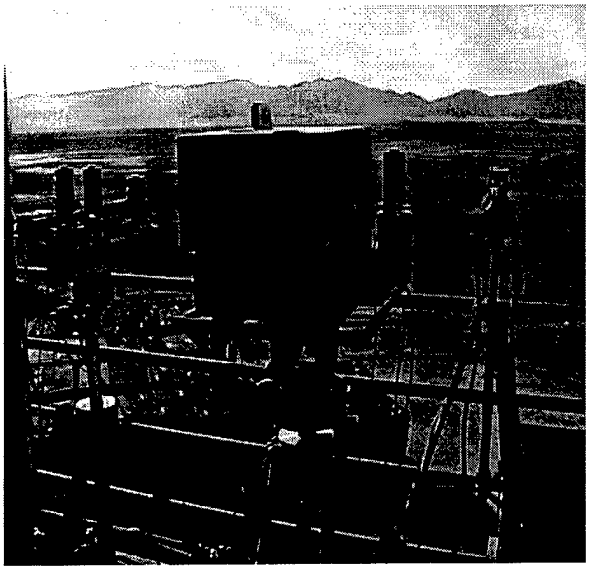

Figure 3.4. Spectroradiometer Deployment

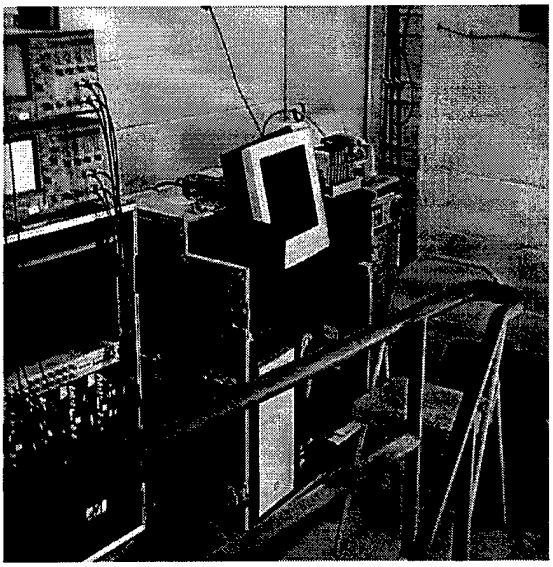

Figure 3.5. Control PC Deployment

The control PC was deployed with a Bomem, 128 megabyte, data acquisition card to receive continuously receive data from the MR-154. Two Bomem software packages were loaded to facilitate collection and quick look analysis, *Acquire* and *Grams*. The control PC was equipped with an AMD 450 Mhz processor and 128 Mbytes of random access memory. A color printer was deployed to provide graphical outputs for the test director and chief scientist. To utilize the Wyle CD read/writer, the PC was networked to two Wyle control PCs.

Two blackbodies were used as calibration sources. Each blackbody was set up on its own tripod on the roof of the West Tower and located 67 inches from the front of the spectroradiometer optics. Both blackbodies were leveled and the center of the blackbody aperture was aligned to the center of the SMY04 aperture. Blackbody one was positioned near the edge of the tower and blackbody two was located near the roof access door. A clear view of the relative position of blackbody one is provided by Figure 3.6.

Figure 3.6. Blackbody One Deployment

All blackbodies used had calibration certificates within the last 1.5 years. The spectroradiometer and associated detectors and camera units were brand new and had been verified by Bomem prior to shipment to the Air Force Institute of Technology in March of 1999. This deployment was the first major use of the MR-154 and associated equipment. A summary of equipment used by model and serial number is provided in Table 3.2.

Table 3.2. Equipment Information

Description	Make	Model	Serial Number
Spectroradiometer	Bomem	MR-154	74005
Camera Control Unit	Elmo	CC421E	162718
Video Display Unit	JVC	TM-550U	11334132
InSb Detector	Cincinnati Electronics	IOH1137	827-I153
HgCdTe Detector	Bomem	SPH37006	6199
Cold Reference Source	Bomem	SMA19006	SMA19017
Control PC	Gateway	AMD 450 Mhz	9706327
GPS Receiver	True Time	560-5900	N/A
Hi-8 Video Recorder	Sony	EVO-9850	N/A
Blackbody Three	Electro Optics	LS1050-1001/AM	4106

Radiant Brass 3B

Test Description. The RP3B test was also conducted at the Fallon Range Training Complex over the period of 25-29 October 1999. The primary test objectives remained the same as all previous Radiant Brass tests. The secondary objective of this series of tests was to determine the repeatability of detonation events and to recreate a static equivalent of the zero degree aircraft run-in vector from Radiant Brass 3A.

NSAWC provided planning, logistics, and operations support for this test. NPMOD provided meteorological data. The NAS Fallon EOD detachment provided ordnance and range support. Four different ground truth teams were deployed to the West tower for this test. Wyle Labs/DXDO was the primary collection team and had priority over all space and team functions. Air Force Research Labs from Hanscom AFB deployed a spectral device, Patrick AFB deployed a radiometric suite, and AFIT deployed the Bomem MR-154 spectroradiometer.

This test comprised of 23 statically detonated events over the course of two nights. The schedule and quantity of detonation events was modified from the original plan due to two nights of inclement weather. Three different explosive types and three different explosive amounts were used during this test. The test layout is provided in figure 3.3. To simulate the air-dropped configurations from RB3A, the ordnance was situated on solid ground and propped up on wooden tripods at a 45 degree elevation angle tail high. Each bomb face was pointed toward the West Tower. The larger bombs were placed in clay craters tail high at the largest elevations possible. A complete description of all events and conditions are provided in Appendix A.

Equipment Deployment. In general the equipment configuration was the same for this test as previously described in the RB3A deployment. Only the items that are different will be discussed here. The MR-154 set up was similar with the following exception; the temperature controller was set to 33°C, as the temperature outside was approximately 40°F.

Only one blackbody source was used for this test. Blackbody three was placed on its tripod and positioned 76 inches from the front of the MR-154 optics. This blackbody was brand new and had calibration certificates dated October 1999.

IV. Experiment Procedures and Analysis Methods

Introduction

This chapter describes the procedures followed in collecting and processing event signatures. Analysis methods applied to the processed signatures are also discussed. First, calibration and measurement collection procedures are described for both the Radiant Brass 3A and 3B tests. Posttest procedures used to manipulate each signature into usable radiance information are detailed. Next, features of the collected data and methods of analysis are discussed in the tradeoff section. The concept, application and uncertainties of the temporal overlap analysis are presented. Lastly, the procedures followed to provide sensor fusion along with related uncertainties are described.

Calibration Procedures

RB3A. Before calibration procedures commenced, all equipment was deployed as described in the previous chapter. Headphones from the roof of the West tower to the control PC operator provided continuous communications. Both the operator on the roof as well as the control PC operator monitored the calibration process. The first step in calibration was alignment.

Alignment was completed by visually pointing the spectroradiometer at Blackbody One. The source aperture was aligned for the center of the field of view (FOV) of both video displays. Slight alignment adjustments were made until maximum signal intensity was displayed on the control PC. The control PC monitored each detector's intensity via the *Acquire* software. The maximum signal was consistently low and left in the camera FOV. This position became the pointing reference position. Once

aligned, the aperture was changed to .200". A radiometric reference was taken at 700°C. The aperture was changed to .001" and a background reference point was taken.

The spectroradiometer was then aligned with Blackbody Two by a similar method. A radiometric reference and background reference was taken at 810°C and 900°C. The use of two blackbodies was to minimize the time required to complete a calibration sequence. The approximate time for either blackbody to stabilize for each temperature was 30 minutes. This calibration procedure was performed before and after the scheduled events each day. This provided amble data to facilitate posttest calibration and analysis.

RB3B. Due to posttest analysis with the RB3A data, the calibration procedures were greatly modified. These modifications include more references points, different calculation methods for the calibration coefficients, and different alignment procedures.

As in RB3A, all equipment was set up and verified in operational order. The spectroradiometer was aimed at blackbody three and aligned as previously described. A major change was the azimuth and the angle of the MR-154 was marked on the tripod to facilitate re-alignment. For all reference points, the signal strength of each detector was recorded and verified with pretest measurements. Once aligned, the blackbody aperture was changed to .200". Putting a cold black material between the blackbody faceplate and the source aperture comprised the background reference. This totally eliminated the source from the MR-154 FOV. After the background reference was acquired, the aperture was rotated away from the .200" aperture to eliminate heating of the faceplate surrounding the aperture.

The primary goal was to take seven reference points at 300°C, 400°C, 500°C, 600°C, 700°C, 810°C and 900°C. These seven points allowed for a four point linear InSb calibration and a four point quadratic HgCdTe calibration. Three points would be available for verification. At each temperature, 4 reference files were acquired. The four files were source and background collected at 16 cm^{-1} and 4 cm^{-1} resolution respectively.

The first three references collected were always 700°C, 810°C, and 900°C. This was the complete calibration sequence from RB3A testing. Before any event measurement was collected, this two-point calibration was processed and verified as accurate. Only then was the spectroradiometer declared operationally ready. Due to the time needed for the blackbody to stabilize at each temperature, the rest of the calibration references were interspersed between event measurements.

Measurement procedures

RB3A. The measurement procedure started each day with verification of equipment. This was accomplished by a collected measurement from Black Body One at 700°C. This measurement was compared to previously collected data to assure equipment functionality. Calibration procedures commence after this initial verification.

Next, the MR-154 was bore sighted to the event target. The control PC initiated the save all interferogram mode in the *Acquire* software. This saved all measurements and references as an interferogram for post processing and analysis.

For each event, the *Acquire* software was programmed to collect a minimum of 500 measurements with no wait time between measurements. The zero scan mode was selected to cause each interferogram to be one sweep direction of the Michelson interferometer. Therefore, each measurement was one interferogram, commonly called

one scan. All 500 scans were saved into one multi-scan file. The Acquire software program provided this multi-scan feature.

The test coordinator was the primary communication source. He was the only communication with Naval Strike and Air Warfare Center (NSAWC) personnel and monitored pilot communications. He was located outside the West tower in clear view of the target and incoming flight paths. The test coordinator would provide a 4-minute warning prior to ordnance release. When the F-18 pilot would release ordnance, he would announce 'pickle'. The test coordination would repeat 'pickle' over the headphone system connected to the third floor and roof of the West Tower. A ten second countdown started for the approximate free fall time of the ordnance. At approximately five seconds prior to impact, the data acquisition of the MR-154 was initiated. At 16 cm^{-1} resolution, approximately 23 seconds of data was collected for each event.

All data was saved to disk between each event. A quick look was completed with the first event to verify if saturation of the detectors occurred and to verify the event signature was captured. This quick look time was limited to five minutes due to F-18 fuel issues. The MR-154 quick look was limited to review of the saved interferogram. No quick look calibrated spectrum was available due to processing time.

At the end of each collection day all data was transferred to ZIP disk and to CD for permanent record and data backup. At any time the test director and coordinator had authority over ground truth collection. The pilot had go or no go say on each event based on operational safety.

RB3B. Measurement procedures for the RB3B test were very similar to RB3A. Both, Wyle Labs and the AFIT ground truth team verified a 700°C measurement prior to

calibration. One difference between tests was all deployed teams would measure a common source and compare radiance information.

The test coordinator provided communications between the NSAWC, Naval Pacific Meteorology and Oceanography Detachment (NPMOD), Explosive Ordnance Disposal (EOD) personnel and the ground truth teams. For each event, EOD would drive all terrain vehicles (ATVs) on the range to fuse the next event. An ATV would point its headlights toward the West tower in direct line of the event. The ground truth teams would boresight the instruments on these headlights. When the EOD team returned to a safe distance, a two-minute warning was issued. The test coordinator provided time hacks of one minute, thirty seconds and a ten second count down to coordinate the ground truth teams and EOD. At approximately five seconds before detonation, the acquisition of the MR-154 was initiated. The rest of the collection procedures were similar to RB3A.

Posttest Processing Event Signatures

Posttest processing of each event signature was an important but repetitious task. Little automation was possible in the *Acquire* software. The basic posttest process was outlined in the Theory chapter and summarized by Figure 2.4. Post processing was a two step process, creating calibration files and event signature manipulation.

Calibration files. The process of collecting reference measurements was described in the previous calibration section. Calibration is based on relative energy values, so each temperature reference was compared to the other temperature reference points to verify correctness. All background files were subtracted from their source references. With the appropriate high and low reference files, *Acquire* calculated a

radiometric correction file. An intermediate temperature interferogram was converted into a complex spectrum and applied to the radiometric correction file. This calibrated file was compared to the appropriate black body curve and previous calibration results.

For RB3B testing, numerous reference temperatures were collected. Each reference point was scrutinized for correctness. Multiple combinations of reference temperatures were input to radiometric correction files and verified with intermediate temperature reference points. This was accomplished for reference files with and without background subtraction. The radiometric correction file that best recreated as many intermediate points as possible was used to calibrate all events for that particular day.

Event manipulation. Processing each event, required many manipulations. This repetitious process created eleven files for each detector and each event. Manipulations started by applying the process described on the right half of Figure 2.4. Once the radiance file was calculated all scans were scrutinized for errors. Approximately five seconds of background information was collected prior to each event.

One of the background scans was extracted into a separate file. *Acquire* would make this extracted file into a four-scan multifile relating to the real and complex spectrum of each scan arm direction. Only the real spectrum of one sweep direction contained the required radiance information and the other three scans were deleted. This manipulated file was then subtracted from its respective event in *Acquire* and saved as a subtracted radiance file.

After the proper background was subtracted, the final ten scans of data from each event were analyzed for system related spectra errors. Erroneous scans were deleted from each event. Data reduction was accomplished by deleting excessive time scans. A

minimum of 1 second of data prior to and 5 seconds of data after event initiation was kept. Once all these manipulations were completed, the event was exported to an ASCII file. On the last day of RB3B testing, no background subtraction was completed. The background subtraction manipulation steps were therefore eliminated.

Analysis Tradeoffs

The previous sections described the process required to collect and manipulate the MR-154 data into a usable form for analysis. The event data is a three dimensional matrix of wavenumber, time, and energy information. Many data features are available for analysis. A tradeoff in the selection of the performed analysis is inevitable due to time constraints place on this thesis effort. Each feature represents a possible source of information to identify the ordnance or event condition. An attempt to break down the various features and analysis methods is provided in Figure 4.1:

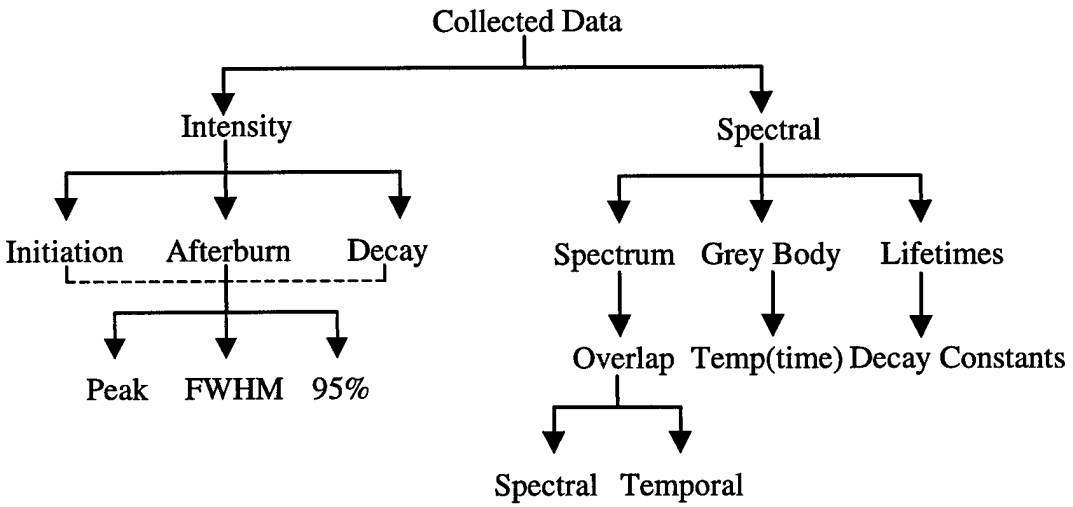

Figure 4.1. Collection Features and Analysis Methods

The first and second rows detail features of the data matrix. The third and fourth rows describe various methods for characterizing each feature. Analysis could be any one or

combinations of these methods and features. This figure is not intended to be all-inclusive, but provide a qualitative description of possible analysis methods.

The primary analysis tradeoff is determining which feature to analyze and what analysis technique will provide the greatest amount information about the differences in event spectral content. To maximize the overall picture of the collected data, overlap analysis was the selected analysis technique.

The method of applying an overlap function is to hold spectral bins constant and overlap temporal vectors. This is similar to comparing radiometric filter bands provided by other ground collection teams. The advantage of this analysis is the spectral bin size is 7.707 cm^{-1} covering a potential spectral range of 500 to 6000 cm^{-1}. A greater description of this analysis method is provided in the next section of this chapter.

Overlap Analysis

Theory. The overlap analysis method is comparing two different detonation events by taking the vector dot product of each spectral bin according to equation 4.1:

$$\cos(\theta) = \frac{A \bullet B}{|A||B|} \tag{4.1}$$

This provides a scalar number between zero and one that represents the overlap of the time dependent vector for each spectral bin. The scalar value representing cos(θ) is the amount of similarity in the two vectors. In a mathematical sense, a value of zero means the vectors are orthogonal and a value of one means A and B are the same vector. This calculation is repeated for all spectral bins. Equation 4.1 divides by the magnitude of both vectors, therefore the units used to describe the energy data prior to applying the overlap function are immaterial.

Procedure. The first step in overlap analysis was post processing the event interferogram into an ASCII file as described in previous sections. The overlap analysis was performed by custom Maltab code 'get_overlap'.

The 'get_overlap' code does many operations. First, two different files were input. A specific wavenumber bin was selected in an atmospheric pass band region. A *Matlab* form of derivation was used to determine the time scan that contains the maximum rate of change from the previous time scan. This maximum derivative was used to locate the event initiation. Both events were aligned to the event initiation to equate time scales.

A user defined time window was established and extracted from each data matrix. The absolute value of this time window was taken to eliminate any negative values caused by system noise and background subtraction. The overlap was calculated, displayed on the PC screen and written to an ASCII file for later manipulation.

Another *Matlab* script, 'combine_overlap', was written to combine multiple overlap files. The overlap values in the atmospheric regions were not usable valid data. This code set all atmospheric absorption bands to zero to remove clutter on outputted graphs. The user is able to graphically display, manipulate and combine any numbers overlap files. This script also provides the ability to create a combined ASCII file. Details of this code are found in appendix B.

Uncertainties. The overlap analysis is only valid if both event files are of the same time scale and spectral resolution. Time scales or resolution of the data must be equated prior to using the 'get_overlap' code. Lastly, atmospheric absorption regions do not provide quality information as noise dominates these regions.

Sensor Fusion, Radiometric Comparisons

Overview. Derivation of the size correction factor used to compare the MR-154 spectroradiometer data to the Wyle InSb radiometer data was presented in the Theory section. The Wyle InSb radiometers were deployed to the left of the MR-154 as shown in Figure 3.4. Since both collection instruments were deployed in the same location with similar look angles, the signal path from the source to both detectors are identical. This eliminated the need to account for the transmission losses over the source signal path. Apparent intensity was therefore compared.

The Wyle radiometers collected energy over four spectral bands relating to the respective filters used. Four bands were defined, Band A 4348 – 4651 cm^{-1}, Band B 3226 – 3704 cm^{-1}, Band C 2509 – 2621 cm^{-1}, and Band D 2153 –2245 cm^{-1}. An overview of these bands with respect to a collected spectrum is provided by Figure 4.2.

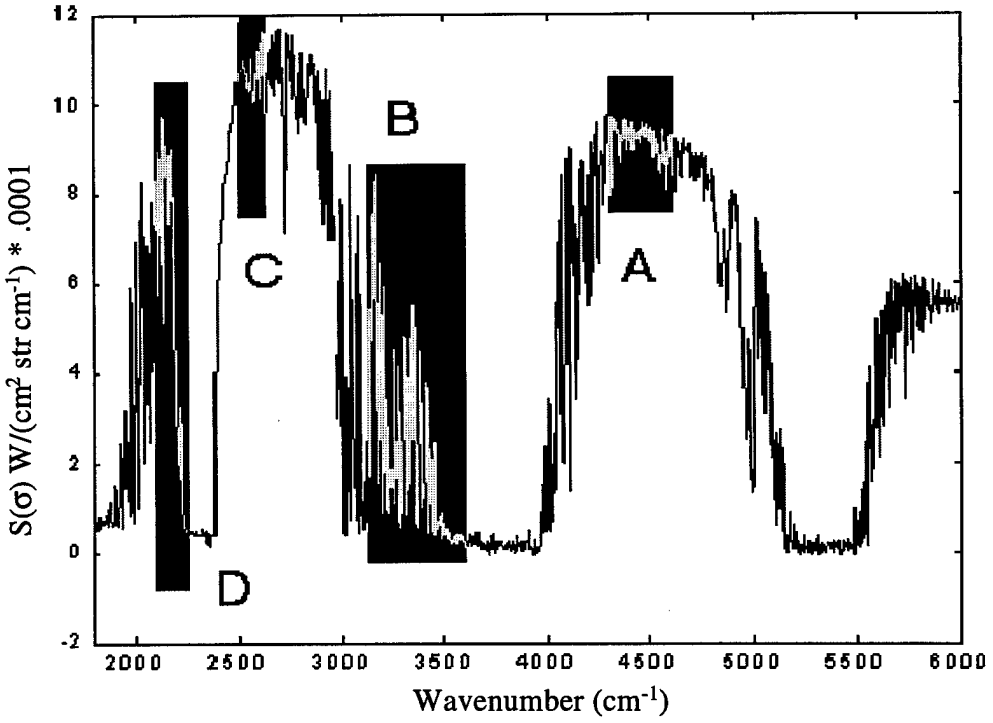

Figure 4.2. Comparison Bands for Sensor Fusion

Since all Wyle instruments contained a filter, $Tr_{filt}(\sigma)$ in equation 2.7 could not be ignored. The filter function was the primary difference in collection methods between the Wyle radiometers and the spectroradiometer. To insure accurate determination $Tr_{filt}(\lambda)$ for each band, AFIT's Bomem, Model B1575 serial number SZM60018, spectrometer was used to calculate transmittance as a function of wavenumber. Wyle Labs applied these filter transmittance functions during posttest processing. The transmittance functions for all filters are provided in Figure 4.3.

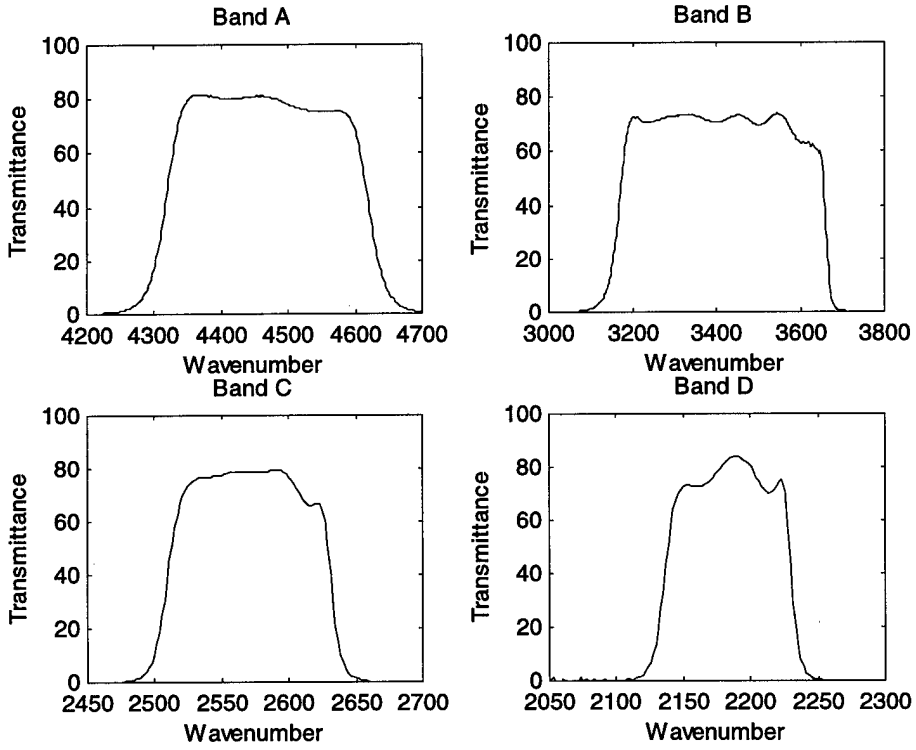

Figure 4.3. Filter Transmittance for Bands A, B, C, and D

Process. The initial step for sensor fusion was posttest processing the radiometric and MR-154 data. The details of Wyle's application of calibration, filter transmittance, and unit conversions are not included in this paper.

Once posttest processing of the MR-154 event data was completed, the *Matlab* code, 'make_temporal', input an ASCII event file and extracted the appropriate wavenumber pass band determined by the filter functions in Figure 4.3. Next, the code summed all wavenumber bins within each band and multiplied by the respective spectral width. The size correction factor derived in equation 2.26 was applied. Finally, each pass band value was converted from units of per wavenumber to per micron. This process was repeated for each time increment. The *Matlab* script created another ASCII file with the time scale in the first column and the appropriate filter bin intensity values, W / (str μm), in succeeding columns.

The final step was to use another *Matlab* code, 'compare_to_spectrometer'. This code input the ASCII file created by 'make_temporal' and the prepared radiometric data. The radiometric data was down sampled by averaging. Finally, a graphical output was displayed comparing the 200 Hz and time averaged radiometer data to the MR-154 data. Tom Fitzgerald provided 'make_temporal' and 'compare_to_spectrometer' (9).

Uncertainties. One uncertainty in the sensor fusion process was the method of applying the transmission filter to the spectroradiometer data. Each filter was not a perfect step function and the full width half-maximum points used to determine the cutoff frequencies of the filters were not exact. A second processing uncertainty was due to the MR-154 wavenumber bins. Each frequency bin was 7.707 cm^{-1} for 16 cm^{-1} resolution data. It was unknown exactly how the MR-154 weights the intensity as a function of wavelength in each frequency bin. These two uncertainties create a small total error in absolute radiance. The last uncertainty was the method of down sampling the 200 Hz

Wyle data. This created a larger uncertainty than the frequency bin or application of the filter response uncertainties.

Down sampling the data from 200 hertz to 20 hertz was required to compare measurements. The standard TMS procedure for down sampling data was to low pass filter the data to eliminate high frequency aliasing and then to decimate the data by only keeping every M^{th} observation (1, 8-47). This technique was not valid for detonation events as decimation could remove the initiation spike. Instead the appropriate method was to average the data.

Averaging the radiometric data created a timing uncertainty. The shape of the averaged curve depends on the start of the average window. For example, assume a ten sample average window. If the event initiation spike occurs on the first of ten samples, the resultant value will be very large. If the initiation spike occurs on the tenth sample, the resultant value will be much smaller. This uncertainty affects the magnitude of the initiation spike and the shape of the averaged curve. Once a detonation event reaches its afterburn, this averaging uncertainty becomes insignificant, as the time scale of the event is much slower. To reduce the averaging uncertainty, the comparison between the MR-154 outputs and the Wyle radiometers were computed from the afterburn.

V. Results

Introduction

This chapter details the observations made during the Radiant Brass 3A and 3B tests. The collection efforts for both tests were extremely successful. One hundred percent of RB3B and 88% of RB3A events were collected. High quality and reliable spectral and intensity information was obtained on all collected events. Over two gigabytes of data in over 3,000 files was processed and analyzed. Due to the large amounts of data, only a portion of the events and data will be described in this chapter and in the following appendices. A complete set of data is available on CD-ROM.

Objectives for this work were to collect robust detonation signatures, discern spectral bands that best discriminate ordnance and characterize the event space for identification. To better quantify the first objective, a data space overview, temporal and spectral characteristics of event data, and system related collection issues will be discussed. Sensor fusion results will be described. Overlap analysis and its results relating to objective two, are discussed next. The third objective is addressed with a qualitative discussion of the gray body and temperature decay trends, as well as a preliminary principal component analysis.

Collection Overview of Data

The collection of detonation signatures was a large success. Once processed according to the previous chapter, each event data matrix contained three dimensions of information. These dimensions are organized as wavenumber x time x energy. Each data matrix was approximately 546x500x1 or 715x500x1 at 16 cm^{-1} resolution and

2179x300x1 or 2853x300x1 at 4 cm^{-1} resolution for the InSb or HgCdTe detectors respectively. A portion of a size small, explosive A, event matrix collected with the InSb detector, is provided in Figure 5.1.

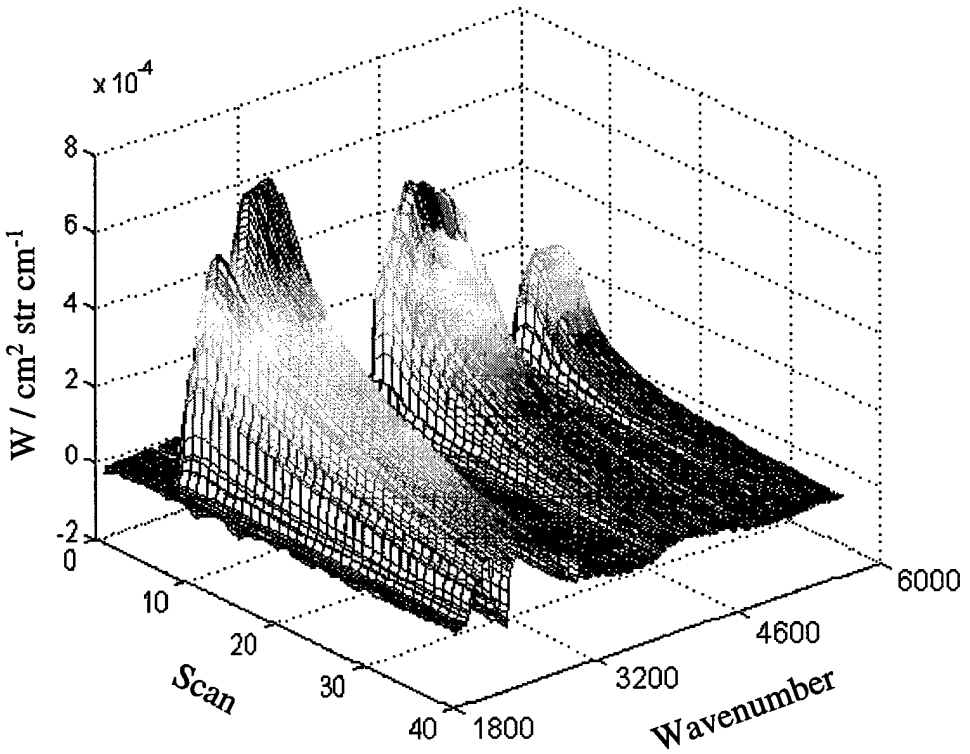

Figure 5.1 Three-dimensional View of a Typical Event

This particular event was collected at 16 cm^{-1} resolution. Each wavenumber bin is 7.07 cm^{-1}. The scan axis directly relates to time by the temporal resolution of .047 seconds per scan. This figure represents 1.88 seconds of event data. The third axis is the apparent radiance, $S(\sigma)$, calculated by the *Acquire* software. The explosive initiation occurred during scan eight and the maximum afterburn is observed at scan thirteen. By scan forty the event is still decaying. The null regions in the spectra are due to atmospheric absorption. The viewpoint for Figure 5.1 is looking down on the decay of the spectra.

Spectral Characteristics. A three dimensional plot provides a good overview of the collected spectra but does not adequately describe all the features present in each dimension of the data matrix. Taking a slice of the data matrix in the energy versus wavenumber plane provides a graphical representation of the spectrum. A comparison of typical spectra collected from the InSb and the HgCdTe detectors is shown in Figure 5.2.

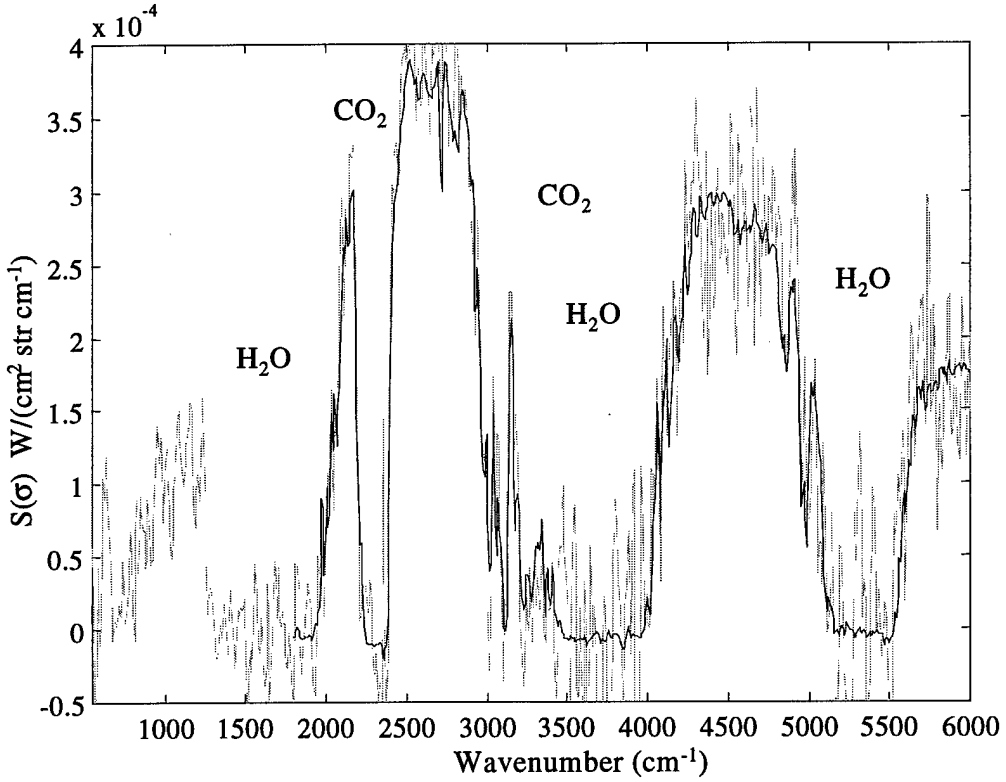

Figure 5.2. InSb (Blue) and HgCdTe (Dark Purple) Detector Spectra

The spectral resolution for Figure 5.2 is 16 cm^{-1}. The spectra collected with the InSb detector is the darker spectra ranging from 1800 to 6000 cm^{-1}. This event was approximately 4825 meters from the collection instruments and the atmospheric absorption bands are very prevalent at this distance. The primary atmospheric absorption molecules are listed in this figure for reference. The background signature for a similar

event was presented in Figure 2.2. The background was subtracted from the detonation event for the data used in Figure 5.2.

Background subtraction adds noise to the signal. The HgCdTe noise levels were large, +/- .0001 W/(cm^2 str cm^{-1}) while the corresponding noise levels of the InSb detector were approximately +/- .00002 W/(cm^2 str cm^{-1}). The HgCdTe noise levels also increased with wavenumber.

Event signatures were collected at two different spectral resolutions. Data collected at 4 cm^{-1} resolution was a secondary collection objective. An example of the 4 cm^{-1} resolution data is provided in Figure 5.3.

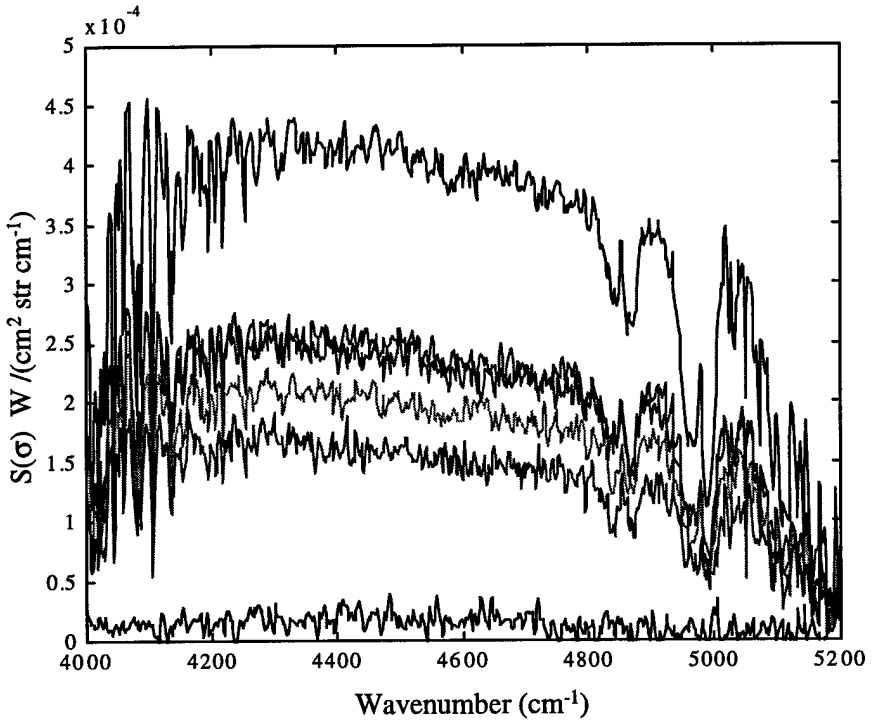

Figure 5.3. Event 36 Spectra at 4 cm^{-1} Resolution
(Scan #, Top Purple 2, Green 3, Red 4, Blue 5,
Violet 6, Bottom Purple Background)

This figure contains the background, bottom, and the second through the sixth scans after the event initiation. The top curve was scan 2. The next two overlapping scans (3 and 4) depicted the afterburn peak. The next curve was scan 5 while scan 6 was immediately below 5. These spectra covered approximate .6 seconds of event. The individual curves look very similar but displaced from each other in magnitude. The spectrum appears to be dominated by the emissions based on the total fireball radiation energy and atmospheric absorption.

Temporal Characteristics. The second plane to slice the 3-dimensional data matrix is the apparent radiance, energy versus time. Analyzing this slice of the data matrix provided an interesting result. During the posttest analysis two different time evolution modes were identified. A graphical description of these two modes is provided by Figures 5.4 and 5.5.

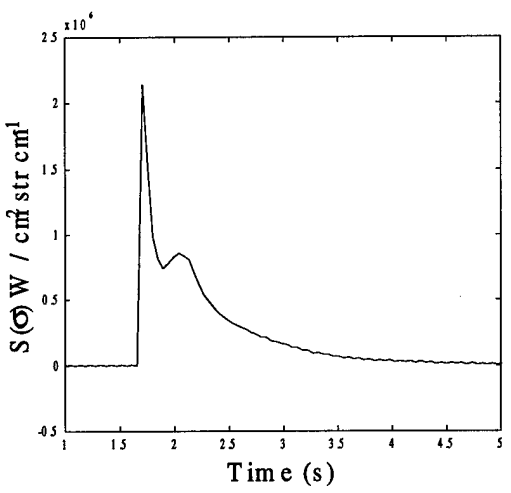

Figure 5.4. Time Evolution Mode One

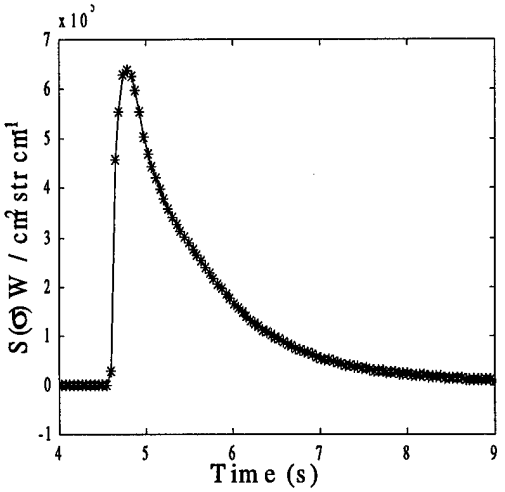

Figure 5.5. Time Evolution Mode Two

For this discussion, the first time evolution mode is defined by Figure 5.4. This mode was the expected time decay mode described in chapter I and contained two well-defined peaks. The first peak, the initiation, was much larger than the second peak, the afterburn.

In general, a significant decay in energy between the initiation and the afterburn peak occurred. For a few events, the afterburn peak was barely discernable from the initiation decay. Temporal mode one described most of the collected data.

The second time evolution mode is defined by Figure 5.5. In the second mode, the intensity of the detonation initiation spike was less than the afterburn peak. This mode was depicted by an initiation followed by a growth period resulting in the afterburn peak becoming the largest apparent radiance value.

To further describe mode two, event 17 (size large, explosive B, air dropped at 355 degrees) event was analyzed. Wyle Laboratory's radiometric data sampled at 200 Hz was compared to the MR-154 20 Hz data. The MR-154 data was collected with the InSb detector. This comparison is shown in Figure 5.6.

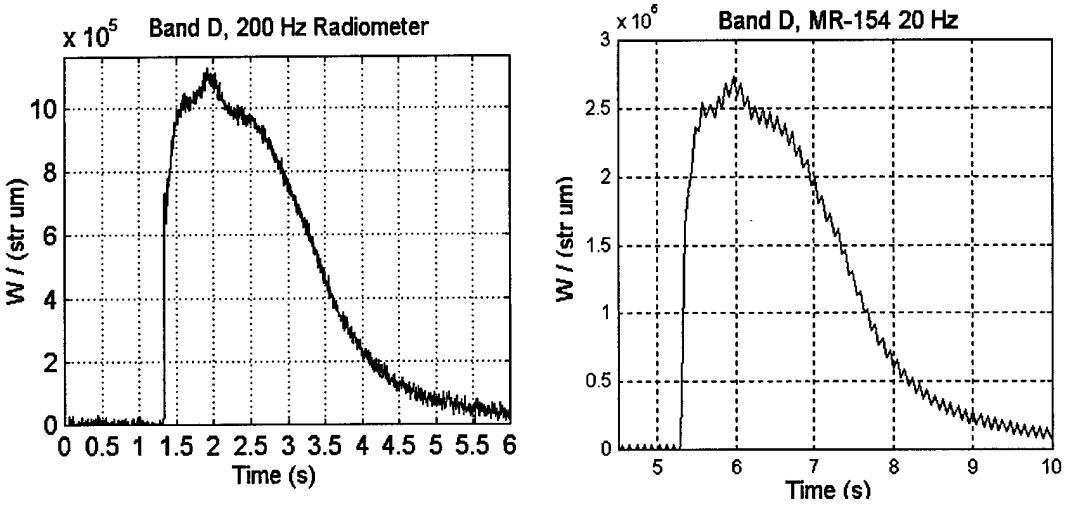

Figure 5.6. 200 Hz versus 20 Hz Collection Rate for Band D

In Figure 5.6, the event initiation spike was seen at 1.4 seconds and 7 W/str μm in the left graph. This initiation spike was not captured by MR-154 collection system. The MR-154 averages out the initiation peak, while the 200 Hz radiometric collection discerned the initiation. This time average uncertainty was discussed in Chapter IV.

Despite missing the initial spike, the relative shapes of both curves were the same. The small humps at 1.6 and 2 seconds in the 200 Hz data were captured in the 20 Hz data. The relative shapes of the temporal distribution were similar for all events collected not just Band D of event 17. In Figure 5.6, absolute radiance of the MR-154 data can not be compared to the Wyle data. The MR-154 detector gain settings changed for this event. The effects of changing the detector gain have not been characterized.

System Errors. An issue visible in the MR-154 data in Figure 5.6 was the every other scan saw tooth pattern. This saw tooth pattern was a function of the MR-154 collection system zero scan. This effect was easily identifiable in the calibrated radiance data, background signature and processed data. Background subtraction amplified this error in specific spectral regions. This scan error is summarized in Figure 5.7.

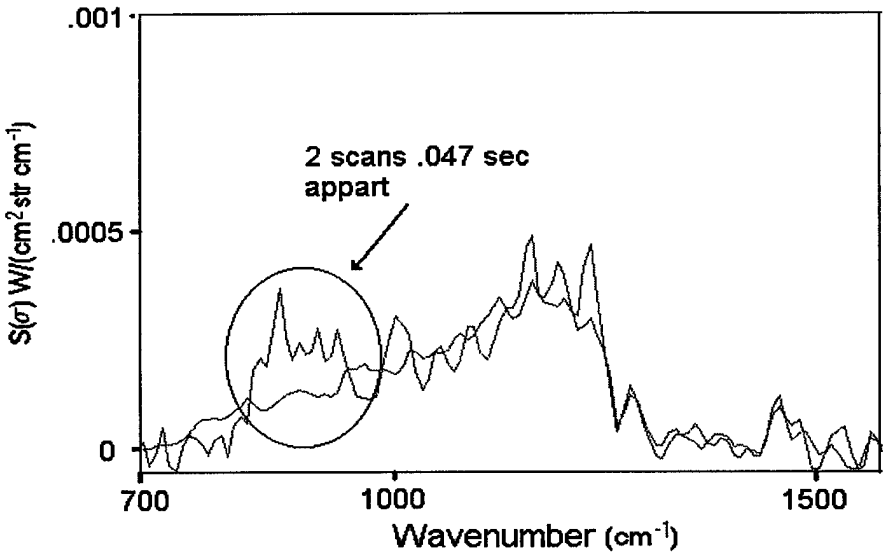

Figure 5.7. Zero Scan Background Signature Error

This figure depicts the worst error region 800 to 1200 cm^{-1}. A large spike was identified from 800 to 950 cm^{-1} for every other scan. This error was in the center of the 8 to 12 μm atmospheric pass band of the HgCdTe detector.

The second system related error analyzed was a loss of the zero reference level depicted by the atmospheric absorption region's apparent radiance values being negative. This error was not noise induced and only occurred during the first few scans of very intense radiant events. This error was attributed to the rapidly changing radiance values of the event signature changing faster than the scan rate of the MR-154.

A complete listing of all collected and processed events are provided in Appendix A. This appendix describes the collection parameters for each event, quantifies the time evolution mode, and describes system related issues of each event.

Sensor Fusion

Sensor fusion was obtained by comparing the Wyle collected 200 Hz InSb radiometer to the MR-154 data. This comparison was a measure of how well the two different collection instruments and collection methods agreed in absolute energy. The quality of this comparison got better each collection sequence based on improved calibration techniques with the MR-154 and better characterization of the filter responses in Wyle's calibrated data.

The calibration of the MR-154 improved over each test due to changes in collection environment and better calibration techniques. The environment for RB3A was an August collect with temperatures varying each morning from 60 to 95° F. The RB3B test was performed at night in October where the average temperature was 35 degrees. Furthermore, posttest analysis from RB3A determined that Black Body One was out of calibration. It also determined the collection optics FOV was not perfectly parallel to the ground and alignment was critical. Better alignment procedures coupled with more robust calibrations greatly improved comparison values.

The final results from sensor fusion were excellent with comparisons in Bands A, C and D normally within 8% absolute radiance and band B within 30%. One example of the comparison is provided in Figure 5.8a through 5.8d. For event 43 the approximate variance of afterburn values were; Band A < 5%, Band B 20 %, Band C 2% and Band D 12%. Even more impressive was the approximate comparison of the peak values, Band A 8%, Band B 47%, Band C 2% and Band D 12%. From chapter IV, comparison values were to be determined from the afterburn peaks to eliminate time average uncertainties. These comparison values are much better than sensor fusion results form previous Radiant Brass tests. In Figure 5.8, the MR-154 spectroradiometer, red curve, results are shifted in time for graphical clarity. The purple curve represents the 200 Hz temporal resolution Wyle radiometer results and the black curve superimposed on top of the purple curve is the time averaged Wyle radiometer results. More sensor fusion data is available in Appendix C.

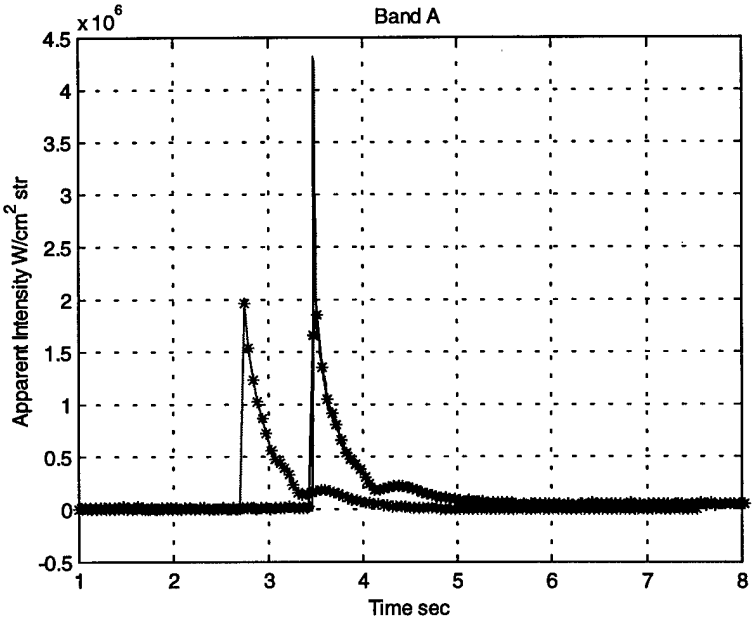

Figure 5.8a. Sensor Fusion for Event 48, Band A (MR-154 Time Shifted Left Red -*-, 200 Hz Radiometer Purple, Averaged Radiometer Black -*-)

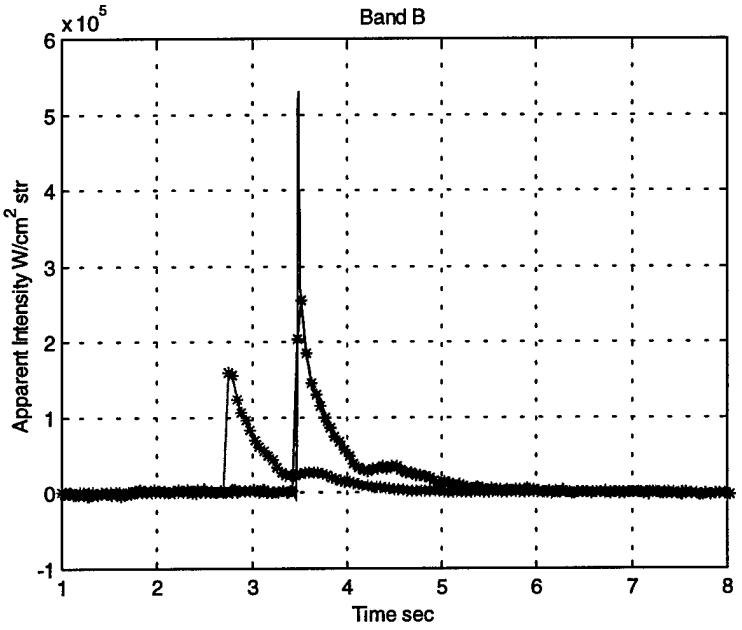

Figure 5.8b. Sensor Fusion for Event 48, Band B (MR-154 Time Shifted Left Red -*-, 200 Hz Radiometer Purple, Averaged Radiometer Black -*-)

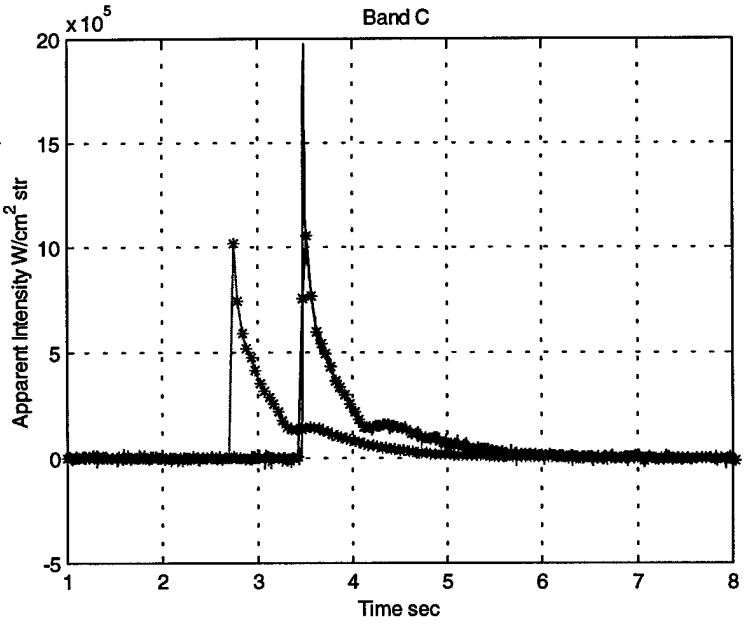

Figure 5.8c. Sensor Fusion Event 48, Band C (MR-154 Time Shifted Left Red -*-, 200 Hz Radiometer Purple, Averaged Radiometer Black -*-)

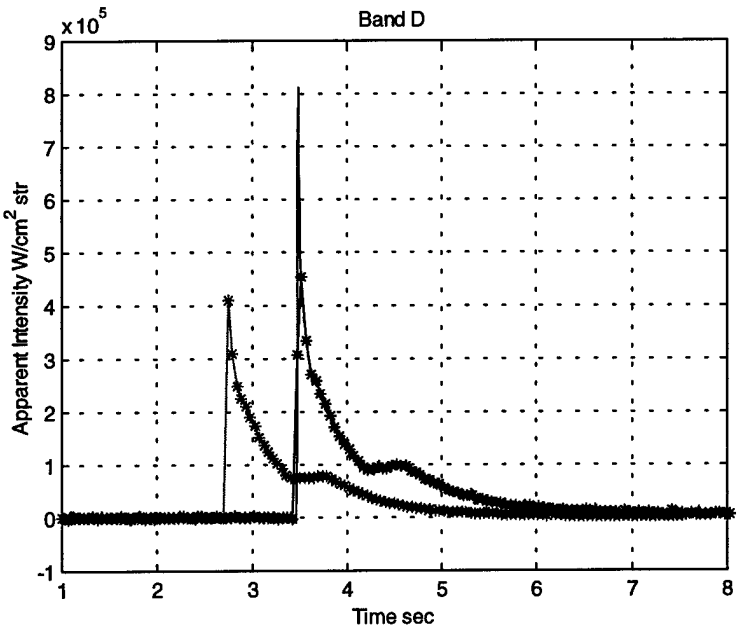

Figure 5.8d. Sensor Fusion Event 48, Band D (MR-154 Time Shifted Left Red -*-, 200 Hz Radiometer Purple, Averaged Radiometer Black -*-)

Overlap Analysis

Overlap analysis was primarily a method of reducing half a million data points into one 2x546 array to describe the similarities and differences in two events. Holding the wavenumber bin constant and varying the time window of the overlapped matrices comprised this analysis. Overlap analysis does not identify what variable or variables causes each overlap to be different. The number of events in any one test state was dramatically limited. This eliminates many statistical methods of analysis. For this reason, results are qualitative in nature.

The most tightly controlled test variable for Radiant Brass 3A was the look angle while for Radiant Brass 3B it was repeatability of an event. Repeatability in the overlap of events under similar conditions was analyzed first to establish a baseline result for future comparisons.

Repeatability. The first variable analyzed was the repeatability of an event. To start with six, size small, explosive A, ordnance configured at 45° elevation, tails high were compared. By holding as many variables as possible constant, the overlap analysis was applied to characterize the repeatability of an event. Events 37, 38, 39, 40, 41, and 43 were all detonated on the same night to eliminate atmospheric variability. All fifteen possible overlap combinations are shown in Figure 5.9.

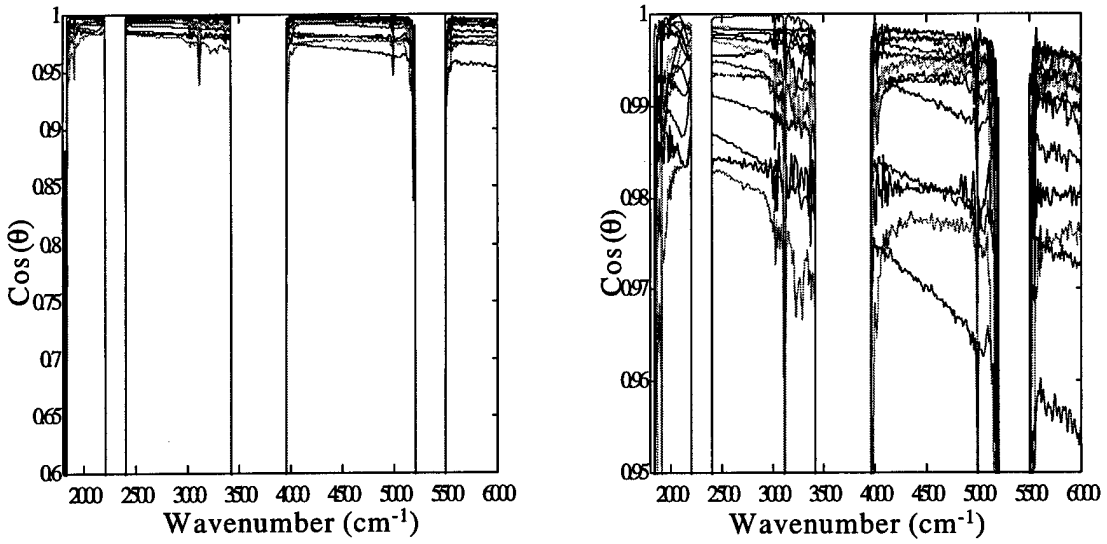

Figure 5.9. Repeatability for Static, Explosive A, Size Small, Type Detonations (Left Scale .6 to 1, Right Scale .95 to 1)

The magnitudes of all combinations were above .95. The $\Delta \cos(\theta)$ over the 1800 to 6000 cm^{-1} spectral range on all but three events were relatively flat +/- .01. Three events had negative $\Delta \cos(\theta)$'s ranging from .02 to .04. The graph on the right in Figure 5.9 represents was provided to show enhanced the detail by event.

Looking at the graph on the left, all combinations seem vary repeatable. The detailed graph shows the true complexity and the variability within ordnance class in the most controlled test environment possible. All of these events were on the Lone Rock

mesa where the ground was relative hard, but ground interaction or explosive variance could be the cause of the variability. Applying overlap analysis to similar events on the second day of static testing provided similar results.

The next set of events examined was the size large static events (34,35,48,49, & 50). These events occurred over two consecutive days. The configuration of each munition was tail high at elevations specified in Table 3.3. The munitions were located on a softer clay surface, propped on the side of a crater facing the West tower. Event 34 was the only large munition collected containing explosive A. The other four events contained explosive B. The overlap comparison is given in Figure 5.10.

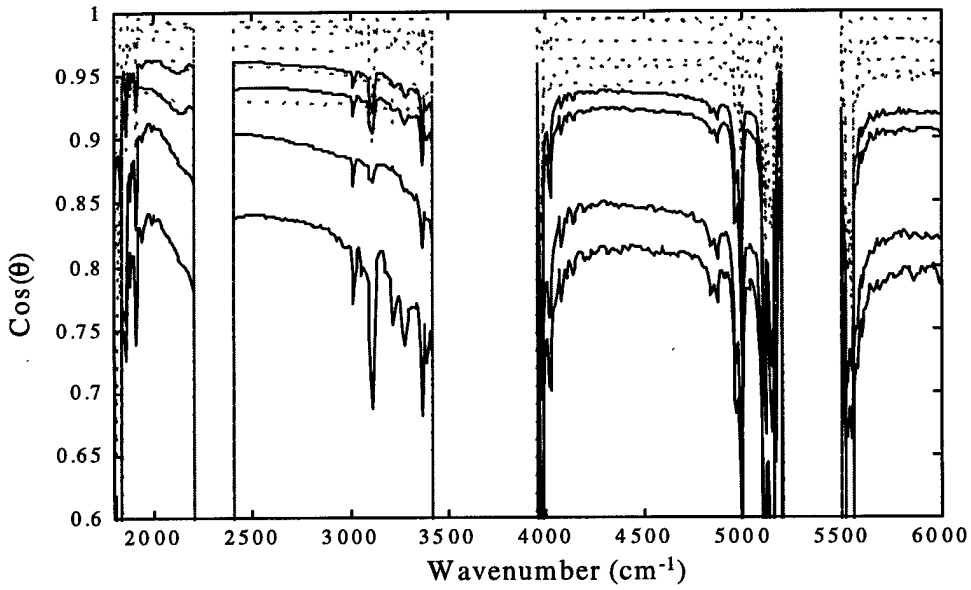

Figure 5.10. Repeatability for Static, Explosive A and B, Size Large, Type Detonations (B versus B Magenta Dashed, A versus B Purple)

The six dotted (Magenta) lines represent all combinations of the explosive B events. These six combinations established a guideline for determining the repeatability of large static events in the same test conditions. These six overlaps had magnitudes greater than .95 and a negative $\Delta \cos(\theta)$ trend by wavenumber of less than .05.

Explosive Type. After completing the repeatability of static events, the overlaps of different explosive types were analyzed. Figure 5.10 not only shows the repeatability of large ordnance on a soft surface, it shows combinations of explosive A with B. Distinct differences in the overlaps are shown. The differences were characterized by large negative $\Delta \cos(\theta)$ variations in the 2000 to 2200 and 3000 to 3500 cm^{-1} regions.

Two of the four overlaps with explosive A are between .9 and .95. Based only on the subjective criteria previously determined, the top two combinations of explosive A and B do not qualify as different. With this said, all four overlaps of explosive A verus B can be distinguished by large slopes ($\Delta \cos(\theta)$) in the 2000 to 2200 cm^{-1} and 3000 to 3400 cm^{-1} spectral regions. The extracted time window for this comparison was one second. The first scan of each event was not included due to the system zero level reference error.

Next explosive C, event 46, was compared to explosive C event 47, explosive B events 48 -50 and explosive A events 45,51, and 54. This is shown in Figure 5.11.

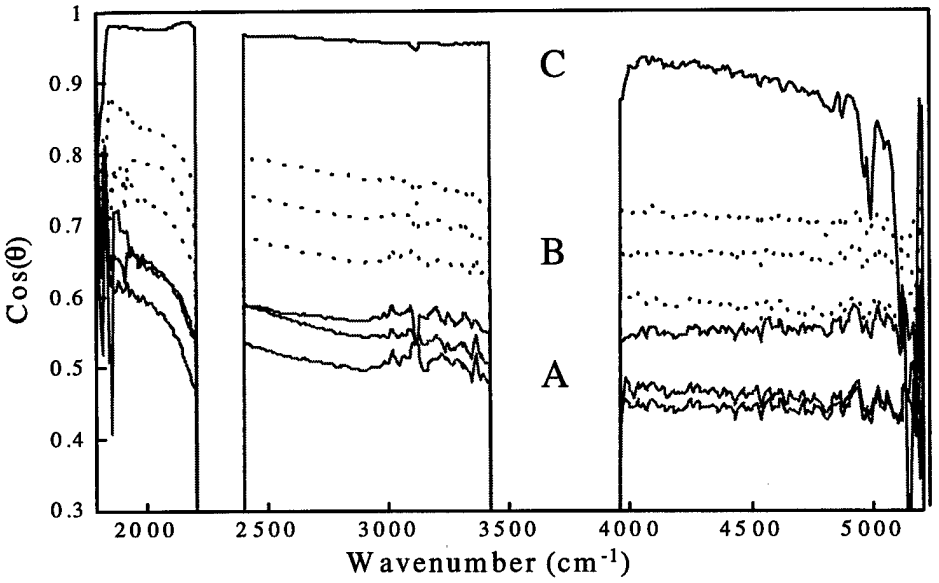

Figure 5.11. Overlap for Static, Explosive C (Red) versus A (Magenta) and B (Purple Dashed) Detonations

In this figure, the initial scan was not used due to saturation of the first scan of event 47. One second of data was overlapped. The comparison of the two explosive C events is described by the top curve in Figure 5.11. The overlap between these two events produce results that do not appear to be repeatable based on standards set by the size small, explosive A repeatability tests. Only two explosive C detonations were collected and the small sample space is a concern. The signatures of explosive C compared subjectively to the explosive C events collected during Radiant Brass 2B. Clear groupings by explosive type were apparent in this figure.

The magnitude of overlap C with A was consistently lower than C with B. This trend was expected due to type of explosive. When the explosive C, event 46, used in Figure 5.11 was replaced with explosive C, event 47, a similar pattern with respect to explosives A and B was exhibited. The relative positions and spacing between explosive A and B were maintained as well as the relative spacing within explosive type.

The large slope in the 2100 to 2200 cm^{-1} spectral region was further investigated. An emission spectra was identified as riding on top of the generalized decay of the spectrum. This emission was in the 2100 cm^{-1} to 2200 cm^{-1} range as shown in Figure 5.12.

This event started at scan 90. Approximately .5 seconds after event initiation, scan 99, the magnitudes of the 2000 to 2200 cm^{-1} and 2400 to 3000 cm^{-1} spectral range were similar. By .8 seconds, the 2100 to 2200 cm^{-1} spectral range had grown 30% larger in apparent radiance than the corresponding 2400 to 3000 cm^{-1} spectral band. This

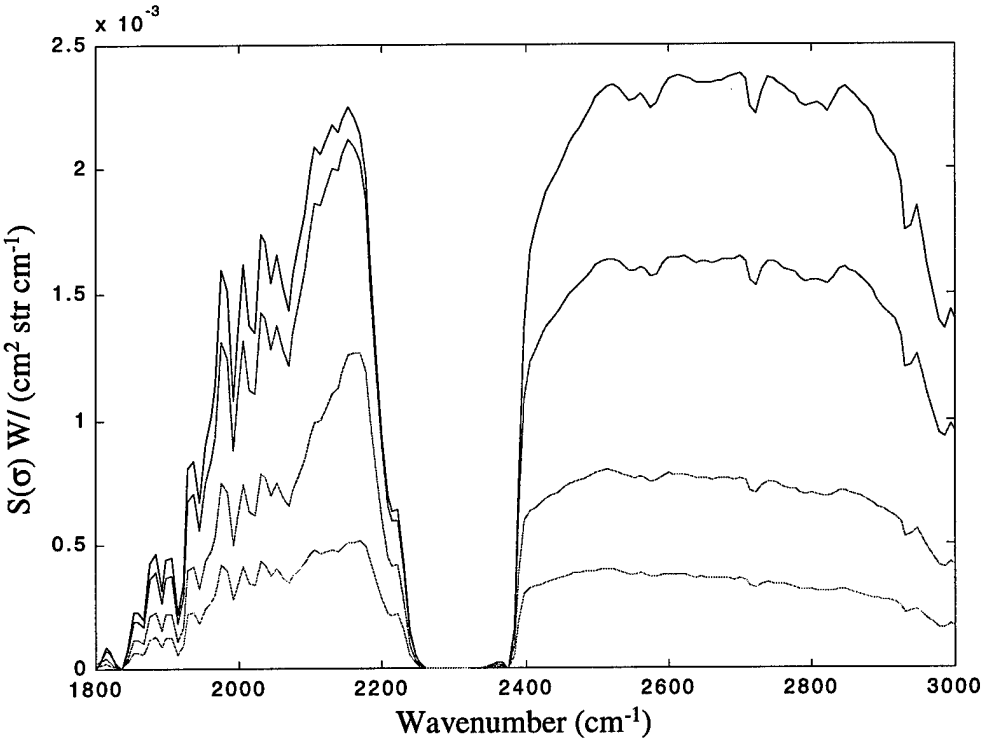

Figure 5.12. Emission Spectra for Explosive A at 16 cm^{-1} Resolution (Scan #, Black 99, Purple 106, Red 114, Magenta 124)

emission continued for approximately one second. An emission of this magnitude was not found in the examination of explosive B events.

According to the 96 Hitran Database, CO has over 390 and CO_2 has over 1260 transistions in the 2100 to 2200 cm^{-1} region alone. This does not include the possible transitions from hundreds of other molecular species existing in the detonation zone. When looking at a specific 4 cm^{-1} resolution peak of range 2168-2170 cm^{-1}, 23 possible CO and CO_2 transitions as well as 59 possible N_20 transitions were identified. In this region the atmospheric absorption profile is relatively flat, further supporting the spike is emisson riding on top of the gray body emission. These molecular species are expected to be in the afterburn of explosives, especially CO according to the equations 2.26 through

2.28. With so many possible transitions spaced so close together, the MR-154 was unable to spectrally resolve any one transition.

To further evaluate the 2000 to 2200 cm-1 region, spectra of explosive A type events were analyzed at 4 cm^{-1} resolution. The typical spectrum from the afterburn of a size small, explosive A event is provided in Figure 5.13.

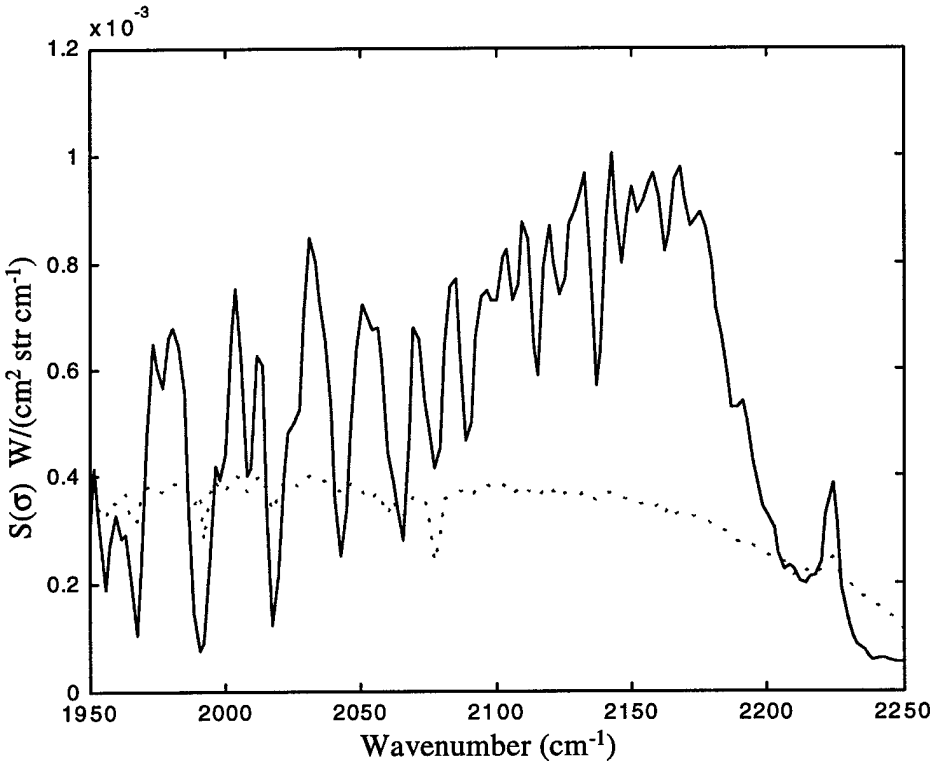

Figure 5.13. Emission Spectrum for Explosive A at 4 cm^{-1} Resolution (Spectrum Purple Solid, Scaled Atmospheric Apsorption Pink Dashed)

This spectrum displayed distinct spectral features not discernable in Figure 5.12. To verify the spectral features are indeed emission, a scaled version of the atmospheric absorption is provided in the dashed pink trace. By comparing both curves, atmopheric absorption can be ruled out as the cause of the features in the 2000 to 2200 cm^{-1} region. As previously stated, the exact molecule or molecules causing emission have not yet been determined.

Look Angle. The next variable analyzed with overlap analysis was look angle. Look angle or azimuth viewing angle was defined as the angle from the observer's collection line of sight or boresight to the vector impact direction of the ordnance. Exact ordnance impact vectors were calculated using the Joint Effectiveness Manual Model. For this analysis the impact vector was determined by the relative run-in heading of the F-18. The approach vectors of the F-18 aircraft were provided in Figure 3.3. The values 65, 155, and 355 reference the approximate F-18 headings upon ordnance release.

The first set of events overlapped were the size large, explosive B, events. This data is presented in Figure 5.14.

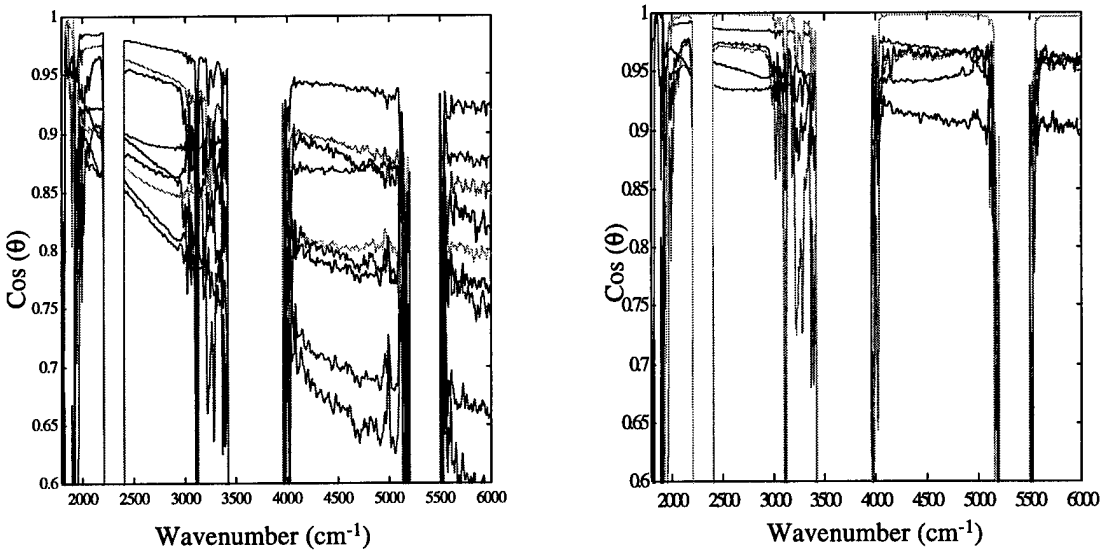

Figure 5.14. Look Angle for Size Large, Explosive B Events
(Right Graph: 355° versus 155° and 65°
Left Graph: 355° versus 355°; Yellow, Purple, Light Blue and
Left Graph: 155° versus 155°; Red, Purple, Green)

Figure 5.14 contained overlaps from three events at 155 degrees, three events at 355 degrees, and one event at 65 degrees. Nine combinations compared 355 to 155 and 65

(left graph), while six combinations compared like events from F-18 run in vectors 155 and 355 (right graph).

The graph on the right is the repeatablity of the air dropped large ordnance. As in the static case, the events were above magnitude .9 and had a maximum negative slope of .07. The graph on the left displays a distinct difference when comparing the 355 versus 155 and 65 approach vectors. Eight of the nine combinations do not meet the criteria for repeatability provided in the right graph. The exception combination was event 18 versus event 8.

To further quantify the look angle, one event from 65 degrees was compared to look angles 155 and 355. This analysis is summarized in Figure 5.15.

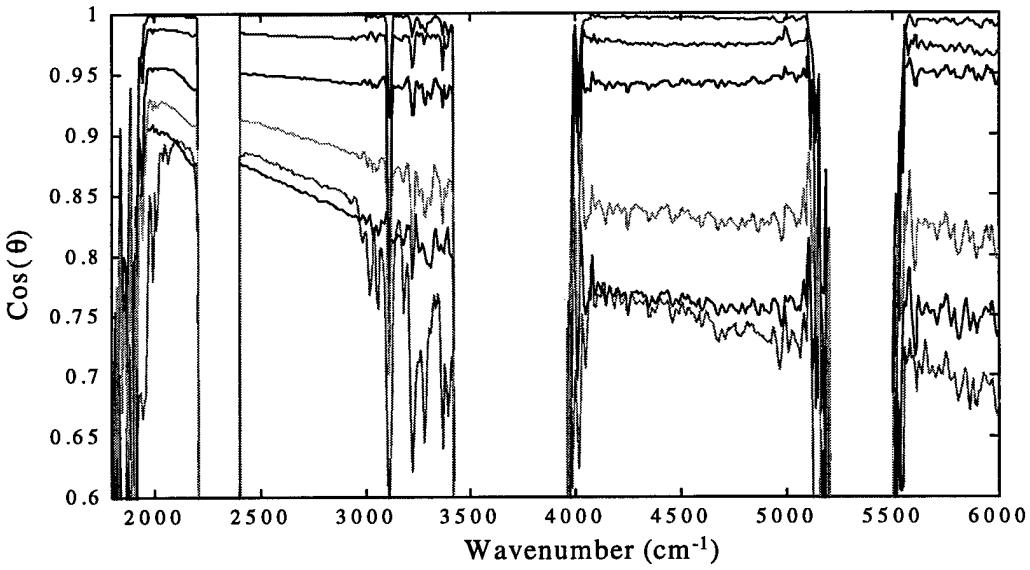

Figure 5.15. Look Angle for F-18 Heading 65° versus 155° (Red, Green, Purple) and 355° (Yellow, Purple, Light Blue)

The combinations of 65 degrees versus 155 degrees were very flat with respect to wavenumber and had magnitudes of .95 or greater. The combinations of 65 versus 355

had negative slopes ($\Delta \cos(\theta)$) in excess of .15 and overlap magnitudes ranging from .93 to .68.

After analyzing the large ordnance, analysis of the size small, explosive A events was completed. Only one event was available from approach vector 355 due to equipment malfunctions on the F-18 aircraft. This event was compared to five events from 155 degrees and four events from 65 degrees. The results are comparable to the large ordnance. The repeatability and look angles are shown in Figure 5.16.

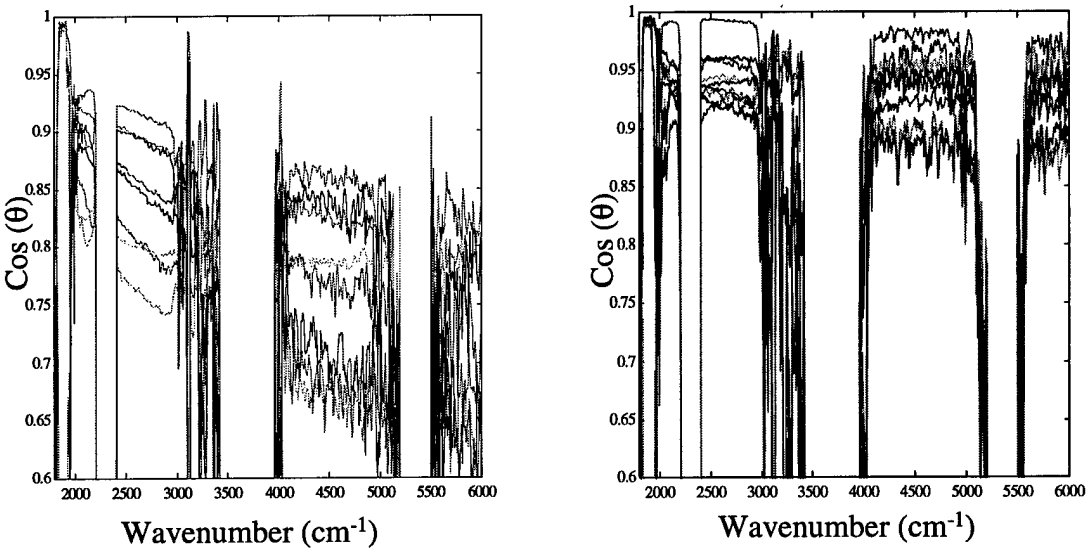

Figure 5.16. Look Angle for Size Small, Explosive A Events
(Left Graph: 355° versus 065° and 155°, Right Graph: 155° versus 155°)

When assessing the left graph of Figure 5.16, a negative slope trend, $\Delta \cos(\theta)$, ranging from .1 to .2 was found with the magnitudes ranging from .94 to .62. The right graph provides all combinations of the five events from one approach vector 155 degrees. As previously described by Figure 5.16, comparing look angles 155 versus 65 provided no obvious differences in overlap.

Overlap analysis provided a subjective method of determining the similarities and differences of two event temporal evolutions by frequency. Spectral regions were found that possibly deliniate explosive type. A distinct difference in event signature was found based on look angle. Changing the size of the explosive or the explosive type did not affect look angle results, see Figures 5.14 and 5.16. This finding suggests the detonation zone is not isotropic.

Gray Body Analysis

The third objective of this thesis was accomplished by characterizing the gray body nature of the emission and a principal component analysis. The spectra emitted by a detonation event was a combination of the emission spectra of the individual particles and by products of each explosion as well as the gray body emission associated with the average temperature of the gaseous mass of the explosion fireball. Since ordnance is designed to deposit maximum amounts of kinetic energy into the surrounding environment, it is not surprising the general decay of each events was dominated by this gray body emission. Numerous events were looked at in *Acquire* by fast forwarding through each spectrum by time. This qualitative feel for the data suggests the dominant spectral decay profile is a gray body with the temperature decaying as an exponential.

A clarification of the term gray body is required for this discussion. The energy decay appears to be a continuous 'black bodyish' decay. Each event does not follow a gray body in the academic sense. The emission does not fit a black body curve scaled down by some constant. The general energy emission was a cross between a selective radiator and gray body.

An example of a decaying temporal mode two, event is provided by Figure 5.17.

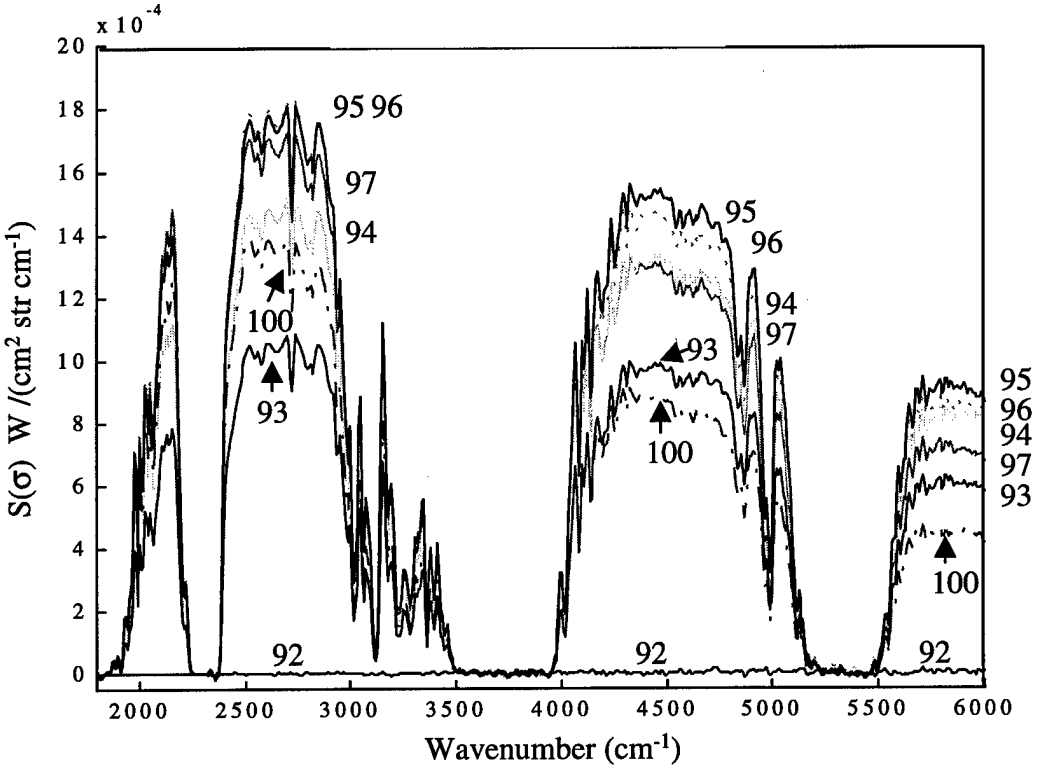

Figure 5.17. Gray Body Decay Displaying Temporal Mode Two, Event 41 (Scan #, Bottom Purple, 92, Purple 93, Yellow 94 Black 95, Lime Green 96, Magenta 97, Red 100)

This figure was derived from a size small, explosive A, 45 degree elevated, static event. The numbers overlaid on the figure relate to the scan number of the event. The data for this figure was collected at spectral resolution 16 cm^{-1} and each scan is separated by .047 seconds. The event initiation occurred at scan 93 while the peak afterburn occurred at scan 95, approximately .141 seconds after the initiation. Scans 96, 97, and 100 depicted the gradual decay of the event.

Even though the event initiation has less apparent radiance than the afterburn peak it appears to be at a higher gray body temperature. The best example of this was comparing scan 93 to 100. The 2400 to 3000 cm^{-1} pass band had scan 100 with greater energy than scan 93. In the 4000 to 5000 cm^{-1} and 5550 to 6000 cm^{-1} ranges, scan 93

clearly contains more apparent radiance or energy and thus was at a higher temperature. Similar arguments can be made for scans 95 versus 96 and scans 94 versus 97.

No attempt to quantify the size of the radiating source by time was accomplished. The growth in apparent radiance was probably due to the increase in size of the emitting infrared fireball. Inspection of the Wyle collection team's infrared imager data supports this statement.

A second decay example, an event displaying temporal mode one is provided in Figure 5.18.

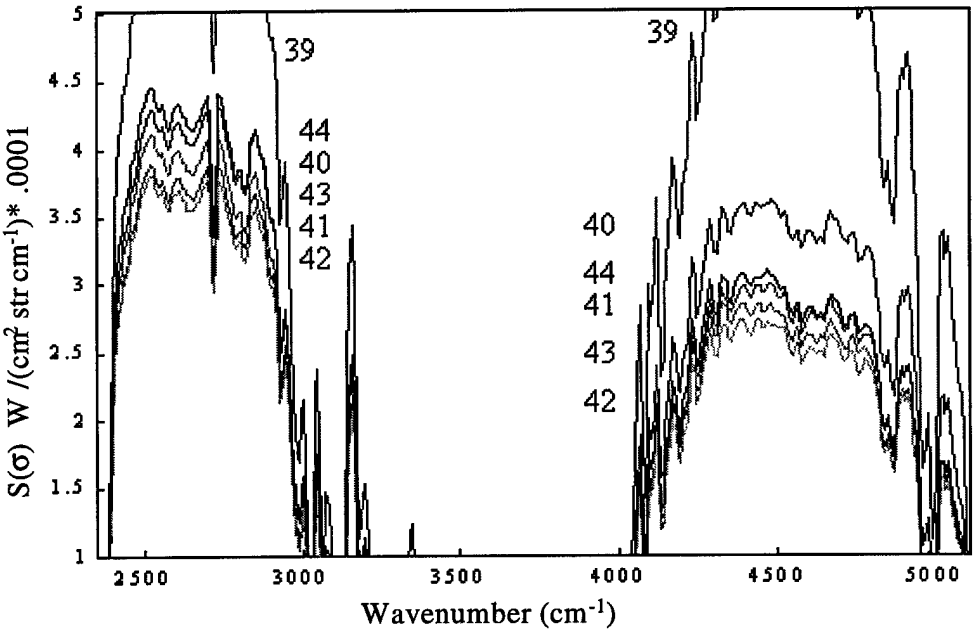

Figure 5.18. Gray Body Decay Displaying Temporal Mode One, Event 9 (Scan #, Top Purple 39, Bottom Purple 40, Red 41, Lime Green 42, Magenta 43, Black 44)

Event 9 was a size large, explosive B event. Explosion initiation occurred at scan 38. This scan's apparent radiance exceeded the Y-axis scale and was deleted for clarity. Scan 44 represented the peak afterburn while scan 42 represented the local minimum

between the initiation and afterburn features. Scans 41 versus 43 and 40 versus 44 both display a decrease in temperature as a function of time due to the energy distribution by wavenumber. This result is similar to results from Figure 5.17.

A possible exception to the decaying temperature versus time trend was Event 34. The explosion initiation for this event was at scan 1. The afterburn for this event, scans 5 and 7, displayed the decreasing temperature versus time, but the temperature appeared to increase between scans 3 and 4. This is shown in Figure 5.19.

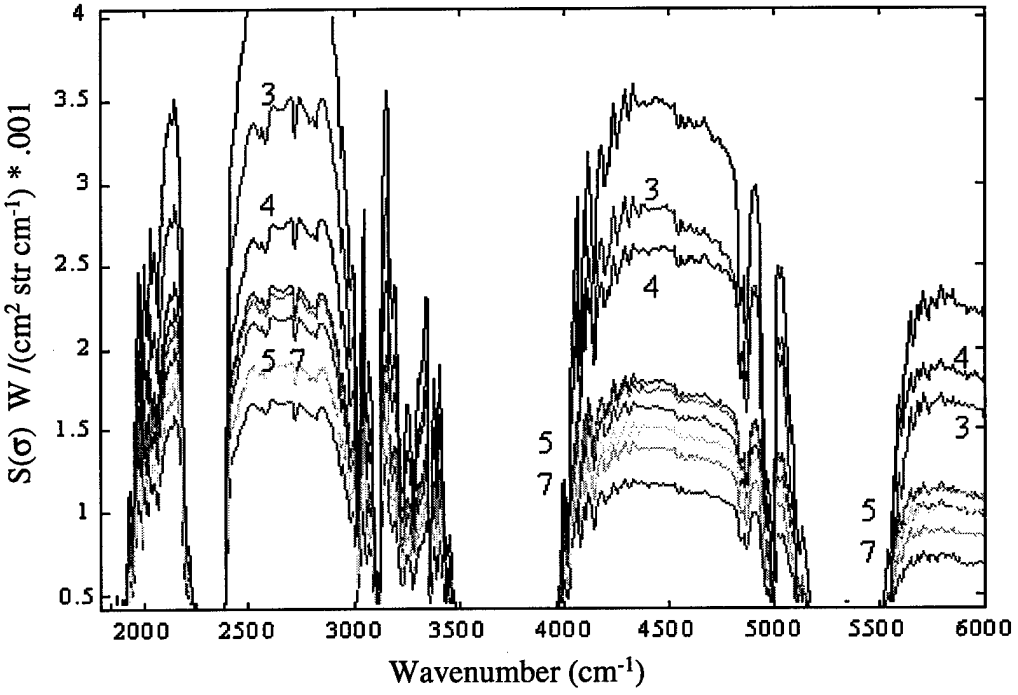

Figure 5.19. Gray Body Decay Displaying a Possible Temperature Increase, Event 34 (Scan #, Black 2, Green 3, Purple 4, Yellow 5, Bottom Red 6, Cyan 7, Magenta 8, Lime Green 9, Top Red 10)

The transition between scan 3 and 4 corresponded to when the background zero point error returned to zero from a negative value for this event. Strong evidence supports the apparent increase in temperature from scan 3 to 4 was a system related error, but this event was unique in size and explosive. Due to the unique nature of the event, it

is not possible to conclude with certainty that the increase in temperature was due to the system error.

This particular event displayed time evolution mode one. Scans 1-6 represented the decay from initiation spike to the minimum point before the growth to the peak afterburn. For clarity, this figure only contains labels for scans 3, 4, 5, and 7.

Principal Component Analysis

A principal component analysis was performed on a sample of the data in cooperation with Howard Mayfield of the Air Force Research Laboratory. The effort was not the primary focus of this thesis and more information on principal component analysis techniques and theory is available in many texts, such as Principal Component Analysis by Jollifee (12). Principal component analysis basically characterizes the variability of n inputs and determines a vector in the n dimensional space that describes the variability. Several attempts at principal components were attempted over a one week period of time. Many attempts produced inconclusive results. One attempt in particular started to group items by test variables and conditions.

For this particular analysis the frequency of the maximum apparent radiance was selected and the temporal features at that specific frequency were characterized. The temporal characterization included four figures of merit. These four figures of merit included: the time from the event initiation to the initial peak, the time between the initial maximum and secondary maximum (afterburn), the time between the secondary maximum and the knee of the decay, and the time for each event to decay back to ambient conditions. These figures of merit were subjectively determined by user

selection from a time versus apparent radiance plot using *Matlab* scripts. The temporal plots used were similar to Figures 5.4 or 5.5.

Two other figures of merit were used, the maximum intensity value corrected for distance to the event and the frequency of maximum apparent radiance. Twenty events were included in this sample space. Table 5.1 details the input information.

Table 5.1. Principal Component Analysis Inputs

Event # Figure 5.19	Freq. max (cm^{-1})	Corrected Intensity	Initial Rise (sec)	Second Maximum (sec)	Decay Knee (sec)	Total Decay Time (sec)
1	4659.0	7.50E+03	0.047	0.752	0.752	2.256
2	4474.5	1.18E+04	0.094	0.517	0.423	1.598
3	4474.5	1.73E+04	0.094	0.329	1.739	5.400
4	4474.0	2.47E+04	0.047	0.000	0.329	3.055
5	2515.0	1.83E+04	0.282	0.282	2.770	5.800
6	4474.0	1.12E+04	0.047	0.564	1.316	3.431
7	2746.4	8.01E+03	0.047	0.423	1.410	4.000
8	2738.0	1.31E+04	0.282	0.000	0.846	3.572
9	2522.7	9.57E+03	0.094	0.141	1.457	4.606
10	2515.0	3.65E+04	0.047	0.235	1.363	4.888
11	2152.0	5.00E+02	0.047	0.000	0.470	2.820
12	2175.0	5.01E+02	0.047	0.094	0.282	1.550
13	2700.0	2.46E+04	0.141	0.141	1.034	4.230
14	2684.7	1.57E+04	0.141	0.141	1.833	4.465
15	2504.0	3.23E+04	0.141	0.000	1.598	4.700
16	2738.7	5.97E+04	0.047	0.470	1.363	3.055
17	2746.4	5.12E+04	0.047	0.000	0.658	2.303
18	2746.4	4.68E+04	0.282	0.000	1.316	4.559
19	2731.0	4.18E+04	0.235	0.000	1.363	4.371
20	2684.0	4.28E+04	0.188	0.000	1.550	5.500
Average	3.07E+03	2.37E+04	1.20E-01	2.04E-01	1.19E+00	3.81E+00
Max	4.66E+03	5.97E+04	2.82E-01	7.52E-01	2.77E+00	5.80E+00
Min	2152.0	500.4	0.0	0.0	0.3	1.6

The results from this particular principal component effort were analyzed. When the second and fourth principal components were compared, some grouping by event

type and condition was established. A plot of principal component two versus principal component four is provided in Figure 5.20.

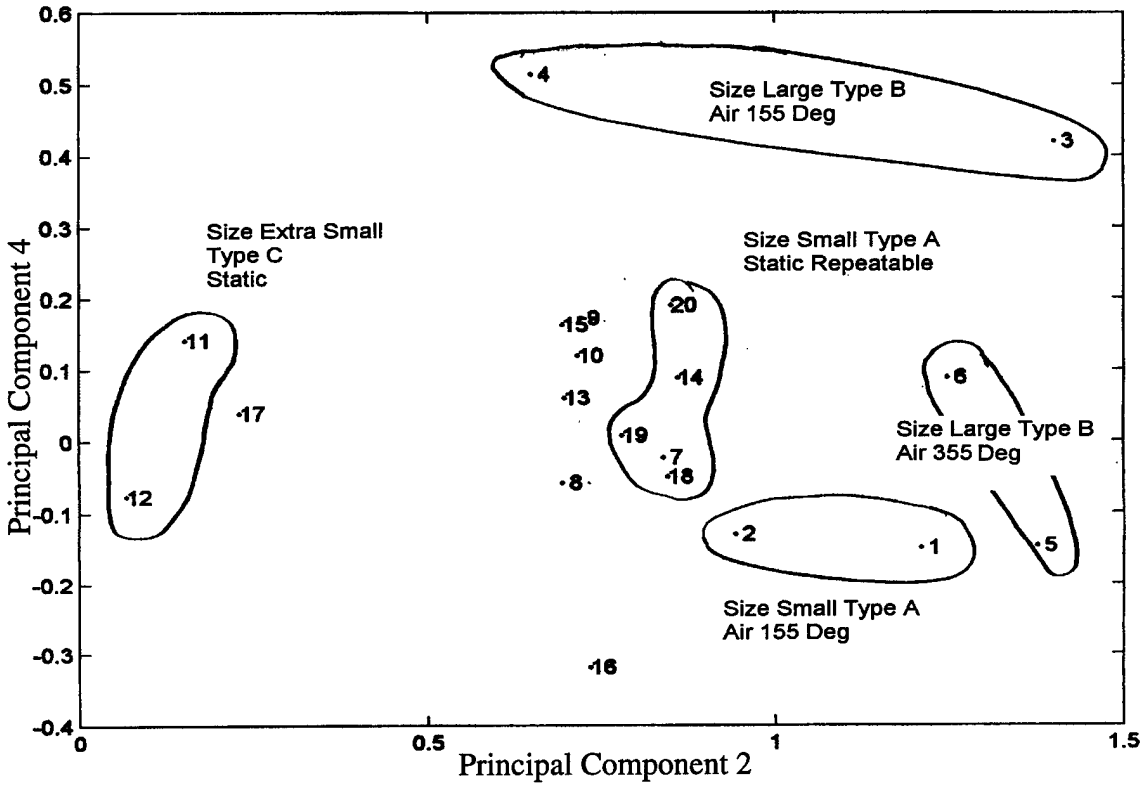

Figure 5.20. Principal Component Analysis of Twenty Random Events

As can be seen in this figure, some grouping by event was attained. The numbers associated on this plot refer to the order of events listed in Table 5.1. The circles attempt to group events by similar test variables. This plot does not identify all ordnance types or event conditions but does show promise for eventual classification.

V. Conclusions

Introduction

This chapter addresses the conclusions reached after collecting signatures from ordnance detonations and analysis of the spectral and temporal content. This chapter will start with a brief summary, address repeatability of ordnance signatures, look angle affects on the signature, characterization of the detonation decay, and a discussion of the ability to identify ordnance or detonation conditions. Finally, a short discussion of the research effort and suggestion for future research are presented.

Summary

A Bomem Fourier Transform Spectroradiometer was used to collect infrared signatures of conventional munitions detonated under field conditions during two Radiant Brass tests. The collection effort was a significant success, collecting 100% of all static events and 88 % of all F-18 dropped ordnance. Comparison of four radiometric bands with an independent collection team's results were within 3% for certain bands and events. This accomplishment is well under the expected uncertainties of 5 to 20% per measurement described by Augustine. The percentage of events collected as well as the quality of the radiance comparison were unparalleled by any other spectral collection during the Radiant Brass testing to date.

The spectral data was analyzed for features that could allow for battle-space characterization. Analysis focused on spectral overlap to establish repeatability of a test scenario. The look angle test condition and explosive types were analyzed to establish frequency ranges for best discrimination. Finally, a preliminary look at a pattern

recognition technique, principal components, was performed to substantiate the ability of unique identification of ordnance or event condition.

Conclusions

Even with such a successful collection, the sample size of events in similar test conditions is limited. Due to this fact, all conclusions are qualitative in nature. The conclusions are supported by analysis performed for this work as well as research performed in conjunction with other technical teams supporting the Radiant Brass program. In general, the collection of spectral and radiometric information with the MR-154 clearly provides better battle-space characterization than radiometric information alone.

First, for size small, explosive A munitions, the event signatures are repeatable. This conclusion is supported by overlap analysis with magnitudes greater than .95 and slopes less than .05 across 1800 to 6000 cm^{-1}, as well as radiometric analysis showing all test events exhibited temporal evolution mode two. The sample space for this conclusion is 13 events detonated over two test periods.

No comment can be made on the repeatability of size large, explosive B events. Radiometric analysis displayed vast differences in the time versus apparent radiance plots over various spectral bands. The repeatability of the size large, explosive B events were established by overlap analysis for comparison purposes. A plausible explanation for the discrepancies in the time versus apparent radiance plots is ground target interaction. These events had 600 to 1000 lbs of explosive detonated on a soft sandy clay surface.

Second, the spectral signatures produced by air dropped ordnance are not uniform within a 360 degree viewing angle of the detonation zone. This implies the detonation

zone is not isotropic. When the ordnance impact vector was 355 degrees or toward the collector boresight, all events exhibited temporal evolution mode two with the increase in the apparent radiance between event initiation and afterburn. When ordnance was dropped with impact vectors 65 and 155, temporal mode one was collected. Temporal mode one was depicted by decay in apparent radiance between the event initiation and the afterburn. Overlap analysis shows distinct differences in all combinations of events that compare look angle 355 to look angles from ordnance delivered perpendicular to and away from the collector's line of sight. No differences between perpendicular and away from ordnance delivery are discernable using overlap analysis.

Third, all detonation signatures can be primarily described as decaying gray bodies where the gray body is a function of wavenumber. Data supports a continuous decline in temperature versus time. This continuous decline in temperature is regardless of whether the apparent radiance of the event was increasing or decreasing. This conclusion is based on subjective evaluation of the analyzed data. This supports statements made by William Miller (18).

Fourth, one frequency range that discriminates explosive A from B is 2100 to 2200 cm^{-1}. In this region, a distinctive emission during the afterburn was identified. This same frequency range showed discrimination between explosives C, B and A. In general, the second frequency range that provides better discrimination is higher frequencies. Overlap analysis supports higher frequency spectra better discriminate look angle and explosive type. In hindsight this conclusion makes sense. The most information that relates directly to the initial detonation conditions should be found in the highest

temperature detonation signatures, thus higher frequency. As each detonation event decays toward ambient conditions, information is lost relating to the initial explosion conditions.

Fifth, a medium-framing rate (20 Hz – 50 Hz) is adequate to temporally distinguish bombs in the battle-space. Repeatedly, the 21 Hz sampling rate of the MR-154 data provided the same information about the temporal history as the 200 Hz radiometers. A medium sample rate may not be able to discern the initial event peak under certain conditions, but does adequately characterize the rest of the event.

Finally, identification of explosives and event conditions in the battle-space is possible. The fact that a region of emission in a specific band was identified over the general gray body decay of the detonation signature provides promise of unique identification. Results from the application of principal components also provided good evidence of event grouping by test condition and explosive type.

Discussion

This research displays promise that with further study a unique identification technique could provide battle-space knowledge of ordnance type and explosive condition for the war-fighter. This research also provides evidence that the gray body like emission of the detonation event dominates the event signature. This makes the identification process more difficult as individual molecular emission or absorption may be difficult to extract from the mass of energy. With this said, an emission region was identified that was different in magnitude between explosive types. This emission region was not spectrally resolvable at 16 cm^{-1} or 4 cm^{-1} resolution.

Overlap analysis provides a measure of similarity and differences between events, but has limitations. These limitations are due to the averaging nature of the analysis. Overlap analysis does have strengths in summarizing the data space and determining if and where munitions or event conditions can be best discriminated.

Further research into characterizing the gray body profile of the detonation event could possible provide unique information about bomb phenomenology. Characterizing the temperature versus time profile would also provide model verification. To accurately accomplish this study, the atmospheric absorption should be removed from the signature. Atmospheric removal code was written but the results were not robust enough to include in this work.

Even with these promising results, the variability in each detonation event is large. Increased sample space and a more in-depth analysis of data collected from the Radiant Brass 2B test could provide greater insights. Collection of a wider range of explosives detonated in field conditions would also provide more robust analysis. Collection from an elevated angle (aircraft) could possibly eliminate some ground signature interaction and would provide a more realistic sensor deployment angle for unmanned air vehicle or space based collection research.

Increasing the spectral resolution without compromising temporal resolution would be beneficial in determining spectral ranges that better discriminate the ordnance types or event conditions. Better spectral resolution could allow for identification of emission spectra riding on top of the gray body emission.

All these different suggestions provide better characterization of the detonation event. A more detailed examination of principal component analysis should include

multiple frequency characterization by time. Using frequency bins that provide better discrimination such as the 2100 to 2200 cm^{-1} band and the larger wavenumbers could increase the robustness of the technique.

Appendix A: Summary of Event Information

This appendix quantifies event specific collection results and test conditions. The test variables associated with each event is provided in Table A.1

Table A.1. Event Descriptions

Event	Static/Air	Impact Vector/ Elevation	Size	Explosive
1	Air	155 degrees perpendicular	Small	A
2	Air	155 degrees perpendicular	Small	A
3	Air	155 degrees perpendicular	Small	A
4	Air	155 degrees perpendicular	Small	A
5	Air	155 degrees perpendicular	Small	A
6	Air	155 degrees perpendicular	Small	A
7	Air	155 degrees perpendicular	Small	A
8	Air	155 degrees perpendicular	Large	B
9	Air	155 degrees perpendicular	Large	B
10	Air	155 degrees perpendicular	Large	B
11	Air	155 degrees perpendicular	Medium	B
12	Air	155 degrees perpendicular	Medium	B
13	Air	355 degrees toward	Medium	B
14	Air	355 degrees toward	Medium	B
15	Air	335 degrees toward	Large	B
16	Air	335 degrees toward	Large	B
17	Air	335 degrees toward	Large	B
18	Air	335 degrees toward	Large	B
19	Air	355 degrees toward	Small	A
20	Air	065 degrees away	Small	A
21	Air	065 degrees away	Small	A
22	Air	065 degrees away	Small	A
23	Air	065 degrees away	Small	A
24	Air	065 degrees away	Small	A
25	Air	065 degrees away	Small	A
26	Air	065 degrees away	Small	A
27	Air	065 degrees away	Small	A
28	Air	065 degrees away	Small	A
29	Air	065 degrees away	Medium	B
30	Air	065 degrees away	Medium	B
31	Air	065 degrees away	Medium	B
32	Air	065 degrees away	Medium	B
33	Air	065 degrees away	Large	B
34	Static	5 degrees elevation	Large	A
35	Static	5 degrees elevation	Large	B

Table A.1 continued:

Event	Static/Air	Impact Vector/ Elevation	Size	Explosive
36	Static	15 degrees elevation	Large	B
37	Static	45 degrees elevation	Small	A
38	Static	45 degrees elevation	Small	A
39	Static	45 degrees elevation	Small	A
40	Static	45 degrees elevation	Small	A
41	Static	45 degrees elevation	Small	A
42	Static	45 degrees elevation	Small	A
43	Static	45 degrees elevation	Small	A
44	Static	45 degrees elevation	Small	A
45	Static	45 degrees elevation	Small	A
46	Static	45 degrees elevation	Ext Small	C
47	Static	45 degrees elevation	Ext Small	C
48	Static	30 degrees elevation	Large	B
49	Static	10 degrees elevation	Large	B
50	Static	3 degrees elevation	Large	B
51	Static	45 degrees elevation	Small	A
52	Static	45 degrees elevation	Small	A
53	Static	45 degrees elevation	Small	A
54	Static	45 degrees elevation	Small	A
55	Static	45 degrees joint fuse	2* Small	A
56	Static	45 degrees joint fuse	2* Small	A

A summary of the collected data by event is provided in Table A.2 In this table four different ground types characterize the impact surface. They are HR, hard rock; SC, sandy clay; HRR, hard rock rubble; and HS, hard sand. The ground types are summarized from the five Radiant Brass Test Reports by Miller. The time mode refers to the time evolution mode described in chapter V. If the event displayed time mode one and no afterburn was apparent, it is described in the notes column as 'no afterburn'. The notes column also describes the system related collection errors by event.

Table A.2. Event Collection Summary

Event	Impact Surface	Collect X = Yes	Res. (cm^{-1})	Time Mode	Notes
1	HR				Collection system error
2	HR				Collection system error
3	HR	X	16	1	
4	HR	X	16	1	
5	HR	X	16	1	
6	HR	X	16	1	
7	HR	X	16	1	
8	HR	X	16	1	
9	HR	X	16	1	Afterburn in Band D only
10	HR	X	16	1	
11	HR	X	16	1	
12	HRR	X	16	1	
13	SC				Event outside field of view
14	HR	X	16	2	
15	HR	X	16	2	
16	HS				Event outside field of view
17	HS	X	16	2	2 afterburn peaks
18	HS	X	16	2	Afterburn in Band D only
19	HR	X	16	2	
20	HRR	X	16	2	
21	HR	X	16	1	
22	HR	X	16	1	
23	HR	X	16	1	
24	HRR	X	4	1	
25	HR	X	4	1	
26	HS	X	4	1	No afterburn
27	HR	X	4	1	
28	HS	X	16	1	
29	HR	X	16	1	
30	HR	X	4	1	No afterburn
31	HRR	X	4	1	
32	HR	X	4	1	
33	HR	X	16	1	
34	SC	X	16	1	1-3 scans lose zero reference
35	SC	X	16	1	1st scan lose zero reference
36	SC	X	16	1	1st scan lose zero reference
37	HRR	X	16	2	
38	HRR	X	16	2	
39	HRR	X	16	2	
40	HRR	X	16	2	
41	HRR	X	16	2	

Table A.2 continued:

Event	Impact Surface	Collect X = Yes	Res. (cm^{-1})	Time Mode	Notes
42	HRR	X	4	2	
43	HRR	X	16	2	
44	HRR	X	4	2	
45	HRR	X	16	2	
46	HS	X	16	1	No afterburn, 1st scan lose zero reference
47	HS	X	16	1	No afterburn, 1st scan saturate
48	SC	X	16	1	1st scan lose zero reference
49	SC	X	16	1	No afterburn, 1st scan lose zero reference
50	SC	X	16	1	1st scan lose zero reference
51	HRR	X	16	2	
52	HRR	X	4	2	
53	HRR	X	4	2	
54	HRR	X	16	2	
55	HS	X	16	2	
56	HS	X	16	2	

Appendix B: Analysis Code

This appendix contains listings of the computer programs used in the manipulation of the MR-154 data and the subsequent analysis. A description of each *Matlab* code and how it works was provided in Chapter 4. The first program is 'get_overlap' code, the second script is 'combine_overlap', the third program is ' make_temporal' and the final code is 'compare_to_spectrometer'. Each code is separated by a solid line and start with general comments.

```
% Matlab script for overlapping temporal vectors by wavenumber
% 'Get_Overlap'
% Started 11 Nov 99
% 1st Lt Jay Orson
% AFIT/GSO/ENP/00M-01
%
% Modified 16 Nov 99 for ascii output
% Modified 17 Nov 99 add checkrow for different wavenumber ranges
%    add notes for time window of overlap
%
% User defined variables
% check_row This is the row to check for event iniation
% time_step This varies the size of the extraction window

[spec_file, spec_dir] = uigetfile('*.txt','Load Spectrometer File');
cd(spec_dir);
spec_in = load(spec_file);

[spec_file1, spec_dir1] = uigetfile('*.txt','Load Comparison
Spectrometer File');
cd(spec_dir1);
spec_in1 = load(spec_file1);

string = [spec_file,' vs ', spec_file1] ;
string1 = strrep(string, '_','\_') ;

% now get sizes

[row_size, col_size] = size(spec_in);
[row_size1, col_size1] = size(spec_in1);

% Strip off vector for wavenumbers

wave_num = spec_in(:,1);
wave_num1 = spec_in1(:,1);

% Select a vector in a pass band to search for bomb iniation
```

```
% to compare brass 2b data, or downsampled InSb or MCT data
%        change check_row to 55
% to compare brass 3a,3b data INSB detectors set check_row 128
% to compare brass 3a,3b data MCT detectors set check_row to 250

check_row = 128;
check_vector = spec_in(check_row,1:end);
check_diff = diff(check_vector);
max_val = max(check_diff);

check_vector1 = spec_in1(check_row,1:end);
check_diff1 = diff(check_vector1);
max_val1 = max(check_diff1);

% find the column of the initiation spike
% start_col and stop_col create the time window to look at
% each column is .047s for Brass 3a and 3b data
% each column is .264S for Brass 2a and downsampled 3a,3b data

time_step = 20 ;

max_col = find(check_diff>=max_val);
start_col = max_col + 2 ;
stop_col = max_col + time_step ;
max_col1 = find(check_diff1>=max_val1);
start_col1 = max_col1 + 2 ;
stop_col1 = max_col1 + time_step ;

spec_out = abs(spec_in(1:end,start_col:stop_col));
spec_out1 = abs(spec_in1(1:end,start_col1:stop_col1));

% figure
% plot (wave_num, spec_out) ;
% figure
% plot (wave_num1, spec_out1) ;

% now that the bomb initiation spikes have been aligned in two
% matrices spec_out spec_out1 area normalize each matrix by each
% row vector

Norm_mat = zeros(row_size,time_step) ;
Norm_mat1 = zeros(row_size,time_step) ;

mag_out = spec_out .* spec_out ;
mag_out1 = spec_out1 .* spec_out1 ;
overlap = zeros(row_size,1) ;

for count = 1:row_size
   adotb = (spec_out(count,1:end)* spec_out1(count,1:end).');
   Norm_A = sqrt(sum(mag_out(count,1:end)));
   Norm_B = sqrt(sum(mag_out1(count,1:end)));
   cross = adotb/(Norm_A*Norm_B) ;
   overlap(count) = cross ;
end

%  plot out the overlap file
```

```
figure
plot(wave_num, overlap,'k-'), set (gca, 'ylim', [.5,1])
set (gca, 'xlim',[1800,6000]), title (string1),
ylabel('overlap'), xlabel ('wavenumber');

% output overlap to ascii file
% make sure to eliminate the .txt and spaces in the given filename

out_file = [wave_num, overlap];

[file_out, path_out] = uiputfile(string,'Click OK to continue');
output_filename = [path_out, strrep(file_out, 'txt','olp')];
eval(['save ' output_filename ' out_file -ascii;']);
```

```
% This program was written to combine multiple files created by
% the get_overlap script.
% 'Combine_Overlap'
% 1st Lt Jay Orson
% AFIT/GSO/ENP/00M-01
%
% User defined variables are num_in number of overlaps to manipulate

num_in = 4 ;

[spec_file, spec_dir] = uigetfile('*.olp','Load one of the overlap
File');
cd(spec_dir);
spec_in = load(spec_file);
[rows,cols] = size(spec_in);
cols_out = num_in + 1 ;
output = ones(rows,cols_out)
output(1:end,1) = spec_in(1:end,1) ;
output(1:end,2) = spec_in(1:end,2) ;

% read in all overlap files from a comparison case to be plotted
% and outputed to one file

for count = 2:num_in,
      [spec_file, spec_dir] = uigetfile('*.olp','Load overlap File');
   cd(spec_dir);
      spec_in = load(spec_file);
      outcol = count + 1 ;
      output(1:end,outcol) = spec_in(1:end,2) ;
end

figure
plot (output(1:end,1) , output(1:end,2:end)),
set (gca, 'ylim', [.5,1]),set (gca, 'xlim',[4000,5100]),
xlabel ('wavenumber'), ylabel ('overlap');

% output overlap files back to ascii
```

```
[file_out, path_out] = uiputfile('defalt' ,'Name the combined overlap
file');
output_filename = [path_out, strrep(file_out, 'm','txt')];
eval(['save ' output_filename ' output -ascii;']);
```

```
% Matlab file to extract 4 pass band regions in the MR-154 Data
%           matrix that relate to 4 filtered Wyle Radiometric Bands
% 'Make_Temporal'
% Sensor Fusion Chapters 2,4,5
% Last Modified 8 Nov 99 by Tom Fitzgerald Wyle Laboratory
% New Filter bands can be created by
% 1st Lt Jay Orson
% AFIT/GSO/ENP/00M-01

start = pwd;

% first read the ascii file that contains the data;
[file_name, path_name] = uigetfile('*.txt');
cd(path_name);

in_data = load(file_name);
wave_num = in_data(:,1);
del_wave_num = wave_num(2) - wave_num(1);
% del_wave_num = 16;

del_time = 0.04734901;

event_distance = input('Enter Distance to event in meters ');

% now get sizes

[row_time, col_spec] = size(in_data);
dummy = ones(row_time,1);

%Filter information
A = dummy * [4319; 4622]';
del_A = A(1,:) * [-1;1];
del_A2 = [A(:,1) - wave_num, A(:,2) - wave_num];
A_m = .1517;

B = dummy * [3171; 3665]';
del_B = B(1,:) * [-1;1];
del_B2 = [B(:,1) - wave_num, B(:,2) - wave_num];
B_m = 0.4249;

C = dummy * [2508;2629]';
del_C = C(1,:) * [-1;1];
del_C2 = [C(:,1) - wave_num, C(:,2) - wave_num];
C_m = 0.1812;
```

```
D = dummy * [2137;2230]';
del_D = D(1,:) * [-1;1];
del_D2 = [D(:,1) - wave_num, D(:,2) - wave_num];
D_m = 0.1941;

%find the values that correspond to the filter bins

A1 = find(abs(del_A2(:,1)) == min(abs(del_A2(:,1))));
A2 = find(abs(del_A2(:,2)) == min(abs(del_A2(:,2))));

B1 = find(abs(del_B2(:,1)) == min(abs(del_B2(:,1))));
B2 = find(abs(del_B2(:,2)) == min(abs(del_B2(:,2))));

C1 = find(abs(del_C2(:,1)) == min(abs(del_C2(:,1))));
C2 = find(abs(del_C2(:,2)) == min(abs(del_C2(:,2))));

D1 = find(abs(del_D2(:,1)) == min(abs(del_D2(:,1))));
D2 = find(abs(del_D2(:,2)) == min(abs(del_D2(:,2))));

A_data = in_data(A1:A2,2:end);
B_data = in_data(B1:B2,2:end);
C_data = in_data(C1:C2,2:end);
D_data = in_data(D1:D2,2:end);

[rows_A, cols_A] = size(A_data);
[rows_B, cols_B] = size(B_data);
[rows_C, cols_C] = size(C_data);
[rows_D, cols_D] = size(D_data);

ones_A = ones(1,rows_A);
ones_B = ones(1,rows_B);
ones_C = ones(1,rows_C);
ones_D = ones(1,rows_D);

A_data_int = ones_A * A_data * del_wave_num;
B_data_int = ones_B * B_data * del_wave_num;
C_data_int = ones_C * C_data * del_wave_num;
D_data_int = ones_D * D_data * del_wave_num;

% now scale to intensity and divide by bandwidth
z_cal2 = 72.5^2; % distance to aperture
a_cal = 0.1^2 * pi; % area of aperture
z_bomb2 = (event_distance * 100)^2; % distance to bomb in cm squared

size_fac = a_cal * z_bomb2 / z_cal2; % Size Factor Correction Chapter 2

time_A = 0:del_time:del_time*(cols_A-1);
time_B = 0:del_time:del_time*(cols_B-1);
time_C = 0:del_time:del_time*(cols_C-1);
time_D = 0:del_time:del_time*(cols_D-1);

A_inten = A_data_int * size_fac * 1/A_m;
A_inten = A_inten - mean(A_inten(:,1:10));

B_inten = B_data_int * size_fac * 1/B_m;
B_inten = B_inten - mean(B_inten(:,1:10));
```

```
C_inten = C_data_int * size_fac * 1/C_m;
C_inten = C_inten - mean(C_inten(:,1:10));

D_inten = D_data_int * size_fac * 1/D_m;
D_inten = D_inten - mean(D_inten(:,1:10));

figure
hold
subplot(2,2,1),plot(time_A, A_inten,'k*-'), set(gca,'xlim',[0,10]),
title('Band A'), grid;
subplot(2,2,2),plot(time_B, B_inten,'r*-'), set(gca,'xlim',[0,10]),
title('Band B'), grid;
subplot(2,2,3),plot(time_C, C_inten,'g*-'), set(gca,'xlim',[0,10]),
title('Band C'), grid;
subplot(2,2,4),plot(time_D, D_inten,'b*-'), set(gca,'xlim',[0,10]),
title('Band D'), grid;

[file_out, path_out] = uiputfile('default.cal','Click OK to continue');
out_cal = [path_out, strrep(file_name,'txt','cal')];
%eval(['print -djpeg75 ' out ]);
% [file_out, path_out] = uiputfile('default.cal','Click OK to
continue');
data_out = [time_A; A_inten; time_B; B_inten; time_C; C_inten; time_D;
D_inten]';
eval(['save ' out_cal ' data_out -ascii;']);


%backg = mean(in_data(:,2:10)')';
%dummy1 = ones(1,col_spec);
%backgs = backg * dummy1;
%in_data_s = in_data - backgs;
%figure
%surf(in_data_s(:,2:end));
```

```
% Script to compare spectrometer and radiometer data
% Radiometer format is TDDDD (T = time, D = data)
% spectrometer format is TDTDTDTD
% 'Compare_to_Spectrometer'
% Tom Fitzgerald Wyle Laboratory
% Modified 16 Nov 99 to add plot boundaries
% 1st Lt Jay Orson
% AFIT/GSO/ENP/00M-01

[rad_file, rad_dir] = uigetfile('*.cal','Load Radiometer File');
[spec_file, spec_dir] = uigetfile('*.cal','Load Spectrometer File');

cd(rad_dir)
rad_in = load(rad_file);
cd(spec_dir);
spec_in = load(spec_file);

time_out1 = downsample(rad_in(1:5000,1),10);
rad_out_A1 = downsample(rad_in(1:5000,2),10);
```

```
rad_out_B1 = downsample(rad_in(1:5000,3),10);
rad_out_C1 = downsample(rad_in(1:5000,4),10);
rad_out_D1 = downsample(rad_in(1:5000,5),10);

time_out = (rad_in(1:5000,1));
rad_out_A = (rad_in(1:5000,2));
rad_out_B = (rad_in(1:5000,3));
rad_out_C = (rad_in(1:5000,4));
rad_out_D = (rad_in(1:5000,5));


figure
plot(time_out,rad_out_A),  set(gca,'xlim',[1,8]);
hold
plot(spec_in(:,1),spec_in(:,2),'r-*'),set(gca,'xlim',[0,10]);
plot(time_out1,rad_out_A1,'k-*'),set(gca,'xlim',[0,10]);
title('Band A');
legend('Radiometer','Spectrometer','Downsampled Radiometer');

grid

figure
plot(time_out,rad_out_B),set(gca,'xlim',[0,10]);
hold
plot(spec_in(:,3),spec_in(:,4),'r-*'),set(gca,'xlim',[0,10]);
plot(time_out1,rad_out_B1,'k-*'),set(gca,'xlim',[0,10]);
title('Band B');
legend('Radiometer','Spectrometer','Downsampled Radiometer');
grid

figure
plot(time_out,rad_out_C),set(gca,'xlim',[0,10]);
hold
plot(spec_in(:,5),spec_in(:,6),'r-*'),set(gca,'xlim',[0,10]);
plot(time_out1,rad_out_C1,'k-*'),set(gca,'xlim',[0,10]);
title('Band C');
legend('Radiometer','Spectrometer','Downsampled Radiometer');
grid

figure
plot(time_out,rad_out_D),set(gca,'xlim',[0,10]);
hold
plot(spec_in(:,7),spec_in(:,8),'r-*'),set(gca,'xlim',[0,10]);
plot(time_out1,rad_out_D1,'k-*'),set(gca,'xlim',[0,10]);
title('Band D');
legend('Radiometer','Spectrometer','Downsampled Radiometer');
grid
```

Appendix C: Additional Sensor Fusion Results

This appendix contains sensor fusion results from six events. Events will include examples of explosive A, B, and C, time evolution modes one and two and a example of two simultaneous detonations. The red curve and -*- notation identifies the MR-154 data. The solid purple curve is the 200 Hz Wyle Radiometer data and the black curve,-*-, superimposed on the purple curve is the time averaged Wyle data. For a review of the sensor fusion bands or process refer to Chapter IV and Chapter II.

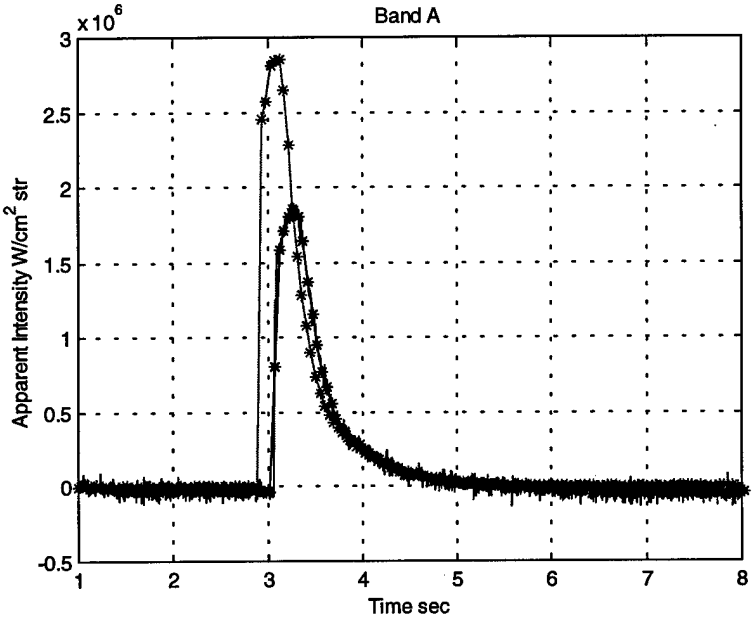

Event 45, Explosive A, MR-154 Offset Left
(MR-154 Red -*-, 200 Hz Radiometer Purple,
Averaged Radiometer Black)

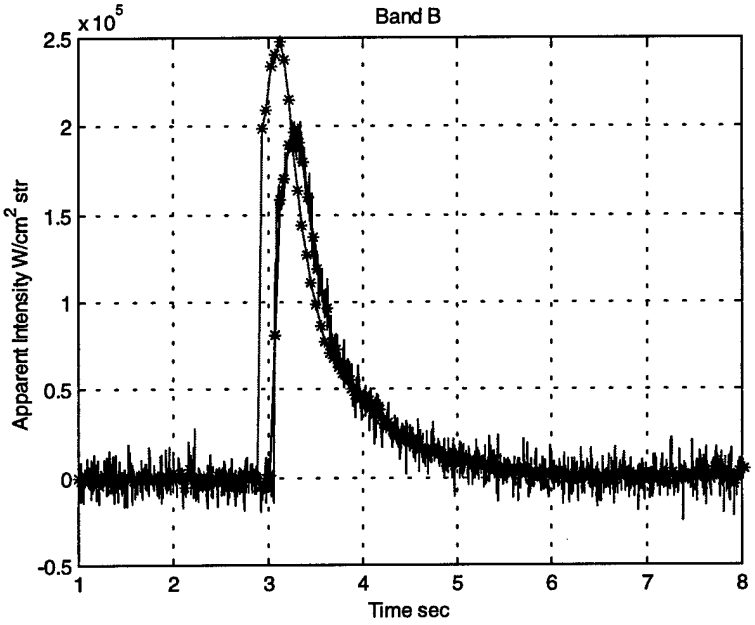

Event 45, Explosive A, MR-154 Offset Left
(MR-154 Red -*-, 200 Hz Radiometer Purple,
Averaged Radiometer Black)

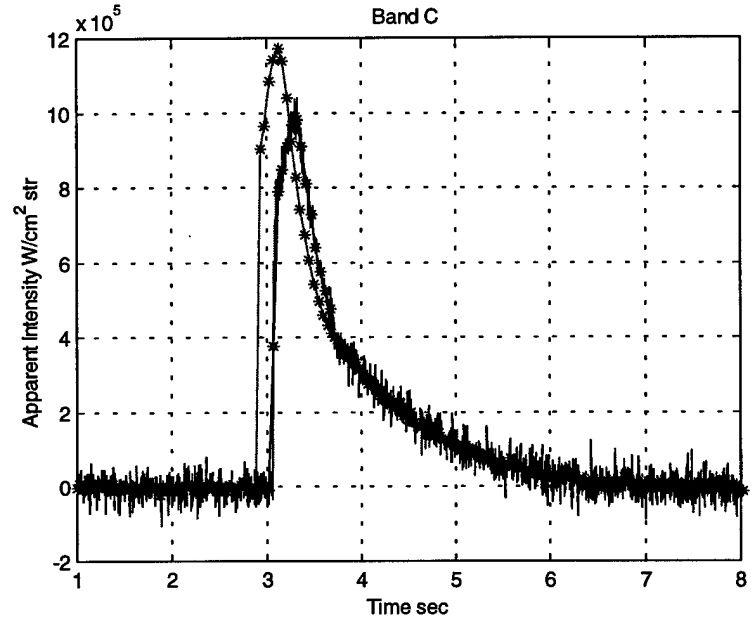

Event 45, Explosive A, MR-154 Offset Left
(MR-154 Red -*-, 200 Hz Radiometer Purple,
Averaged Radiometer Black)

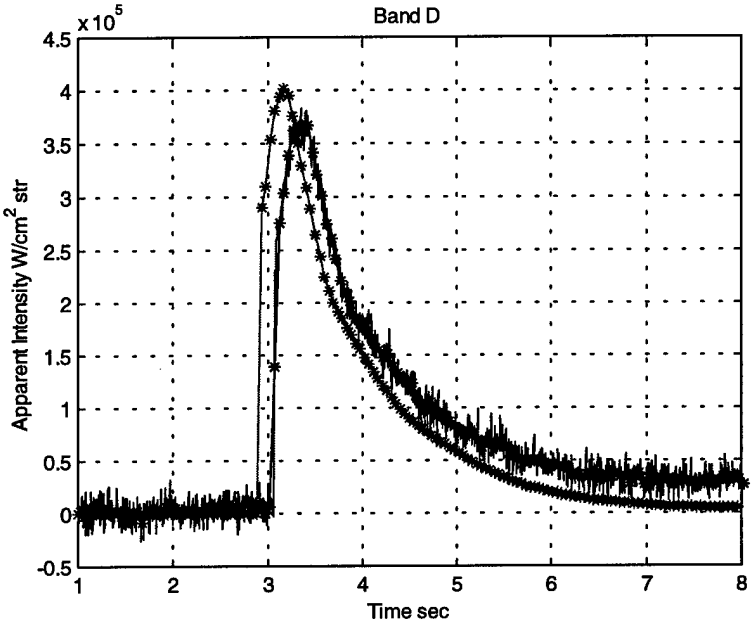

Event 45, Explosive A, MR-154 Offset Left
(MR-154 Red -*-, 200 Hz Radiometer Purple,
Averaged Radiometer Black)

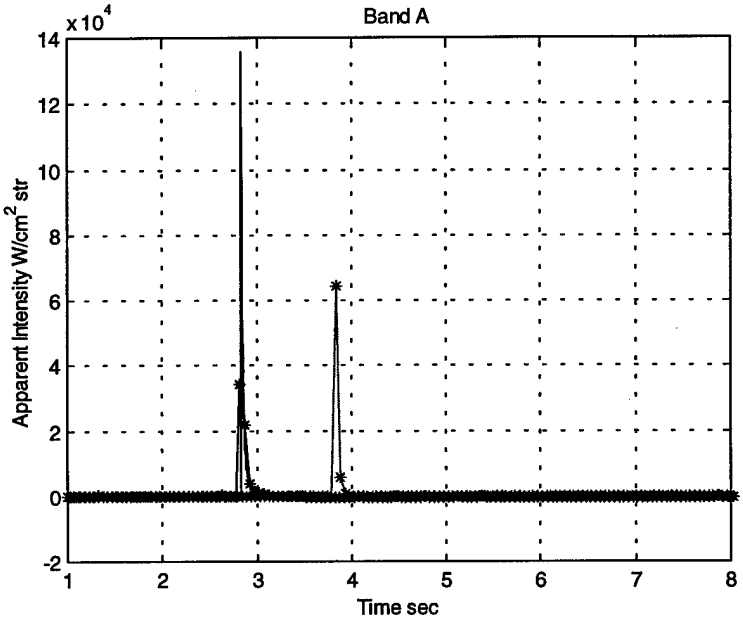

Event 47, Explosive C, MR-154 Offset Right
(MR-154 Red -*-, 200 Hz Radiometer Purple,
Averaged Radiometer Black)

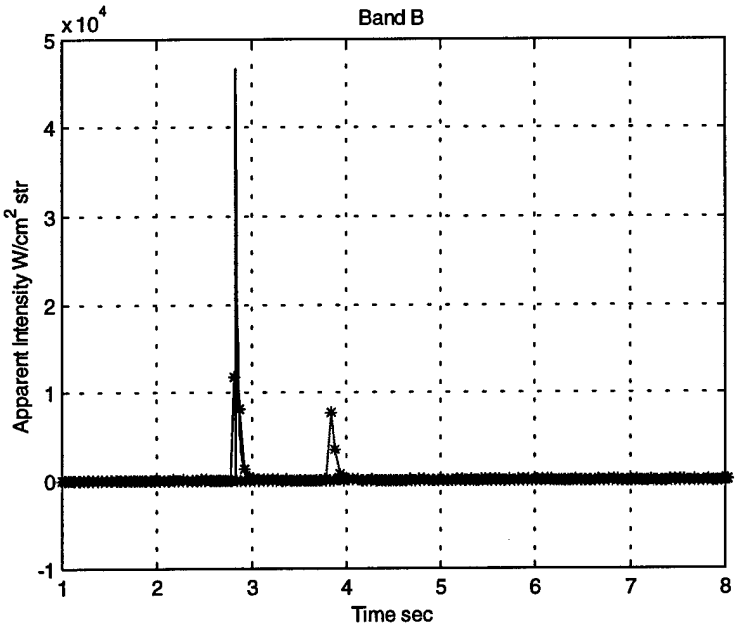

Event 47, Explosive C, MR-154 Offset Right
(MR-154 Red -*-, 200 Hz Radiometer Purple,
Averaged Radiometer Black)

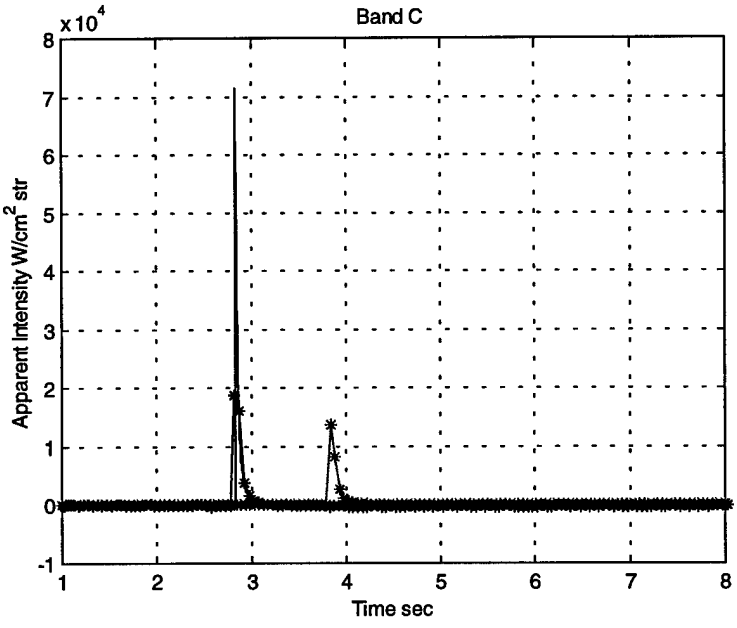

Event 47, Explosive C, MR-154 Offset Right
(MR-154 Red -*-, 200 Hz Radiometer Purple,
Averaged Radiometer Black)

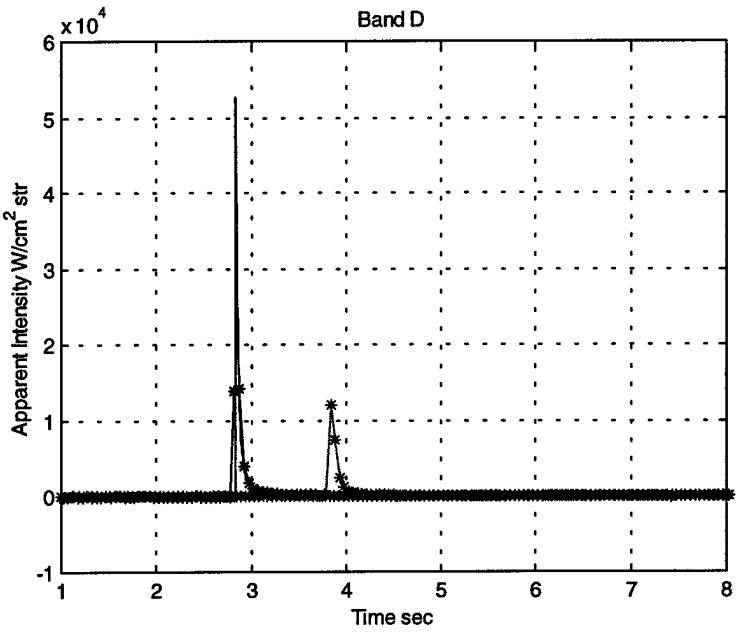

Event 47, Explosive C, MR-154 Offset Right
(MR-154 Red -*-, 200 Hz Radiometer Purple,
Averaged Radiometer Black)

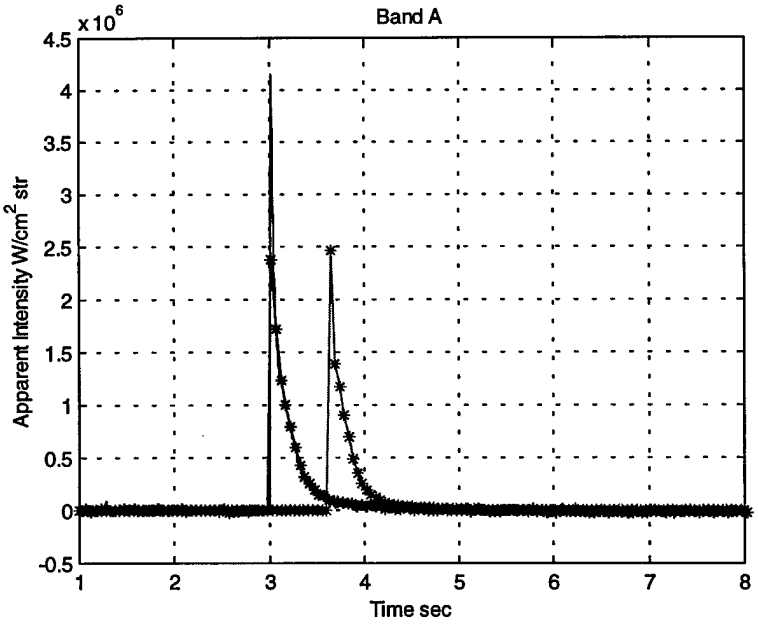

Event 49, Explosive B, MR-154 Offset Right
(MR-154 Red -*-, 200 Hz Radiometer Purple,
Averaged Radiometer Black)

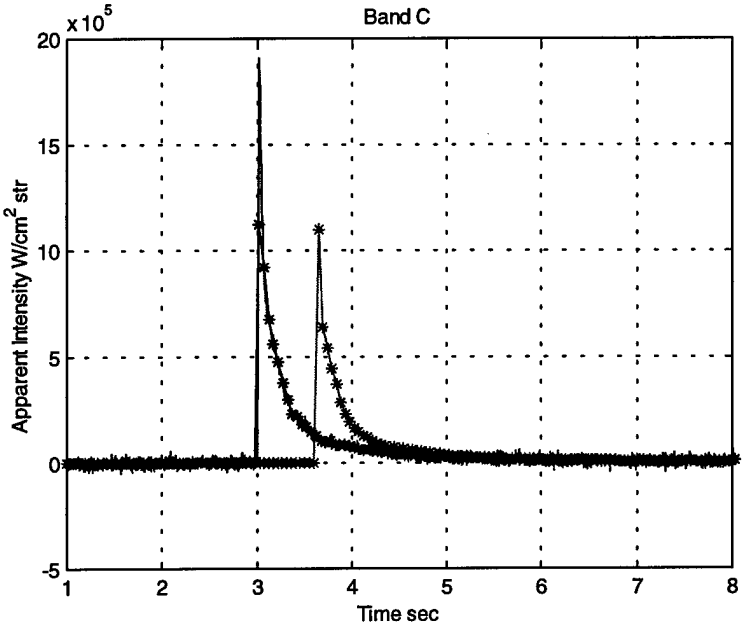

Event 49, Explosive B, MR-154 Offset Right
(MR-154 Red -*-, 200 Hz Radiometer Purple,
Averaged Radiometer Black)

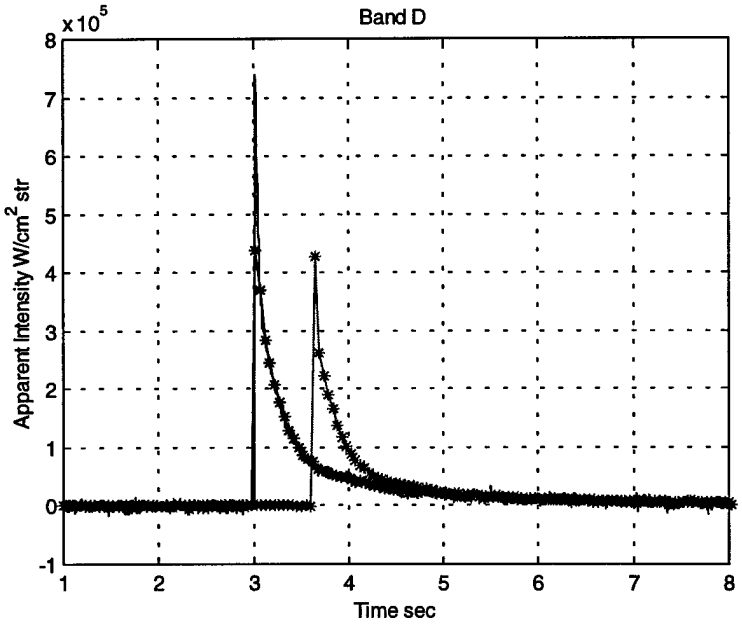

Event 49, Explosive B, MR-154 Offset Right
(MR-154 Red -*-, 200 Hz Radiometer Purple,
Averaged Radiometer Black)

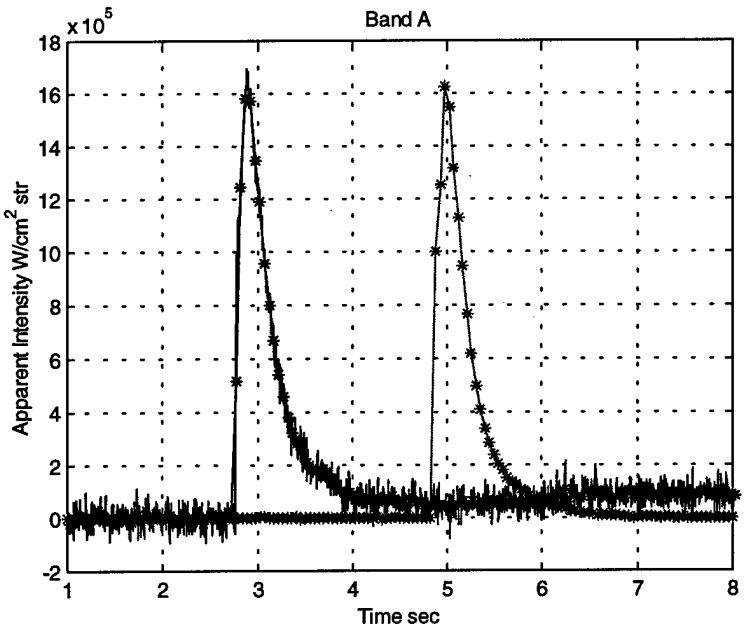

Event 51, Explosive A MR-154 Offset Right
(MR-154 Red -*-, 200 Hz Radiometer Purple,
Averaged Radiometer Black)

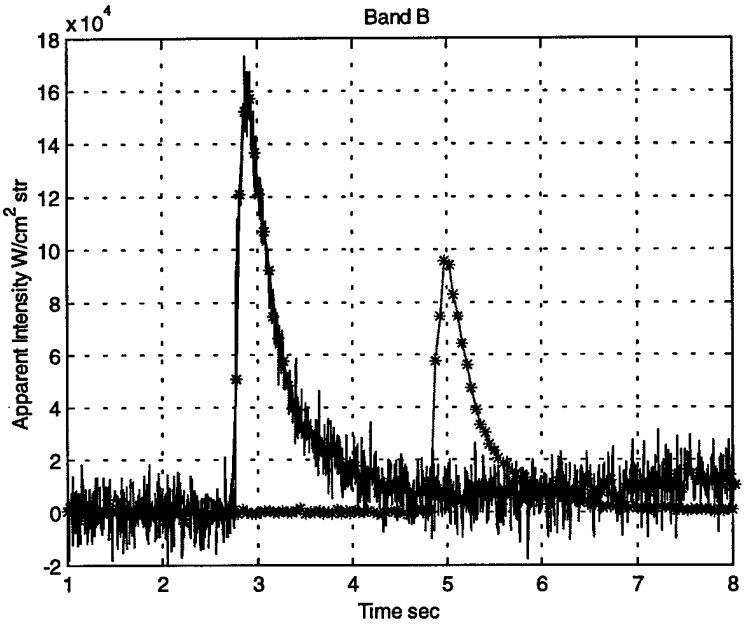

Event 51, Explosive A MR-154 Offset Right
(MR-154 Red -*-, 200 Hz Radiometer Purple,
Averaged Radiometer Black)

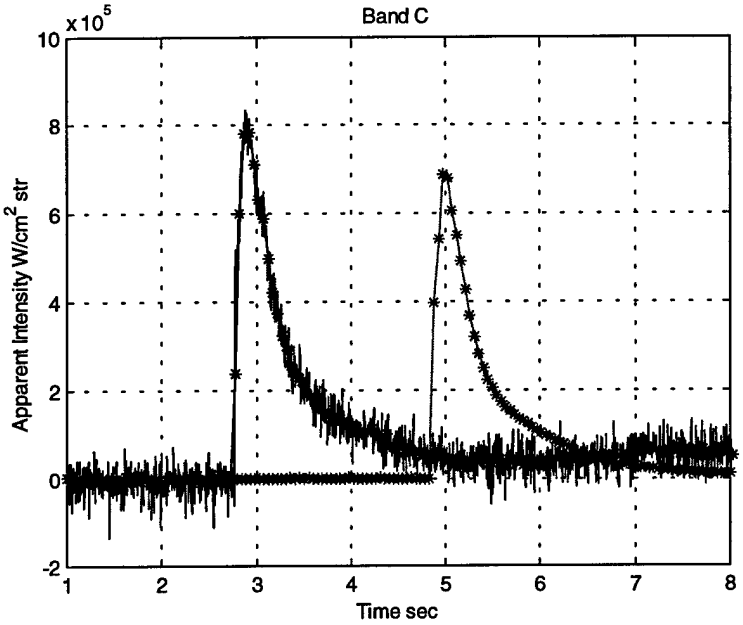

Event 51, Explosive A MR-154 Offset Right
(MR-154 Red -*-, 200 Hz Radiometer Purple,
Averaged Radiometer Black)

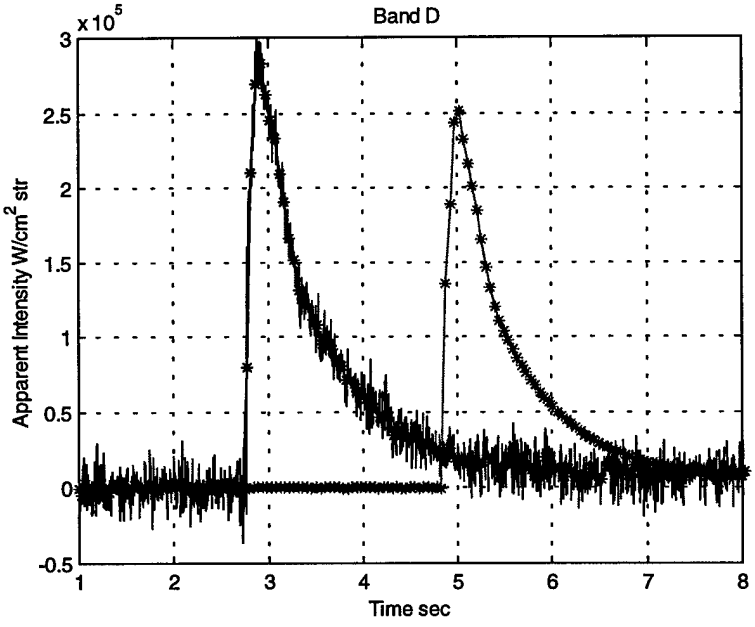

Event 51, Explosive A MR-154 Offset Right
(MR-154 Red -*-, 200 Hz Radiometer Purple,
Averaged Radiometer Black)

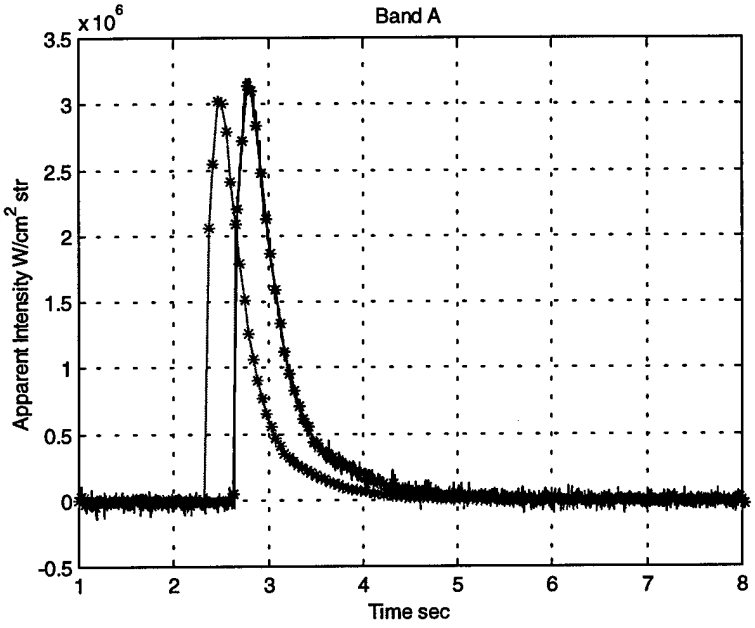

Event 55, Explosive A, 2 Simultaneous Detonations
MR-154 Offset Left (MR-154 Red -*-, 200 Hz Radiometer Purple, Averaged Radiometer Black)

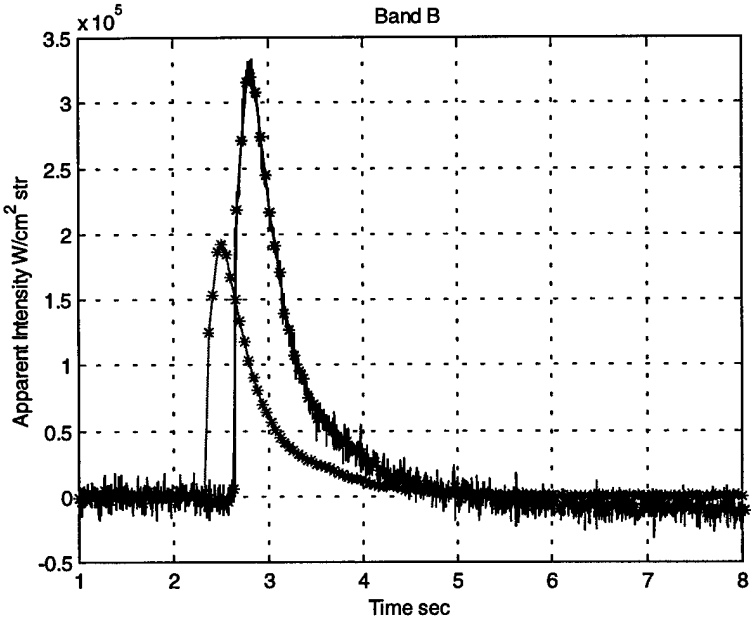

Event 55, Explosive A, 2 Simultaneous Detonations
MR-154 Offset Left (MR-154 Red -*-, 200 Hz Radiometer Purple, Averaged Radiometer Black)

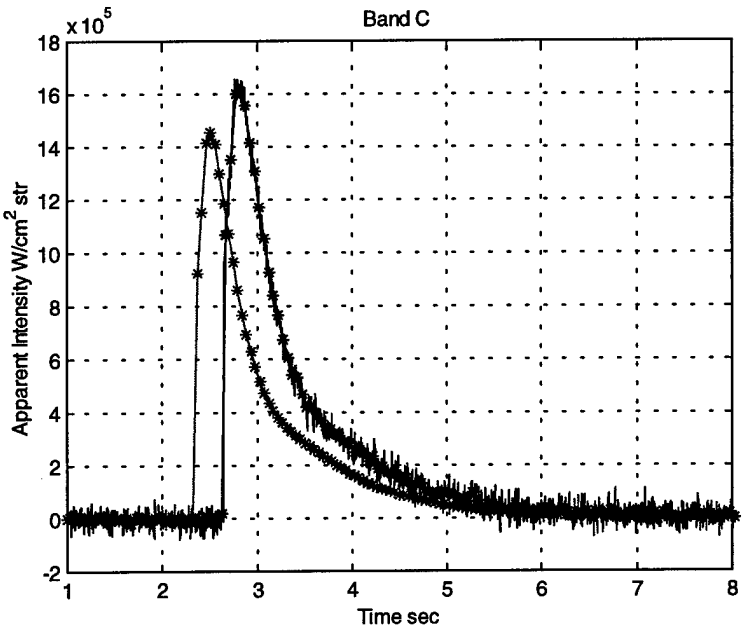

Event 55, Explosive A, 2 Simultaneous Detonations
MR-154 Offset Left (MR-154 Red -*-, 200 Hz Radiometer Purple, Averaged Radiometer Black)

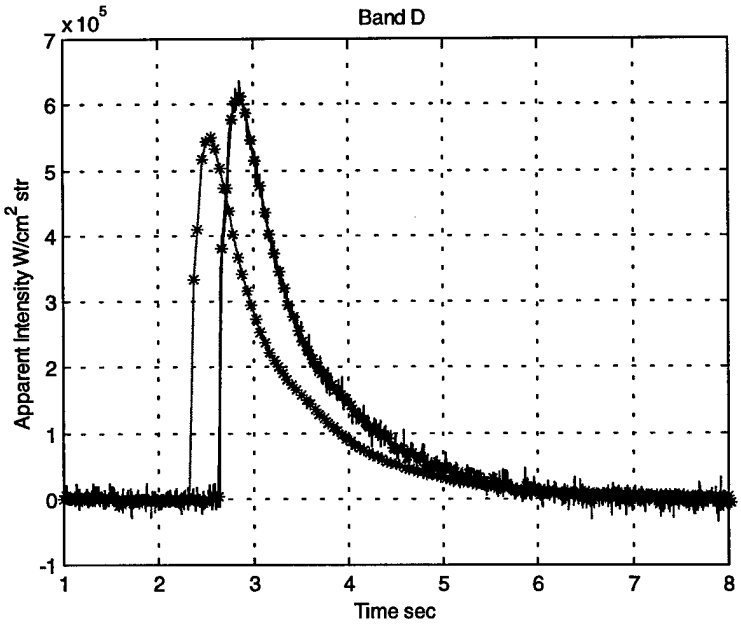

Event 55, Explosive A, 2 Simultaneous Detonations
MR-154 Offset Left (MR-154 Red -*-, 200 Hz Radiometer Purple, Averaged Radiometer Black)

Bibliography

1. Augustine, H. and others. Tactical Missile Signatures Measurement Standards Handbook. Michigan: Environmental Research Institute of Michigan, 1997.

2. BOMEM Users Manual. MR Series FT-Spectroradiometer Design Overview and Theory. Version 1.0, May 1995

3. BOMEM Users Manual. MR Series FT-Spectroradiometer Research Acquire Radiometric Software Manual. Version 3.0, August 1999

4. Cook, A. H. Interference of Electromagnetic Waves. Oxford: Clarendon Press, 1971.

5. Cooper, Paul W. Explosives Engineering. New York: Wiley-Vch, 1996.

6. Department of Defense. Multispectral Users Guide. August 1995

7. Elachi, Charles. Introduction to the Physics and Techniques of Remote Sensing. New York: John Wiley & Sons, 1987.

8. Evans, Howard. Paper, "Study: On the Sampling of Explosive Signatures." Ball Aerospace & Technologies Corp. March 1998.

9. Fitzgerald, Tom. Senior Engineer, Wyle Laboratory. Sensor Fusion Data. 1999.

10. Hauser, Robert G. Survey of Military Applications for Fourier Transform Infrared (FTIR) Spectroscopy. MS thesis, AFIT/GM/ENP/99M-07. School of Engineering, Air Force Institute of Technology (AU), Wright-Patterson AFB OH, February 1999.

11. "HITRAN 1996." CD-ROM. ONTAR Corporation, 9 Village Way, North Andover, MA.

12. Jolliffe, I. T. Principal Component Analysis. New York: Springer-Verlag, 1986.

13. Miller, Sean C. and Miller, William J. Radiant Brass Test Report. Florida: Science Applications International Corporation, August 1998.

14. -----. Radiant Brass Test Report Phase 2A. Florida: Science Applications International Corporation, October 1998.

15. Miller, William J. and Miller, Sean C. Radiant Brass Phase 2B Test Report. Florida: Science Application International Corp., January 1999.

16. -----. Radiant Brass Phase 3A Test Report. Florida: Science Application International Corp., October 1999.

17. -----. Radiant Brass Phase 3B Test Report. Florida: Science Application International Corp., November 1999.

18. Miller, William J. Chief Scientist Radiant Brass Test Program, SciTec Inc. Personal Interview. 11 November 1999.

19. Seyrafi, Khalil and Hovanessian S. A. Introduction to Electro-Optical Imaging and Tracking Systems. Norwood: Artech House, Inc, 1993.

20. Struve, Walter S. Fundamentals of Molecular Spectroscopy. New York: John Wiley & Sons, 1989.

REPORT DOCUMENTATION PAGE	Form Approved OMB No. 074-0188

1. AGENCY USE ONLY (Leave blank)	2. REPORT DATE	3. REPORT TYPE AND DATES COVERED
	March 2000	Master's Thesis July 1999 - March 2000

4. TITLE AND SUBTITLE

Collection of Detonation Signatures and Characterization of Spectral Features

5. FUNDING NUMBERS

6. AUTHOR(S)

Jay A. Orson, 1st Lieutenant, USAF

7. PERFORMING ORGANIZATION NAMES(S) AND ADDRESS(S)

Air Force Institute of Technology
Graduate School of Engineering and Management (AFIT/EN)
2950 P Street, Building 640
WPAFB OH 45433-7765

8. PERFORMING ORGANIZATION REPORT NUMBER

AFIT/GSO/ENP/00M-01

9. SPONSORING / MONITORING AGENCY NAME(S) AND ADDRESS(ES)

NAIC/DXDI
Attn: Capt William T Caldwell
4180 Watson Way
WPAFB OH 45433-5625 DSN: 787-2575 COM: 937-257-2575

10. SPONSORING / MONITORING AGENCY REPORT NUMBER

11. SUPPLEMENTARY NOTES

Advisor: Lt Col G. P. Perram ENP DSN: 785-3636 ext 4504 COM:937-255-3636 ext 4504 Glen.Perram@afit.af.mil

12a. DISTRIBUTION / AVAILABILITY STATEMENT

APPROVED FOR PUBLIC RELEASE, DISTRIBUTION UNLIMITED

12b. DISTRIBUTION CODE

ABSTRACT (*Maximum 200 Words*)

The remote observations of the temporal and spectral characteristics of the infrared (IR) emissions from exploding ordnance have been correlated with explosion conditions. A Bomem MR-154 Fourier Transform Interferometer with two detectors, InSb and HgCdTe, and a 75 mrad telescope was used to record spectra in the 1.3 - 20 μm range. Data was collected at spectral resolutions of 16 cm^{-1} and 4 cm^{-1} and temporal resolutions of 0.045 s and 0.123 s respectively. Two field tests were conducted: (1) a set of dynamic drop explosions and (2) a series of static detonations.

Sensor fusion between the FTIR instrument and four 200 Hz InSb radiometers is promising. The FTIR temporal profiles, calibrated for absolute radiance, compare within 8% in three independent bands and within 30% in the fourth band. The degree of temporal overlap as a function of frequency for a pair of detonation events, provides a direct indication of the ability to discriminate between explosion conditions. Overlap analysis provides quantification of the repeatability of an explosive condition, and the discrimination between look angle and explosive type. Additional preliminary analysis mechanistically describes all events as decaying gray bodies.

14. SUBJECT TERMS	15. NUMBER OF PAGES
Remote Sensing, Detonations, Infrared, Spectral Signatures, Conventional Munitions, Ordnance, Spectroscopy, Fourier Transform Infrared Spectroscopy FTIR	113
	16. PRICE CODE

17. SECURITY CLASSIFICATION OF REPORT	18. SECURITY CLASSIFICATION OF THIS PAGE	19. SECURITY CLASSIFICATION OF ABSTRACT	20. LIMITATION OF ABSTRACT
UNCLASSIFIED	UNCLASSIFIED	UNCLASSIFIED	UL